THE UNIVERSITY
of ADELAIDE

FACULTY OF SCIENCES
SCHOOL OF PHYSICAL SCIENCES

EQUATION OF STATE OF ROTATING NEUTRON STARS

WASIF HUSAIN

SUPERVISORS :
PROF. ANTHONY THOMAS
PROF. DEREK LEINWEBER

Contents

List of Figures

List of Tables

Abstract

In this thesis a very comprehensive model of rotating neutron stars has been constructed, which is based on the Quark-Meson Coupling model (QMC model), using the method developed by Hartle for slowly rotating compact stars. To determine tidal Love number method suggested by 'Hinderer' is adopted. In this thesis, neutron star properties are calculated at the rotation frequency of 500 Hz and compared for three EoSs which are based on pure nuclear matter, full baryon octet (both are constructed by taking nuclear structure into consideration) and finally strange quark matter (which is based on the MIT bag model) at the core in β equilibrium. Various universalities have been predicted among the neutron star properties such as dimensionless quadrupole moment vs compactness, dimensionless moment of inertia vs M/R, dimensionless moment of inertia vs dimensionless quadrupole moment and dimensionless moment of inertia vs dimensionless tidal deformability. The significance of the low energy density region and crust is also shown.

Declaration

I certify that this work contains no material which has been accepted for the award of any other degree or diploma in my name, in any university or other tertiary institution and, to the best of my knowledge and belief, contains no material previously published or written by another person, except where due reference has been made in the text. In addition, I certify that no part of this work will, in the future, be used in a submission in my name, for any other degree or diploma in any university or other tertiary institution without the prior approval of the University of Adelaide and where applicable, any partner institution responsible for the joint-award of this degree.

I give permission for the digital version of my thesis to be made available on the web, via the University's digital research repository, the Library Search and also through web search engines, unless permission has been granted by the University to restrict access for a period of time.

I acknowledge the support I have received for my research through the provision of an Adelaide Scholarship International.

Acknowledgment

This thesis is supported by Adelaide Scholarship International, without the aid this study could not have been possible.

I would like to thank my family for their support, particularly Saba for believing in me and my friends Anthony Kalaitzis and Zeno Kordov for his valuable corrections. I would like to thank my co-supervisor Prof. Derek Leinweber for his valuable advices and suggestions. At last but not the least, I would love to thank my guardian angel, Prof. Anthony William Thomas who is like my father being here in the University of Adelaide for supporting me. It is my immense pleasure toworkwithhimwithouthimIcouldnothavecompletedmyresearch.

Wasif Husain

1 Introduction

Neutron stars are special stars. Unlike the ordinary stars, they are extremely compact objects that are much tinier, amongst the fastest spinning and some of the largest order of magnetic field, in Universe. Neutron stars come into being when an ordinary star dies. They are created after the death of a star in a supernova remnant. They are the densest (excluding black hole) and the most neutron rich objects found in the Universe. Typically, all neutron stars that have been found, have mass from 1 to 2 solar masses. When an ordinary star of mass, 8 - 25 solar masses [1] runs out of its fuel (nuclear fusion), i.e runs out of possibilities to counter itself against gravitational collapse, it can no longer sustain itself and collapses under its own gravitational pull. At this point, first the inner core of the progenitor star collapses and releases a ripple of very high energy to the outer layers and blows them away into the Universe, as a type-II, Ib or Ic supernova explosion.

What is left after the explosion depends upon the mass of the progenitor star. If the mass of the progenitor star is less than 8 solar masses, the explosion results in a white dwarf and if the mass of the progenitor star is greater than 25 solar masses, the explosion results in a black hole. In 8-25 solar mass range of the progenitor star, after the explosion a very small, sometimes called microscopic, super dense and hot star is left, that is a neutron star. The star is named a neutron star because it is made of neutrons mostly.

It has been a big challenge among physicists to determine the properties of matter under the extreme conditions of pressure and energy density and understand the strong force. For determining the properties of compact stars and various other astrophysics phenomena, it is essential to know the relation between the pressure and energy density of the system, i.e its equation of state [2][3]. But, at such extreme conditions of energy density, the laws of physics which govern them, are not properly discovered yet. Luckily, The Universe has blessed us with

compact objects in form of white dwarfs and neutron stars which serve as astrophysical laboratories [4] for understanding and testing our knowledge under extreme conditions. They are the objects that pair the strong force with the general theory of relativity.

The study of neutron stars requires expertise from several different fields : particularly, hadron physics, general theory of relativity, high-energy physics, nuclear physics and quantum-chromodynamics. Various attempts have been made and significant advances in the understanding of neutron stars have been achieved. Large advances have also been made in the observational data of neutron stars.

1.1 Historical Background

After the discovery of the neutron [5], in 1934 Baade and Zwicky [6] proposed the idea of a neutron star and suggested that these stars would have enormous central density and a very small size. They also suggested that these kinds of stars could be created in supernova explosions. Neutrons stars are some of the densest objects of universe after black holes. Due to their enormous gravitational pull, neutron stars compress their matter to several times the density of atomic nuclei, which makes them ideal for discovering new physics.

In 1935, Tolmann [7] and independently Oppenheimer and Volkoff [8] calculated the structural equations of a neutron star, assuming that the core of the star is made of an ideal gas of free neutrons at very high density. In their calculation, Oppenheimer and Volkoff calculated that stable, static neutron stars could not be heavier than 0.7 times the mass of the Sun, which is a value much smaller than the Chandrasekhar mass limit of white dwarfs : 1.44 solar mass. This low value of the mass predicted for neutron stars was the result of the fact that the neutrons were considered to be non-interacting. In the 1950s Wheeler [9] calculated the equation of state of a non-interacting neutron-proton-electron gas under β-equilibrium. In 1959, a Skyrme-type [10] force was considered by Cameran [11] to study the

effects of the nucleon-nucleon interaction on equation of state (EoS). He calculated a maximum mass of neutron stars, of around 2 solar masses, which was a clear indication that there could be other particles like muons and hyperons, in the core rather than just electrons-protons-neutrons. Many authors have suggested the possibility of pion and kaon condensation inside the core of neutron stars. After the proposal of the quark model by Gell-Mann [12], Ivanenko and Kurdgelaidze [13][14] proposed the possibility of quark deconfinement in the core.

Although the existence of neutron stars had been theoretically suggested, the possibility was ignored for almost 3 decades due to their tiny size. In 1967 first radio Pulsar PSR B1919+21 was discovered by Bell and Hewish [15] with a frequency of 82MHz and a rotation period of 1.4sec. At that time, pulsars were not identified as neutron stars, but later Gold [16] showed that pulsars are indeed rotating neutron stars.

1.2 Pulsars

Rapidly rotating neutron stars are generally accepted as *Pulsars*[17][18][19][20], which have a very regular periodicity. Neutron stars have high magnetic fields and spin, so they radiate energy. Magnetic poles of pulsars are not aligned to their axis of spin. So, when a pulsar rotates, its radiation sweeps and their radiation is only observed if an observer is in its line-of-sight, which is why their radiation has a pulsating nature, detected as turning on and off, therefore they are named after the phenomenon : pulsars. Sometimes they are also referred to as 'light houses of the Universe'. Most of the pulsar's radiation falls into the radio region of the electromagnetic spectrum but there are a few pulsars that have radiation in the optical, X-ray and gamma regions.

The first radio pulsar was detected in 1967 by Jocelyn Bell [21][22]. PSR J1748-2446ad is the fastest spinning pulsar, discovered to date with the frequency of 716Hz, by Jason W. T. Hessels [23] of McGill University on November 10,

2004 and was later confirmed on January 8, 2005. Over 2000 pulsars have been detected and some commonly known pulsars are Crab, Vela, PSR 1937+21 and PSR 1957+20. There are some rotating neutron stars which are called magnetars because they have magnetic fields of the highest order, billions of times the magnetic field of the Earth. Pulsars can be categorized on the basis of the order of the magnitude of the magnetic fields they have. Some of the prominent kind of pulsars are described as follows.

1.2.1 Ordinary Pulsars

These pulsars are unaccompanied pulsars that have rotational periods from a few milliseconds to few seconds. They have magnetic fields, typically $B = 10^{11} - 10^{13}G$ and age, typically from $t_{PSR} = 10^5$ to 10^8 years [24]. The X-ray spectrum of thermal emission from normal pulsars has been estimated, which permits the cooling theory to be applicable to their study. Unlike the neutron stars case, lacking pulsation, the measurement of t_{PSR} and magnetic field make the class of thermal structure models certain and therefore prevent the scattering of possible cooling curves.

1.2.2 Millisecond Pulsars

Millisecond pulsars have magnetic fields lower than ordinary pulsars, B = 10^8 to $10^{10}G$, and age of a few million years to several billion years t_{PSR} = 10^9 to 10^{10} years [24]. These pulsars, which have relatively lower magnetic fields may have undergone accretion processes during their evolution, which induced a magnetic field and increased their angular momentum by interaction with accreted matter with magnetic fields, details can be found in [25][26]. Some millisecond pulsars radiating X-rays display thermal component in their spectral yield by emission from hot polar caps [27].

1.2.3 Anomalous Pulsars

Anomalous pulsars are young, isolated and highly magnetized neutron stars. They have magnetic fields B = 10^{13}-$10^{15}G$. Due to their large magnetic fields, they are widely referred to as magnetars. They have luminosity 10^{33}-10^{35} ergs/sec and long periods of 6 - 12 sec [28,29]. A possible explanation for their properties is grounded on the assumption that neutron stars of magnetic field $10^{12}G$ acquire matter from the accretion disk left after the supernova explosion [30].

1.3 Neutron star binary system

A neutron star binary is a system that has a neutron star coupled with another compact star like neutron star, white dwarf or ordinary star. A binary system with a black hole is still to be detected. Determinations of parameters of binary systems give additional information about neutron stars, particularly about their mass.

As the matter of the accompanied object falls into the neutron star, radiation of energy takes place, which makes the system a source of X-ray radiation. For the purpose of study, these systems can be divided into two classes of systems. First, low-mass X-ray binary systems - systems in which a neutron star is accompanied by a low mass object ($M < M_{\odot}$), it could be white dwarf, red giant or neutron star. Second, there are relatively short lived massive systems. In these systems, the accompanying object has mass tens of times the mass of the Sun ($M > 10M_{\odot}$) and the accretion of mass by a neutron star in these systems is extremely intense.

X-ray binaries serve up periodic as well as irregular radiation, and can be categorized in two sub classes as permanent and temporary. Rotation of neutron stars enhances the radiation of some systems but others are channeled by quasi periodic oscillations (QPO), and burst (neutron stars suffer from thermonuclear explosions, burning accreted mass).

QPO was discovered in 1985 [31] and takes place in low mass X-ray binaries that have a neutron star, white dwarf or black hole [32][33][34]. They are likely

to originate in the accretion disk. Some hypotheses have suggested that they are associated with the Kepler frequency. If these hypotheses are believed to be true, QPO in low-mass X-ray binaries systems can serve as a tool to measure parameters of neutron stars.

The X-ray luminosity of bursts can go up to the Eddington limit ($L = 1.3 \times 10^{38}(M/M_{\odot})$) erg/sec. At such high luminosity, radiation pressure on plasma due to Thomson scattering takes over the gravitational force. Flashes of such high luminosity are of particular interest because their spectra and intensity allow us to calculate parameters of neutron stars [35][36].

During quiescent periods the spectra of certain soft X-ray transients show thermal radiation components of neutron stars located in the system. This permits curves that explain the cooling process to be compared with observations, as in the case of a single neutron star, with the only difference that energy emitted by accretion must be taken into account.

Quasi permanent transients (those which are active and inactive for years) are of special interest. In a model [37], thermal radiation in the quiescence is suggested, due to cooling of the crust after a long period of deep heating due to accretion. Such cooling is independent of the structure and matter composition of neutron stars, but its analysis gives information regarding the physics of different regions (envelopes). KS 1731-260, MXB 1659-29 and AXJ175.2-2754 [38] are sources of this kind. Analysis of luminosity of such objects and its dependence on time provides information regarding the heat capacity and thermal conductivity of the crust [38n].

Calculating mass of neutron stars by Kepler parameters in X-ray binary systems is not a very reliable method because of theoretical uncertainties, such as the shift of angular momentum due to accretion. The most exact values are obtained for the binary systems of two neutron stars, in the absence of accretion. Several accurate mass measurements are available in the literature with errors $< 0.2M_{\odot}$ for several binary systems. These measurements range from 1.1 $M_{\odot}$ to 1.7 $M_{\odot}$.

1.4 Source for super-dense matter

Neutron stars have very thin atmospheres, but not so thin crusts (a few kilometers thick). For bulk compact stars most of the mass of a neutron star is contained in its highly compressed core. In comparison with the core, the crust mass is very small and can be ignored since it does not play a significant role in determining most of their properties apart from determining radius which highly depends on crust. Bulk stellar properties like mass and moment of inertia, depend only on the core [39][40]. For this reason, the highly dense part (i.e the core) plays a significant role in determining the properties of heavier neutron stars of over one solar mass. The equation of state (EoS) of neutron star matter up to a few times the nuclear saturation density [41][42][43] is not well known, but at nuclear drip density and below, it is well known [44][45][46]. Physical properties of matter at such high density, known as the super-nuclear regime, differ with the equation of state used, some hypotheses suggest hyperons (Σ, Λ, Ξ) along with neutrons and protons, some suggest deconfined quark matter and strange quarks. So the actual physics or equation of state of a neutron star is poorly known. All derived models (EoS) largely depend on what techniques are used in solving many body problem, which model is used to define the nucleon-nucleon interaction, how electric charge neutrality is defined in β equilibrium, how kaon and pion condensation is treated and possible phase transitions from confined hadronic matter to deconfined quark matter.

The nuclear equation of state of a neutron star is quite different from the equation of state (EoS) of nuclear matter. Normal nuclei are approximately isospin symmetric and bound together by the strong force. Whereas, in neutron stars, nuclear matter is highly isospin-asymmetric and is not bound by the strong force but the gravitational force alone. Strange stars are hypothesized to be self-bound by confinement [47][48][49] and gravity just increases their density a little bit. Another feature of a neutron star that must be acknowledged is that the origin of neutron star matter violates conservation of strangeness by the weak interac-

tion, this gives a significant amount of net strangeness to the neutron stars which is either contained in hyperons [50][51][52][53][54][55][56][57] or exists in the form of strange quark matter that coexists with hyperons in chemical equilibrium [58][59][60][61].

There have been many attempts made, based on different hypotheses to determine nuclear matter properties at higher densities and model neutron stars Glendenning is recognized among the first people who used modern theories and techniques (available that time) to determine the EoS for superdense matter. He began by using all baryon states that may be populated in the superdense medium, constructed the relativistic Lagrangian and derived the equation of motion using the relativistic Hartree approximation. Of course, his work had limitations (still good enough to set up a direction) for example π contribution and the tensor coupling of the ρ meson, were not included and the incompressibility of nuclear matter does not achieve agreement with large σ meson self-interactions. Some drawbacks of the model have been removed by using the Hartree-Fock approximation, like the π meson contributions are included in the exchange term, the ρ meson tensor coupling is included and smaller incompressibility is included.

At high densities, above nuclear density, matter may undergo phase transitions and new exotic states may form. The existence of these states relies on the strong interaction and the structure of baryons.

1.4.1 Meson condensation

In 1960 [62] it was suggested that the core of neutron stars may have mesons (pions-the lightest meson). Generally, the Bose condensation of pions in nuclear matter is hindered by repulsive forces between nucleons. However, in a superdense medium, collective excitations (pion like quasi-particles) may take place [63][64][65][66] and condense, with loss of transition invariance. Some studies have displayed the significance of correlations among nucleons for the possibility of creating a new phase of pion condensation, and possible creation of ordered

structure with pion condensation.

Kaons may appear in the core by the processes

$$e + N \rightarrow K^- + N + \nu_e \quad ,$$

and

$$n + N \rightarrow p + K^- + N \quad ,$$

where N represents a nucleon and their presence in the process ensures conservation of energy and momentum in a highly dense medium. In 1980 [67] the possibility of Bose condensation of Kaons at densities above three times nuclear matter density was explained. Since then it has been addressed by many authors, see for instance Ref. [68].

In neutron stars the Bose condensation process is possible by involving K^- mesons instead of neutral-K mesons because of their smaller mass. A theoretical approach to explain the process is suggested in [69] on the basis of strong interactions. Formation of K condensation highly depends on the presence of hyperons and greatly affects nuclear matter properties. The strength of attractive forces between kaons and nucleons is the main cause behind the first and second order phase transition and the presence of either of the above mentioned condensations makes the EoS softer (not so compact at the core).

1.4.2 Quark deconfinement

Hadrons are made of quarks, whose degrees of freedom may play a significant role in determining properties of nuclear matter at high density. Single quarks can't be observed in a free state in low energy density regimes, they are always bound together with other quarks, called quark confinement and their binding force grows at low energy density [70]. But as the energy density increases, baryons may decompose into their constituent quarks. Invanenko and Kurdgelaidze [71] in 1965 showed that neutron stars core may be made of deconfined quark matter. With the development of quantum chromodynamics (QCD), non-interacting quark matter properties were calculated with the help of perturbation theory but such calcu-

lations [72][73] were limited to energy density $>> 1GeV/fm^3$, and it is very unlikely for a particle's chemical potential to reach that value in a neutron star core. Later, more models were suggested to explore compact stars. In [74], series of phase transitions were shown in neutron star interiors at different energy densities.

All current existing neutron star models have drawbacks. Quark and baryon phase transition models lack self-consistency, which is paramount and calculations are done with the use of perturbation theory at relatively low energy densities, at which they predict phase transitions, are unrealistic. For these reasons, the existence of a deconfined or free quark core in a neutron star is highly unlikely.

1.4.3 Existence of mixed phases

This can be realized as a co-existence of two different phases in the form of droplets. Since 1990, such phase transitions have been considered by many authors [75][76] to explain compact stars . Co-existence of two different phases, is possible by the virtue of the implicit assumption of electro-neutrality in phases. Electric charge of one transition phase is counterbalanced by the other coexisting transition phase and the structure of matter is calculated by balancing surface tension (at the edge between droplets), energy density, kinetic energy of ingredient particles and electrostatic energy. Mixed phases are more convenient for both quark matter and meson condensation.

1.4.4 Crystallization in the core

Initially, it was assumed that the strong nucleon-nucleon short range repulsive force may lead to a solid inner core of neutron stars [77][78]. But later in 1970's, it was realized that the nucleon-nucleon interaction is generated only by the exchange of vector mesons and the more accurate calculations were performed and it was realized that effect potential of neutron-neutron do not crystallize the core.

However, another possibility of crystallization was suggested [79] as the tensor component of a mid-range nucleon-nucleon interaction [80], but it was countered by reference [81], which suggests that tensor interactions lead to structures which have neutrons pinned in a plane with opposite orientation of spins and each such plane serve oppositely oriented protons and neutrons spins (called alternating spin - ALS). If the increment in binding energy, during the formation of these structure (ALS) exceeds the loss in kinetic energy of the particles, then the structure may become energetically feasible for phase transition in this state.

In other words, there are numerous models based on different hypotheses, explaining composition and structure of the core of neutron stars, differing in the details of microscopic interactions and none of them is fully accepted.

2 Puzzling Characteristics of Rotating Neutron Stars

Up to now, over 2000 rotating neutron stars have been discovered in the Universe and they posses remarkable characteristics. Some of the important properties of these stars are given below.

2.1 Mass

Since the discovery of neutron stars, it has been a puzzle to answer how massive a neutron star can be. Unlike black holes, neutron stars can't have arbitrary mass because there is no physical force, excluding neutron degeneracy pressure, to counter the gravitational collapse. Most of the neutron stars found in the Universe have masses around 1.4 $M_{\odot}$, but Ter 5I and Ter 5J [82], M5B [83], PSR J1903+0327 [84], and PSR J0437-4715 [85] all have masses of about 1.7 $M_{\odot}$ with 95$\%$, confidence limit. While the recent discovery of pulsar PSR J0348+0432 surprised the astronomical community with the mass of 2.01 solar masses. The upper limit of mass that a neutron star can have is not known, but PSR J0348+0432 sets up a maximum mass constraint of at least 2 solar masses. A successful Equation of state (EoS) must satisfy this value and predict a maximum mass of 2 solar masses, at least. Determination of the gravitational mass is of great importance because it combines gravity with nuclear theory and gives us a chance to understand and test our knowledge at higher densities. The mass of a neutron star is determined by the mass function which is a function of five Keplerian parameters : binary period P_b, eccentricity, projection of the neutrons star's orbital semi-major axis on the line of sight, $x = a_1 sin(i)$, where i represents inclination of the orbit and longitude of periaston(ω_0) and time(T_0). These parameters are related to the mass of a neutron star (M_p) and its partner star (M_c) by Kepler's third law [86][87][88]

$$f(M_p, M_c, i) = \frac{(M_c sin(i))^3}{(M_p + M_c)^2} = \frac{P_b v_1^3}{2\pi G}, \tag{1}$$

where v_1 given by $2\pi a_1 sin(i)/P_b$, is the projection of the neutron star's orbital velocity on its line of sight. The relativistic advance of periastron angle, ω, has also been measured, which helps the getting the value of the system's total mass. To get the mass of the individual star, the combined effect of the transverse Doppler shift and the gravitational redshift allow the measurement of each pulsar mass.

2.2 Spin -

Neutron stars rotate with a typical frequency of around 600-700Hz. This incredibly high rate of rotations can be understood by the law of conservation of angular momentum, because the initial a star has low spin and large radius as its radius reduces (10-15 kms) its spin must go up. The fastest spinning neutron star discovered till today is PSR J1748-2446ad, with frequency 716 Hz [89]. Neutron stars are born with high magnetic fields about the order of 10^{12-15} G, Because of the loss of energy/mass as electromagnetic radiation, their spin should come down significantly over a period of time. Common acceptance among physicists is that neutron stars get their high spin due to mass accretion from low density companions (e.g. white dwarfs), which increases their spin due to conservation of angular momentum of the system. This mass accretion could have happened right at the birth of the star or some time after in the stellar evolution.

When pulsars have lost enough energy they do not radiate much any longer (almost stop radiating). These are called quiet pulsars but at some point of time they could acquire mass by mass accretion and their spin goes up and they start radiating again they are called recycled pulsars. This phenomena describes that pulsars are old neutron stars which undergo mass accretion.

There is a claim of a neutron star having frequency 1122 Hz, observed from oscillations in x-ray bursts from XTE J1239-285 [90]. This is controversial because the observation has not been repeated and the signal could have errors due to the burst mechanism like burning material. The maximum frequency a neutron

star can have is called the Kepler frequency and it occurs at the mass-shedding limit. Frequencies of 716 Hz and 1122 Hz both impose a weak constraint on the EoS because both the values are well below the Kepler frequency.

2.3 Magnetic Field -

Because of their high magnetic fields, pulsars radiate waves of different wavelengths up to gamma rays. They are detected when the radiation is pointed towards Earth. They have magnetic fields of around 10^{12} Gauss at their surface. Neutron stars with magnetic fields higher than this are called magnetars. Such a high magnetic field is quite a strange property because neutron star matter is supposed to be neutral. The possibility of such magnetic fields has been addressed by many authors, yet the mystery is still not solved. One of the hypotheses is, assuming magnetic flux conservation, if the progenitor star has a magnetic field of 10-100 Gauss then after the explosion it may give rise to a magnetic field of 10^{12} Gauss in a newly born neutron star. One interesting idea is a possible transition to a ferromagnetic state in the liquid interior of the neutron star [91][92].

There is no consensus and solid theory that can define the origin of such a high magnetic field. If one could come up with an equation of state that can define the structure of a neutron star, then we might solve this problem. The magnetic field is also the matter of a great puzzle. Neutron star matter is supposed to be neutral because neutrons are charge-less particles and the left-over electrons and protons cling together, so it is not expected to have a charge distribution or magnetic field. Also, the magnetic field axis is not the same as the axis of rotation. It is tilted slightly and the reason for this is unknown. So, it becomes a point of research to understand the structure of neutron star by defining its equation of state.

2.4 Glitch -

In 1967, Pacini [93] showed that rapidly rotating neutron stars with strong dipole magnetic fields can transfer their rotational energy into electromagnetic radiation and can emit particles to a very high energy. Neutron stars, by losing their rotational energy steadily, decrease their frequency. Neutron stars show incredible accuracy (and consistency) in their rotational period, while the accuracy of their spin can be measured over years [94][95], yet there can be a small increment in their rotation frequency observed after a certain time that is called a glitch. Generally observed relative glitches ($\frac{\Delta\nu}{\nu}$) are between $10^{-11} - 10^{-5}$, followed by an increase in the spin down rate of the pulsar.

Many authors have tried to address the mechanism behind it [96]. There are no changes in observed radiation data in almost all pulsars associated with such events, suggesting its origin is internal. In this context, a rapid transfer of angular momentum from neutron super-fluid in the inner crust to the rest of the pulsar is often considered to be the cause of the glitch [97][98]. But, magnetars or high magnetic field pulsars like J1119-6127 and J1846-0258 sometimes exhibit changes in observation radiative data and could have a different origin [99] of the glitch. The reason for this is not known. The young pulsar PSR B1757-24 [100] shows a huge glitch of order 10^{-6} sec. Pulsar glitches of such high order are shown by only 7 pulsars out of 800 known ones.

There are some attempts made to use the glitch to inspect the interior of pulsars by putting constraints [101][102][103][104][105] on the EoS. Studies done on the rotations of the Crab and Vela pulsars suggest that effects of glitches over the long-term spin evolution are proportional to the effects powered by magnetic braking or stellar winds [106][107][108]. McKenna and Lyne [109][110] suggested that the glitch activity has a linear behavior with the spin-down rate. Later, Espinoza [111] confirmed that result and showed that the glitch activity decreases heavily in pulsars with low spin-down rate. They also suggested that young pulsars exhibit glitches more often than old ones.

2.5 Radius

Neutron stars are microscopic objects (relative to other astronomical objects) with radii ranging from 10 - 15 kms. Direct determination of their size is not possible due to their tiny size and large distance from the Earth, which is why it took more than 30 years to find one, after their prediction. One possible way of determining radius is by their thermal emission that is X-ray flux (F), temperature (T) and distance

$$r = \sqrt{\frac{FD^2}{\sigma T^2}}, \tag{2}$$

$$R = r\sqrt{1 - 2\frac{GM}{c^2 R}}, \tag{3}$$

where r is the effective radius, R is the radius of the neutron star, M is the mass, D is the distance and σ is the Stefan-Boltzmann constant. A major concern about measuring the radius is the uncertainty in temperature, which can mislead the value by a huge margin. Steiner's analysis suggested that the neutron star radius may range from 10.4 kms to 12.9 kms [112][113].

Yancoulos developed the technique of calculating radii by using gravitational lensing around pulsars [114]. With better instruments in the future, radius may be measured with 10% precision but if the temperature on the surface is not uniform then the value can deviate by up to 50%.

2.6 Moment of Inertia

The moments of inertia of neutron stars span a range of order of 10^{43} to $10^{45} gm.cm^2$, depending on the stiffness of the core and based on the calculations done on the energy lost from neutron stars [115]. Most authors calculated the moment of inertia of the Crab pulsar, based on luminosity, as ranging from 4x$10^{44} gm.cm^2$ to 8x$10^{44} gm.cm^2$ [116][117][118]. But, in the double pulsar PSR J0737-3039 the moment of inertia of pulsar A may be determined with an accuracy of 10% in the

immediate coming years [119] by measuring the increment of the system's periastron, and conclusions from some EoSs have been drawn in [119][120][121]. By getting relatively accurate values of both the moment of inertia and mass of the same star together one can put a stronger constraint on determining the radius of the neutron star. Recently, during a thermonuclear burst of two low mass X-ray binaries the mass and radius was estimated, M = 1.4$M_{\odot}$and R = 11 km or M = 1.7 $M_{\odot}$and R = 9 km for EXO 1745-248 [122] and M = 1.8 $M_{\odot}$ and R = 10 km for 4U 1608-52 [123]. Both radii were estimated to have deviations of 1 Km. These measurements more depend on models rather than the actual measurement of the moment of inertia of PSR J0737-6069A. However the precision of the measurement of the moment of inertia remains to be determined.

2.7 Surface Temperature

Analysis of the photons emitted by the neutron stars is useful to determine their temperature. Neutron star spectra are treated as being of a blackbody type, although they are not a blackbody because they have some elements (Hydrogen, Helium etc) present in their atmosphere. However, their spectra can be modified due to the presence of strong magnetic fields at their surface. The effective surface is temperature reduced when realistic atmosphere models are considered to fit the measured spectra. The point must be noted, comparing to observational data, that temperature is not useful but luminosity (L) is, because luminosity is proportional to the fourth power of temperature and any uncertainty in temperature will create a huge difference in luminosity.

$$L = 4\pi R^2 \sigma T^4, \tag{4}$$

where σ is the Stefan-Boltzmann constant and R is the observational distance.

2.8 Gravitational redshift -

The gravitational redshift at the surface is a useful measure to determine the structure of a neutron star. Calculation of the red shift is done by the determination of a ratio of frequencies in terms of the mass and radius of the neutron star. When a photon leaves the neutron star from its surface, the frequency (v_{E}) of the photon from the neutron star, i.e emitter, is inversely proportional to the proper time between two consecutive troughs or crusts. The same expression holds true for the receiver as well which is located at infinity (v_{inf})

$$\frac{v_E}{v_{inf}} = \sqrt{1 - \frac{2GM}{c^2 R}}, \tag{5}$$

$$z = \sqrt{1 - \frac{2GM}{c^2 R}} - 1. \tag{6}$$

The determination of the redshift is used to get the M/R ratio [124], which is useful to determine the structure of the star.

Cottam, Paerels, and Mendez [125] claimed that they have observed a gravitational redshift of z = 0.35 in spectral lines from EXO 0748-676. There is also a claim made with a 95$\%$ confidence interval, for measuring the mass-radius of the system using Eddington-limited photospheric expansion x-ray bursts [126] which rules out many EOSs. This claim invites controversies, because the 95$\%$ confidence interval is big enough to rule out much of the parameter space and it is believed that the potential for systematic error is understated. However, the gravitational redshift is consistent in both the claims, which is z = 0.35. Thus we treat z = 0.35 as a tentative constraint. The current NICER mission aims to exploit this to determine the radius with an accuracy of order 5 $\%$.

2.9 Neutron Star Cooling

Newly born neutron stars are extremely hot objects with internal temperature of the order of $10^{11} K$ and they cool down very fast by the neutrino emission process

from the interior region and photon radiation from the surface. The neutrino emission process and cooling rate both depend on number on the baryons participating in the emission process. The direct Urca process is the simplest possible neutrino emission process and it is very fast due to conservation of momentum.

$$n \rightarrow p + l + \overline{\nu}_l \, , \, p + l \rightarrow n + \nu_l \quad .$$

This process is possible when the fraction of protons exceeds a critical limit, x_{DURCA}, between 11-15$\%$ [127]. There are other processes which lead to slow cooling of neutron stars and are active at any density and any proton fraction. These processes are called modified Urca processes.

$$N + n \rightarrow N + p + l + \overline{\nu}_l \, , \, N + p + l \rightarrow N + n + \nu_l \quad .$$

There are other possible processes, bremsstrahlung and Cooper pair formation are possible, depending on the number of baryons taking part in the process. The Bremsstrahlung process is given by

$$N + N \rightarrow N + N + \nu + \overline{\nu} \quad ,$$

while the Cooper pair formation process is possible when the temperature of neutron stars goes below a critical temperature.

$$n + n \rightarrow [nn] + \nu + \overline{\nu} \, , \, p + p \rightarrow + \nu + \overline{\nu}$$

If hyperons are present in the core that may lead to extra cooling mechanisms which lead to neutron star temperatures below what has been observed. Therefore, for understanding the cooling process, hyperon super-fluidity [128][129][130][131] [132][133][134] becomes a point of interest because it may have a role in neutron star thermodynamics.

2.10 Gravitational waves and neutron star binary

Gravitational waves are one of the many predictions of Einsteins' general theory of gravity, which suggest that gravitational waves are nothing but the ripples in the fabric of spacetime, which propagates with the speed of light. For understanding it, one can naively compare it with the waves of water in the ocean but grav-

itational waves require an ideal smooth and unperturbed background, in which gravitational waves propagate. Unlike the water waves, gravitational waves are not the motion of material of medium but the ripple in the fabric of spacetime itself.

Gravitational waves generate from the oscillations of neutron stars (also by black holes and white dwarfs). And carry an important information regarding internal structure of the compact star and the gravitational wave signals can be affected by the deformational effects like tides and rotations. On August 17, 2017 Advanced LIGO and Advanced VIRGO observed the first gravitational wave (event known as GW170817) from the merger of a neutron star binary [135]. This pioneering work has begun a new era in the search for the EoS by imposing new a constraint.

The orbital motion of the neutron star binary generates gravitational waves that can carry out energy and momentum of the system. As the radius of the orbital decreases the spin of the binary system increases. Initially, in a binary system, two neutron stars are separated by a large distance and their orbital frequencies are low. At this point both the neutron stars behave like a point mass and the frequency of the system is determined by the chirp mass M, given by

$$M = \frac{(m_1 \times m_2)^{3/5}}{(m_1+m_2)^{-1/5}},$$

where m_1 and m_2 are the masses of both the neutron stars, respectively. As the orbital radius reduces the relativistic effects become highly relevant and when the orbital radius reduces to approximately the size of the neutron star, the internal structure of the neutron star becomes very significant and the gravitational waves generated at this point contain valuable information about the (internal) matter of neutron stars. The tidal field of one the neutron star develops a mass-quadrupole moment on the other and vice versa. The ratio of induced quadrupole moment and the external tidal field is proportional to tidal deformability. The tidal deformability is also determined by the tidal love number which depends on the EoS.

$$\Lambda = -Q_{ij}/\epsilon_{ij},$$

where Q_{ij} is the star's induced quadrupole momentum and ϵ_{ij} is the external tidal field.

$$\Lambda = \frac{2}{3} K_2 (\frac{c^2 R}{GM})^5 \ ,$$

where Λ is called tidal deformability, K_2 is the second order tidal love number, M is the mass of the neutron star and R represents the radius of the neutron star.

2.11 Different Density Regions Inside Neutron Stars

Neutron stars generally have mass in the range 1-2 solar masses and radii of 10-15 kms. Their average density is 10^{14}gm/cm^3. They have onion like structure divided into two parts, crust and core and both crust and core are divided into two sub parts, inner crust and outer crust, and inner core $\&$ outer core. Most of the mass of a neutron star is contained in the core. The most external part of the star is called the atmosphere, where the thermal spectrum is generated. Atmosphere is typically a few centimeters to a few millimeters thick, depending on the temperature of the neutron star (Fig. 1).

2.11.1 Atmosphere

This region is only a few millimeters thick layer which is made of plasma. In this layer electromagnetic radiation spectrum is formed, which possesses an important information regarding the surface temperature, magnetic fields, mass, radius and chemical composition of the matter. Thickness of this layer could vary up to tens of centimeters for hot neutron stars ($T > 10^{6.5} K$). For cold neutron stars with high magnetic fields, one could have solid or liquid condensed surface, depending on the gravity, temperature, magnetic field and the chemical composition. The density of this layer may vary from 10^{-4} to $10^{6} gm/cm^3$. The atmosphere contains atoms, molecules and ions which change the observed electromagnetic spectrum.

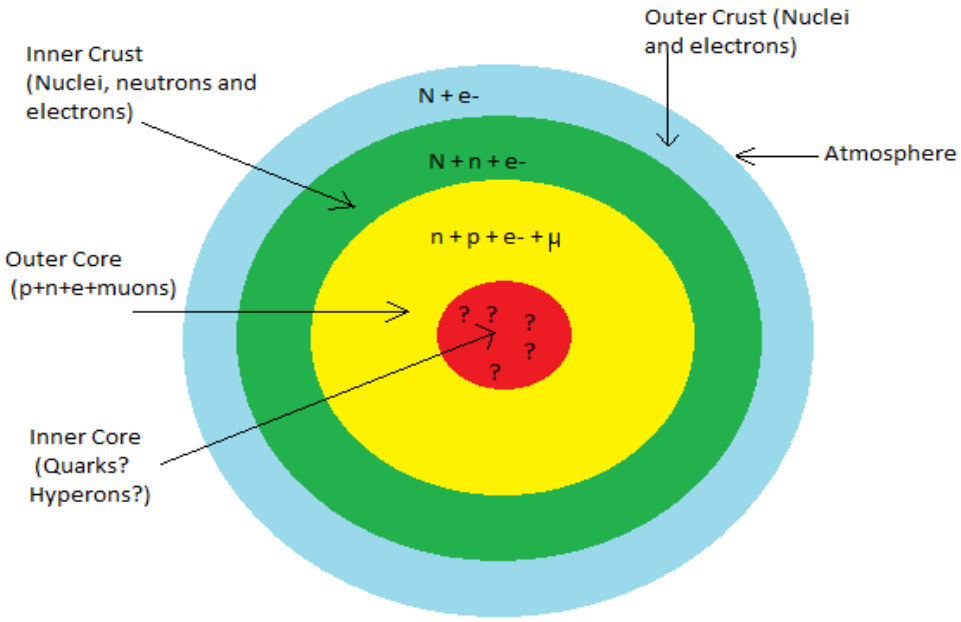

Figure 1: Different density region inside the neutron star and the core is a matter of speculation

The atmosphere has been studied by many authors for decades but still it is not fully understood. Magnetic fields of order 10^{12} - $10^{14}G$ with temperature, approximately $10^{5.5}K$, for the hydrogen atmosphere is explained in Refs. [136][137]. There are models available [138] for partially ionized atmosphere having carbon, oxygen & nitrogen for magnetic field strength 10^{12} - 10^{14} and temperature $10^{5.5}$ - $10^{6.5}K$.

2.11.2 Outer crust

The outer crust extends to a few hundred meters and is typically made of heavy nuclei, with a strongly degenerate relativistic electron gas. It has a density of order $10^6\ gm/cm^3$ to $10^{11}gm/cm^3$. When the density reaches the value of the drip density, neutrons start to drip out of the nucleus. Available models show that neutron

star matter, at the surface is made of ordinary atomic nuclei that are squeezed into an solid lattice with a ocean of electrons moving through the gaps between them. Because of the lesser quantum states available for neutrons than electrons, neutron degeneracy pressure is more than electron degeneracy pressure. Also nuclear forces between the closely packed neutrons cause quantum waves and force neutrons to move along lines that have minimum repulsive nuclear forces [139]. The neutrons behave as a super-fluid (a state where all particles move without resistance and viscosity) and their quantum properties prevail. It is suggested that due to iron's high binding energy per nucleon, the nuclei at the surface of neutron stars are iron. It is also suggested that heavy elements, like iron, simply sit under the surface and leave only light nuclei, such as helium and hydrogen. If the surface temperature is more than $10^6 K$ (for a newly born pulsar), the surface is suggested to be fluid instead of the solid, as observed in cooler neutron stars (temperature $< 10^6$ K) [140][141]. This region is very interesting for solid state physics due to the extreme conditions of density, temperature and magnetic field, which are unlikely to be created in the laboratory [142].

2.11.3 Inner crust

The inner crust region is typically 1-2 kilometers thick with a density of 4×10^{11} gm/cm^3 to half the nuclear saturation density ($0.5\rho_0$). At such high density the neutron drip process takes place. Nuclear chemical equilibrium in terms of beta-capture and beta decay in this layer produces matter of composition (neutron rich nuclei, free neutrons and free electrons coupled in an s-wave form super-fluid [143]) that can't be produced in laboratory. Due to a constant contest between Coulomb and nuclear force, nuclei lose their spherical structure to form exotic structures such as rods, tubes etc and give rise to 'nuclear pasta' phase. The properties of nuclei in the inner crust matter are expected to be very different from those of terrestrial nuclei because their properties are influenced by the gas of dripped neutrons. Hence, the EoS of the inner crust matter is still theoretical

model dependent. The physics of this region is very well explained in [144].

Degenerate neutrons in this region create neutron degeneracy pressure. However, their heat capacity may be decreased by super fluidity, resulting in a decisive contribution of atomic nuclei to the thermal capacity of this region. Nuclei in this layer make up a crystal lattice by Coulomb forces. A possible explanation can be given by considering collective vibrational excitations. Electrons are relativistic and highly degenerate particles. So, they do not contribute to the heat capacity of the inner crust (provided that temperature is not very low). However, if the temperature has gone below the Debye temperature for the crystal, it may contribute significantly [145].

Electrons are the main electric conductors in the inner crust and their scattering process plays a significant role. Atomic nuclei embedded into crystal lattice add no significant conductance. Phonons in the inner crust may become the main agent of heat transfer in the presence of lattice defects or admixture [146]. Neutrons, particularly super-fluid ones, may behave as conductors as well [147]. In this region the spherical shape of the nuclei is expected to be dismantled by the coulomb force and nuclear forces and make up new shapes of droplets : rods, tube etc. But evidence of this has still not been found.

2.11.4 Outer core

This region is several kilometers thick and made of electrons, protons and neutrons with density of order 10^{14} gm/cm^3. This region is a quantum fluid, made up of p-wave super fluid neutrons with a very small amount of s-wave super fluid. As soon as the chemical potential of the muon is equal to the chemical potential of the electron, muons start to appear. For a low mass neutron star the outer core is the entire core, as the density does not change much as one moves towards the center.

2.11.5 Inner core -

This is the most dense region of neutron stars. The composition of this region is only a matter of speculation. Different hypotheses have different views, including hyperons, pions, kaons and quark matter. The possibility of additional degrees of freedom in the core, also called exotic, is the direct consequence of the fact that stars lower their energy with appearance of hyperons or quarks in the inner core. Quark deconfinement and presence of hyperons are one of the most interesting hypotheses that connects neutron stars with Quantum Chromodynamics.

However, some authors have speculated about the appearance of strange compact stars which are unlike the compact stars described in the above paragraph. They are thought to be 'strange stars' because of having the possibility of having a mixture of deconfined up, down, and strange quarks in their cores which is the result of the Bodmer-Witten-Terezawa hypothesis [148][149][150][151][152][153][154].

3 Modeling of neutron stars

Neutron stars are laboratories for theoretical physicists to test their knowledge and hypotheses at extreme energy density and pressure, which is unlikely to be created in a physics laboratory [142]. Modeling neutron stars requires two major theories that are, theory that describes matter properties at extreme energy density (Equation of state) and structural equations. When modeling a neutron star, one of the first questions that arises is, how does matter behave at extreme energy density?

It is a challenging question among nuclear physicists whether the nuclear structure plays an important role in describing the nuclear properties of matter or not. How does the strong interaction work? How would the particles behave if the nuclear density goes up to several times normal nuclear matter density? How and why are quarks in the nucleon confined? What are neutron stars, black holes and other highly dense objects made of? What sustains them against collapsing due to gravity? To answer these burning questions one has to understand the strong interactions that govern the EoS of the dense matter. If one could understand this, it would be a step forward in understanding various physical phenomena.

To understand nucleon structure, Guichon proposed an effective model which is known as quark-meson coupling model (QMC) [153], based on the MIT bag model. It suggested a new kind of saturation mechanism for nuclear matter at the quark level. Since then major enhancements have been made in the model. In 2007, J. Rikovska Stone, P.A.M. Guichon, H.H. Matevosyan and A.W. Thomas [154] suggested a methodology based on the QMC model to calculate the EoS of cold steller matter in β equilibrium for a non-rotating neutron star. In this thesis, a comprehensive comparative study of nucleons only based EoS, i.e N-QMC700, full octet baryon matter based EoS, i.e F-QMC700 and strange matter based EoS using the MIT bag model (Chodos et al. 1974), will be shown for rotating neutron stars. There are observational data available which impose a great degree

of constraint on the EoS. A good equation of state should explain physics within the constraints imposed by observations. There are some strict constraints given below:

(i) Till now over hundreds of neutron stars have been discovered and all of them have radii in the range 10-15 Km. So a good equation of state must predict the radius in this range.

(ii) Most of the neutron stars have mass approximately 1.4 times the mass of the Sun, but recently discovered neutron stars PSR J1614-2230 [155] and PSR J0348+0432 [156] have masses 1.928 and 2.01 solar masses, respectively. So, a good equation of state must predict a maximum mass of at least 2.01 solar masses.

(iii) The moment of inertia is more sensitive to EoS rather than the radius. James M. Lattimer and Bernard F. Schultz [157] showed the values of moment of inertia up to an accuracy of 10%. That leads to an accurate value of radius and pressure. Moment of inertia a serious constraint. Calculated values must follow Lattimer and Schultz work.

(iv) At high energy density, as neutron stars become stiffer their Kerr metric solution should move towards the Kerr solution of a black hole.

(v) Eccentricity and the quadrupole moment should be consistent with the rotation of the neutron star.

(vi) The tidal deformability and the Love number should be consistent [158][159] [160][161] with the empirical analysis [162][163] made on data collected from gravitational wave detection by LIGO and VERGO observatories.

There are other observables like spin, Kepler period, angular momentum, compactness and rotational deformation, but these observables do not impose a serious constraint on the EoS because they cover a wide range of values. But, to calculate all these observables, not only is an EoS required but we also require structural equations based on Einstein's general relativity framework. For that purpose Hartle [164] developed a very impressive and effective methodology to calculate the structural equations for slowly rotating compact stars, taking general relativity

into consideration. The method is a kind of extension of the TOV equation, to which a rotational perturbation is added i.e. a deformation in the star's structure due to rotation and the amount of extra mass that a compact star can possess due to rotation.

By using this method, perturbation terms can be solved step by step in a constructive way. First, the TOV equations and rotational velocity differential equations are solved then the monopole (mass and pressure perturbation) equations based on rotation and finally the quadrupole equations (rotational deformation, i.e equatorial stretching and poles shrinking) can be solved. For the purpose of solving them only the TOV and rotational velocity differential equations are required.

The process can be summarize in the following steps.

(i) Supply the EoS to the TOV equation and integrate them from the center of the star towards the surface.

(ii) Integrate the rotational velocity differential equation based on the EoS (pressure and energy density function).

(iii) Integrate the monopole equations, i.e the mass and pressure perturbation differential equation, to get the extra mass and pressure that compact stars can have due to rotation.

(iv) Integrate the quadrupole equations, i.e the stretching of the radius at the equatorial plane and the contraction of the radius at the poles caused by rotation.

Like most authors, this study avoids working with rapidly rotating neutron stars near its Kepler frequency, because this method only work for slowly rotating stars. For fast rotating neutron stars, determination of the Kepler frequency for a particular star configuration imposes a self consistency condition on the equations derived for a spinning body. However this method works fine for the stars frequency where $R\Omega << c$, where R is the radius of the neutron star, Ω is the frequency and c is the speed of light.

4 Methodology

Many theories have been published to understand, whether or not the quark degree of freedom plays a significant role in nuclear structure? Different authors have predicted various hadron properties at finite nuclei density using relevant nuclear theory.

Here, for the purpose of discovering the role of quark degrees of freedom. We adopted the Quark-Meson Coupling model, which is based on MIT bag model. The results will be compared with the EoS [165] of strange stars which is also based on the MIT bag model.

4.1 Quark-meson coupling (QMC) model

Nuclear structure has been proven very significant in describing the properties of nuclear matter, and in determining the nuclear structure it is important to understand meson's and baryon's relevant degrees of freedom. Although quantum hadrodynamics (QHD) and the quark-meson coupling (QMC) model naively appear to be connected, unlike the QHD model where the structure of baryons is ignored and treated as a point like but in the QMC model baryons are treated as collections of three quarks based on the MIT bag model. The interactions between different bags are generated by exchanging mesons. Inside the bag quarks are confined as color singlet hadrons. At higher densities, where nucleons commence to overlap, their structure is expected to play an important role in determining their properties. A strict restriction on QMC is that quark bags do not overlap.

Guichon [166] proposed this model and suggested a new mechanism for nuclear saturation. Guichon took baryons as bags of quarks which are considered massless, coupled directly to exchange mesons, modifying the quark motion. This model has been successfully defied the doctrine of finite nuclei.

In [167], it is proven that it is feasible to derive a nuclear Hamiltonian consistent with relativity which could be used at high densities. Taking the findings

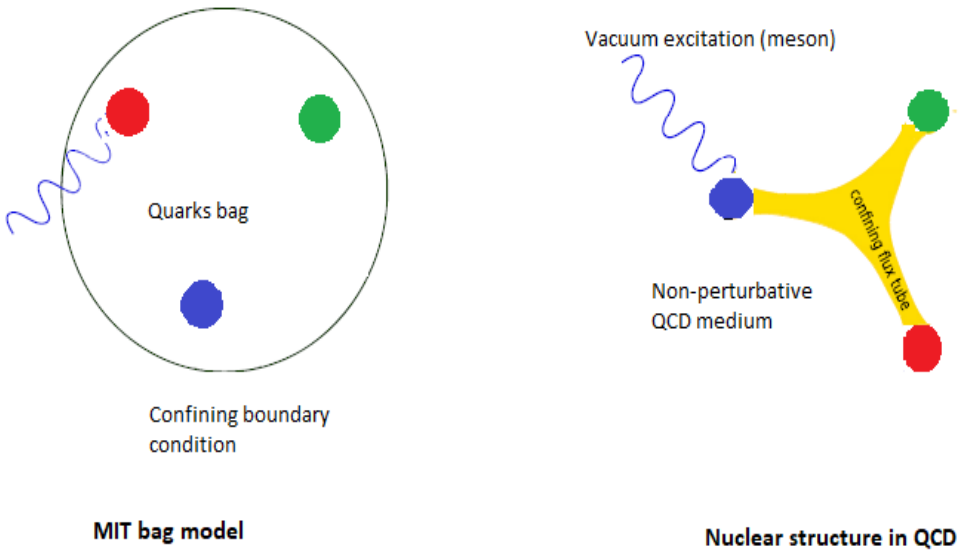

Figure 2: Nuclear Structure

of Ref. [168] a generalization of the formalism to nuclear matter containing a mixture of octet N,Λ,Σ and Ξ baryons was constructed. The QMC model framework is very well suited to describe any kind of baryon (strange or non-strange) , because baryons are taken as bags of quarks and baryons retain their individuality at high energy density. In other words, at higher density having quark bags not allowed to overlap is too restrictive. QCD simulations showed that confined picture of quarks is like a Y-shaped (Fig. 2) string of color attached to the quarks and beyond this area there is ordinary non-perturbative medium where quarks from other hadrons can move without changing its structure. Therefore, the strict condition of non-overlapping of quark bags which restrict quarks from traveling through its boundary, must be considered as an average portrayal of a complex situation, and the boundary and size of the bag should not be attributed a strict physical meaning. Nuclear density is reciprocal to the bag volume and apparently, there is a limit to the density above which QMC model does not work properly. In the first realization of the QMC model, coupling inside the bag seems unnatural but it is

suggested that if we recall the more realistic underlying representation in which quarks are just attached to the color string (gluon), and apart from that the rest of the volume is non-perturbative and nothing prevents quarks from feeling the vacuum fluctuations. In the model the simplest version of the consideration is limited to σ, ω and ρ mesons only.

4.1.1 Effective mass and energy

Using the Born-Oppenheimer approximation [169], for a given position and velocity of the quark bag, the energy of the bag coupled with σ, ω and ρ, is calculated in the nuclear mean field associated with them. The quantum numbers of the octets baryons are given in Table 1. After constructing the full Hamiltonian,

	p	n	Λ	Σ^-	Σ^0	Σ^+	Ξ^-	Ξ^0
t	1/2	1/2	0	1	1	1	1/2	1/2
m	1/2	-1/2	0	-1	0	1	-1/2	1/2
s	0	0	-1	-1	-1	-1	-2	-2

Table 1: Isospin(t), isospin projection(m) and strangeness(s) of octet members

classical and canonical quantization is performed to get the energy. This work is the extension of the previous QMC model where consideration was limited to nuclear matter and finite nuclei (hyperons were excluded) but this model is more general and hyperons are included. Here, work has been limited to consideration of the spin $\frac{1}{2}$ SU(3) octet (N,Λ,Σ,Ξ) and baryons are specified by $|f >= |tms >$ (Table 1).

As hyperons are included, the main working hypothesis is that strange quarks do not couple with the meson field which is based on the results of the fact that mesons represent the correlated pion exchanges, this is also a major part of the explanation of the observed small spin-orbit splitting in Λ hypernuclei, as the strange quark carries all the spin of the Λ hyperon. It is assumed that the couplings

do not violate isospin symmetry and the masses of the up (u) and the down (d) quarks are taken as zero. The energy of f flavored baryon at position $\vec{R}$ (at the center of the bag) in the rest frame of the σ field, is given by

$$E = \sqrt{P^2 + M_f(\sigma)^2} + g^f_\omega \omega + g_\rho \vec{b_\alpha}.\vec{I^t}, \tag{7}$$

where $\vec{P}$ is the momentum of the baryon and $M_f(\sigma)$ is its effective mass and $\vec{I^t}$ is the isospin operator for the isospin t, defined by

$$< tms|\Sigma_q \vec{\tau_q}/2|t'm's' >= \delta_{(tt')}\delta_{(ss')}\vec{I}^{tt'}_{mm'}. \tag{8}$$

Here $\vec{\tau_q}$ is the Pauli matrix acting on the u (up) and d (down) quarks. b_α represents the ρ coupling where α (-1,0,1) is isospin. The Omega coupling to a flavored quark is given by

$$g^f_\omega = \omega^\omega_f g_\omega = (1 + s/3)g_\omega, \tag{9}$$

where g_ω is the ω-N coupling constant. Guichon, in 1988 [153] found that the vector mean field, ω , is linear with the nucleon baryon density while the scalar mean field i.e σ field depends on the source term. In response to the applied scalar field the quark wave function self-consistently adjusts so that the σ field does not increase as fast as ω field does, as the density increases. Nucleon structure introduces an effect that opposes the scalar field. As the density increases the repulsive ω effect increases but the attractive σ does not. In nuclear matter nucleon structure opposes the applied scalar field. By applying the QMC model and solving the quark bag equations one gets the parametrized mass of the baryon. The effective mass of a baryon is given by (see appendix 8.1)

$$M_f(\sigma) = M_f - \omega^\sigma_f g_\sigma \sigma + \frac{d\tilde{\omega}^\sigma_f (g_\sigma \sigma)^2}{2}, \tag{10}$$

d is the scalar polarisability and g_σ is the σ-N coupling constant in free space. An effective Lagrangian can be constructed at the hadronic level and one can proceed to solve the relativistic mean field equations in the usual way [170]. Weightings of the couplings are controlled by the $\tilde{\omega}^\sigma_f$ and ω^σ_f and a first approximation is set $\tilde{\omega}^\sigma_f = \omega^\sigma_f$ = 1 + s/3.

4.1.2 Hamiltonian of the nuclear system

To get the total energy stored in the nuclear system it is essential to add up the baryon energies and the energy stored in the meson fields. If m_σ, m_ω and m_ρ are the masses of σ, ω and ρ mesons then the total energy of the system can be given by

$$\begin{aligned} E_t &= \Sigma_{i=1}^{A} E_B + E_{meson} \\ E_t &= \sqrt{P_f^2 + M_f(\sigma)^2} + g_\omega^f \omega + g_\rho \vec{b}.\vec{I^t} \\ &\quad + \frac{1}{2}\int \vec{dr}[(\nabla\sigma)^2 + m_\sigma^2\sigma^2] \\ &\quad - \frac{1}{2}\int \vec{dr}[(\nabla\omega)^2 + m_\omega^2\omega^2] \\ &\quad - \frac{1}{2}\int \vec{dr}[(\nabla\vec{b})^2 + m_\rho^2\vec{b}^2], \end{aligned} \tag{11}$$

where in the hypothesis meson fields are taken to be time independent. Assuming σ_{sol}, ω_{sol} and ρ_{sol} are the solutions for the σ, ω and ρ meson equations of motion, respectively. So, the Hamiltonian of the nuclear system is given by

$$H(R_x, P_x) = E_t(R_x, P_x, \sigma \to \sigma_{sol}, \omega \to \omega_{sol}, \rho \to \rho_{sol}) \tag{12}$$

$$\frac{\delta E}{\delta\sigma} = \frac{\delta E}{\delta\omega} = \frac{\delta E}{\delta b_\alpha} = 0. \tag{13}$$

The scalar σ meson field is non-linear, as effective mass depends on it and it needs to be solved carefully, whereas ω and ρ are linear and can be solved with no difficulty. For the purpose of solving for the σ field, in Ref. [168] the method to solve it is suggested as

$$\sigma = \bar{\sigma} + \delta\sigma, \tag{14}$$

where $\bar{\sigma}$ is the nuclear ground state expectation value in the nuclear system $\bar{\sigma} =< \sigma >$ and $\delta\sigma$ is a small deviation in the σ field. Referencing to the results of Ref. [168]. The Hamiltonian term depending on the σ meson field in terms of the one body kinetic operator ($K(\overline{\sigma})$) is given by

$$H_\sigma = \int \vec{dr}[k(\sigma) - (1/2)\bar{\sigma} < \frac{\partial K}{\partial\bar{\sigma}} > + (1/2)\delta\sigma(\frac{\partial K}{\partial\bar{\sigma}} - < \frac{\partial K}{\partial\bar{\sigma}} >)], \tag{15}$$

and $K(\overline{\sigma})$ depends on the creation ($a_k^\dagger$) and annihilation operator (a_k). Where k indicates the momentum of a baryon of flavor f

$$K(\overline{\sigma}) = \frac{1}{2V}\Sigma_{k,k',f}e^{i(\vec{k}-\vec{k'}).\vec{r}}(\sqrt{k^2 + M_f[\overline{\sigma}(\vec{r})]^2} + \sqrt{k'^2 + M_f[\overline{\sigma}(\vec{r})]^2})(a^\dagger_{\vec{k}f}a_{\vec{k'}f}). \tag{16}$$

For the mean field approximation setting the meson field variation $\delta\sigma(r)$ to zero is required. The self-consistent solution for a constant $\overline{\sigma}(r)$ meson field in a uniform system is solved in [168], and for the sake of brevity, is directly quoted

$$\overline{\sigma}(r) = -\frac{1}{m_\sigma^2} < \frac{\partial K}{\partial \overline{\sigma}} >, \tag{17}$$

which is needed to be solved numerically and fluctuation in scalar meson field $\delta\sigma$ is given by

$$\delta\sigma(\vec{r'}) = \int d\vec{r'}\frac{d\vec{q}}{(2\pi)^3}\frac{ie^{\vec{q}.(\vec{r}-\vec{r'})}}{q^2+\tilde{m}_\sigma^2}(-\frac{\partial K(\vec{r'})}{\partial\overline{\sigma}} + < \frac{\partial K}{\partial\overline{\sigma}} >), \tag{18}$$

where $\tilde{m}_\sigma$ is the effective meson mass, given by

$$\tilde{m}_\sigma^2 = m_\sigma^2 + < \frac{\partial^2 K}{\partial\overline{\sigma}^2} > . \tag{19}$$

In nuclear matter the energy density is calculated in the Hartree-Fock approximation. The one body kinetic operator and Hamiltonian density from equation (16) are calculated using [154] :

$$< K(\overline{\sigma}) > = \frac{2}{(2\pi)^3}\Sigma_f\int_0^{k_f} d\vec{k}\sqrt{k^2 + M_f^2(\overline{\sigma})}, \tag{20}$$

$$\frac{< H_\sigma >}{V} = < K(\overline{\sigma}) > + \frac{1}{2m_\sigma^2}(< \frac{\partial K}{\partial\overline{\sigma}} >)^2\frac{1}{(2\pi)^6}\Sigma_f\int_0^{k_f} d\vec{k_1}d\vec{k_2}\frac{1}{(\vec{k_1}-\vec{k_2})^2+\tilde{m}_\sigma^2} \times\frac{\partial}{\partial\overline{\sigma}}\sqrt{k_1^2+M_\sigma^2}\frac{\partial}{\partial\overline{\sigma}}\sqrt{k_2^2+M_\sigma^2}. \tag{21}$$

The next step is to construct potentials for ω and ρ meson exchange Fock contributions. The exact solutions for these are given by

$$\frac{< V_\omega >}{V} = \frac{G_\omega}{2}(\Sigma_f\omega_f^\omega n_f)^2 - G_\omega\Sigma_f(\omega_f^\omega)^2\frac{1}{(2\pi)^6}\int_0^{k_f(f)} d\vec{k_1}d\vec{k_2}\frac{m_\omega^2}{(\vec{k_1}-\vec{k_2})^2+m_\omega^2}, \tag{22}$$

$$\frac{< V_\rho >}{V} = \frac{G_\rho}{2}(\Sigma_{tms} m n_{tms})^2 - G_\rho \Sigma_{tmm's} \vec{I^t_{mm'}}.\vec{I^t_{m'm}} \frac{1}{(2\pi)^6} \int_0^{k_F(tms)} d\vec{k_1}. \int_0^{k_F(tm's)} d\vec{k_2} \frac{m_\rho^2}{(\vec{k_1} - \vec{k_2})^2 + m_\omega^2}, \tag{23}$$

where G_σ, G_ω and G_ρ are defined by

$$G_\sigma = \frac{g_\sigma^2}{m_\sigma^2}, \tag{24}$$

$$G_\omega = \frac{g_\omega^2}{m_\omega^2}, \tag{25}$$

$$G_\rho = \frac{g_\rho^2}{m_\rho^2}. \tag{26}$$

In the Hartree-Fock approximation, the long range pion exchange contribution enters through the Fock term only and adds to the energy. For studying the impact of long range pion exchange, a generalized expression is give in [170]

$$\frac{< V_\pi >}{V} = \frac{1}{n_B}(\frac{g_A}{2f_\pi})^2 (J_{pp} + 4J_{pn} + J_{nn} - \frac{24}{25}(J_{\Lambda\Sigma^-} + J_{\Lambda\Sigma^0} + J_{\Lambda,\Sigma^+}) + \frac{16}{25}(J_{\Sigma^-\Sigma^0} + 2J_{\Sigma^-\Sigma^0} + 2J_{\Sigma^+\Sigma^0} + J_{\Sigma^+\Sigma^+}) + \frac{1}{25}(J_{\Xi^-\Xi^-} + 4J_{\Xi^-\Xi^0} + J_{\Xi^0\Xi^0})), \tag{27}$$

where

$$J_{ff'} = \frac{1}{(2\pi)^6} \int_0^{k_F} \int_0^{k'_F} d\vec{p} d\vec{p'} [1 - \frac{m_\pi^2}{(\vec{p} - \vec{p'})^2 + m_\pi^2}]. \tag{28}$$

In the above equations $g_A = 1.26$ is the axial coupling constant of nucleon and m_π is the mass of the pion with $f_\pi = 93MeV$ being the pion decay constant. J_{ff} is a contact term which is not easy to separate from short range contributions of heavy mesons so they are excluded. This only makes small readjustments in G_σ, G_ω and G_ρ which has been checked. In a nut shell, only long ranged pion exchange of the Yukawa type is taken into consideration.

4.1.3 Taking care of parameters

Coupling constant, G_ω, G_ρ and G_σ, meson masses and free nucleons are the ones that need to be fixed. Free nucleon radius does not impact much on results, so best suited value for radius is kept R_N^{free} = 0.8fm which is realistic [172]. Masses of π, ω and ρ are set to their physical values. However the mass of σ meson is not well known due to $\pi\pi$ resonance width which is quite large in physical region. In finite nuclei [168] m_σ = 700 MeV produces the best results. Therefore m_σ is fixed to 700 MeV. In case of study of neutron stars, mass of σ meson, m_σ, is not so significant because it contributes to the nuclear surface which is not present in neutron stars. G_ω, G_ρ and G_σ are set to reproduce the binding energy and the asymmetry energy of ordinary nuclear matter at the saturation point. First pion contributions are set to zero and coupling constants are adjusted so that it give binding energy, $E = -15.865MeV$ and asymmetry energy, $a_s = 30MeV$, of nuclear matter at saturation point of $0.16fm^{-3}$. These couplings, for QMC700 model, are summarized in table 2.

Model	$m_\sigma(MeV)$	π_n	$E(MeV)$	$G_\sigma(fm^2)$	$G_\omega(fm^2)$	$G_\rho(fm^2)$	$K_\infty(MeV)$
QMC700	700	0	-15.865	11.33	7.27	4.56	340

Table 2: Table for Coupling constants

In table last column defines incompressibility, K_∞. For QMC700 accepted value for modulus of K_∞ is ranging from 200 MeV to 300 Mev. But value given in table is clearly above that. For decreasing the same, Fock term is added because it has attractive interaction, which is weakly dependent on density at saturation point, approximately $\rho^{1/6}$. This has been confirmed by by QMCπ1 model where pion contributions are included and incompressibility drops from 340 MeV to 322 MeV.

In Table 2, the column π_n is the number by which pion contribution is multiplied, E denotes binding energy of symmetric nuclear matter and K_∞ represents incompressibility.

4.1.4 Cold uniform neutron star matter

Neutron star matter, after cooling over a long period of time, is in generalized in β equilibrium. All baryons, regardless of their strangeness [173], of octet can come into existence by successive weak interactions. In this study, considered matter is made from octet baryons, electrons and negative muons.
The total energy density is the summation of the baryon density ϵ_B, electron density ϵ_e and muon density ϵ_μ.

$$\epsilon = \epsilon_B + \epsilon_e + \epsilon_\mu \tag{29}$$

under the condition that equilibrium state minimizes the energy and baryon number is conserved and electric charge is neutral (zero). Baryonic contribution is can be given by

$$\epsilon_B = \frac{< H_\sigma + V_\omega + V_\rho + V_\pi >}{V}, \tag{30}$$

where each term in the numerator has been defined previously from equations (22 to 28).
In terms of binding energy per baryon (E)

$$\epsilon_B = \Sigma_f (E + M_f) n_f. \tag{31}$$

Baryonic pressure (P_B) and incompressibility modulus (K_∞) are given by

$$P_B = n_B^2 \frac{\partial}{\partial n_B} \frac{\epsilon_B}{n_B}, \tag{32}$$

$$K_\infty = 9 \frac{\partial P_B}{\partial n_B}, \tag{33}$$

where n_B = $\Sigma_f n_f$ and the derivative with respect to n_B is taken at constant fraction,

$\frac{n_f}{n_B}, f = 1, 2, 3, ..., 8$.
Fermi expression gives the energy density of the free gas of leptons (l)

$$\epsilon_l = \frac{2}{(2\pi)^3} \int_0^{k_{f(l)}} d\vec{k} \sqrt{k^2 + m_l^2}, \tag{34}$$

where m_l is the mass of the lepton and n_l is the number density, given by

$$n_l = \frac{k_f^3(l)}{3\pi^2}. \tag{35}$$

Matter in the neutron star is suppose to be neutral. In equilibrium and under the constraint of charge neutrality, by the Lagrangian multiplier (λ, ν) method, one gets

$$\delta[\epsilon_B(n_p, ..) + \epsilon_e(n_e) + \epsilon_\mu(n_\mu) + \lambda(\Sigma_f n_f - n_B) + \nu(\Sigma_f n_f q_f - (n_e + n_\nu))] = 0, \tag{36}$$

where q_f denotes the charge of flavor f. Equation (36) is the deviation of energy which does not depend on any variation of the Lagrangian multiplier, λ and ν.
Chemical potential is defined as

$$\mu_f = \frac{\partial \epsilon_B}{\partial n_f}, \mu_l = \frac{\partial \epsilon_l}{\partial n_l} = \sqrt{k_f^2(l) + m_l^2}. \tag{37}$$

Putting the chemical potentials back in the equilibrium condition, equation (36), one gets

$$\mu_f + \lambda + \nu q_f = 0, \tag{38}$$

$$\mu_e - \nu = 0, \tag{39}$$

$$\mu_\mu - \nu = 0, \tag{40}$$

$$\Sigma_f n_f - n_B = 0, \tag{41}$$

$$\Sigma_f n_f q_f - (n_e + n_\mu) = 0. \tag{42}$$

To solve equations (38-42), the Lagrange multipliers, λ and ν, need to be eliminated. That is achieved by putting $f = neutron$ in equations (38) and (39).

At a given density n_B, generally some of the densities disappear in equilibrium state, so the equations generated by their variation vanish from equation (38) to (40). Eliminating μ from equations (39) and (40), clearly gives $\mu_\mu = \mu_e$ which is solved by

$$k_f(\mu) = R\sqrt{k_f^2(e) + m_e^2 - m_\mu^2}, \tag{43}$$

where R represents the real part. This relation is always true because electrons enter first ($m_\mu > m_e$), that means if the electron density vanishes then so does the muon density. Quickly coming to the solution of these set of equations (39-43) which are solved in [174], taking the same procedure given. Let relative concentrations are denoted by

$$Z = [z_i] = [\frac{n_p}{n_B}, \frac{n_n}{n_B}, \frac{n_\lambda}{n_B}, ..., \frac{n_e}{n_B}, \frac{n_\mu}{n_B}]. \tag{44}$$

Every element of $[z_i]$ is related (E_i) to equations (32-36). Each of the elements is obtained by taking the variation of ϵ with respect to $\rho_i = z_i n_B$. Suppose at some density, n_B, a solution of Z_0 is found. After finding the solution, one first checks whether or not, by increasing the density by δn the threshold for some particle has been crossed. To check whether a particle has appeared or not, below and across the threshold ($z_i = 0$), one tests if E_i (for that particle) changes sign with increase in density by δn that means that particle has appeared. If this condition is met that means all such equation (E_i) are need to be added in the system of equations. Then the system of equations are solved numerically taking first approximation as Z_0 and incrementing density by δn ($n_B = n_0 + \delta n$). If a certain concentration drops below a small given value, θ, then the corresponding equation is dropped from the system. The value of θ depends on the accuracy of our solution. From [154] the calculation is done by taking the value of $\theta = 10^{-4}$ and checking that 10^{-3} gives the same results. System of equations is solved for pure neutron matter and initial condition is set to $n_B = 0$. Once the equilibrium solution ($Z(n_B)$) has been found for a selected range of baryon densities then the total energy density at equilibrium is calculated. Total pressure ($P(n_B)$) due to leptons and baryons, is calculated

by summing individual pressures. From equations (32-36), at equilibrium total pressure can be given by [174]

$$P(n_B) = n_B^2 \frac{d}{dn_B} \frac{\epsilon(n_B)}{n_B}. \tag{45}$$

Neutron stars are made of matter that covers a wide range of density, from terrestrial iron to several times the nuclear matter density. At density, 2-3 times nuclear matter density, atoms break into their elementary particles and neutron star matter becomes a system of unbound neutrons, protons, electrons and muons. After enough time a state of β equilibrium is reached and all components which have longer timescale than the life-span of the system take part in equilibrium condition. When the density goes higher even heavier mesons and strange baryons may appear and play a role [175][176][177][178][179]. At baryon density below 0.75 times nuclear matter density, nucleons are arranged on a lattice along with neutrons and electron gas. This density region is found in the inner and the outer crust, in this region, QMC700 EoSs are matched with the EoS given by Baym-Pethick-Sutherland (BPS) [201] (Radius of a star must increase at low density region).

Developing a nucleon based EoS using effective interaction (non-relativistic Skyrme, relativistic mean field) was suggested in [180][181] to densities corresponding to maximum mass of neutron star (non-relativistic models are not valid at most masses if $n_B >= 2n_0$). In this study, in the energy density range up to 1200 MeV/fm^3, comparative study among three EoS, pure neutron matter (N-QMC700), full octet baryon (F-QMC700) and strange matter [142] is carried out.

4.1.5 Equation of State (EoS)

For the sake of convenience the parametrized EoSs are given below, which represent pressure and energy density relation. The parameterizations given in Table 3

give EoS of N-QMC700 and F-QMC700.

$$P = \frac{N_1 \epsilon^{p1}}{1 + e^{(\epsilon - r)/a}} + \frac{N_2 \epsilon^{p2}}{1 + e^{-(\epsilon - r)/a}} \tag{46}$$

This fit works well for the energy density 0 to 1200 MeV/fm^3 and values for the constants N_1, N_2, p_1, p_2, 'r' and 'a'.

	N_1	p_1	N_2	p_2	r	a
N-QMC700	0	0	0.008623	1.548	342.4	184.4
F-QMC-700	0.0000002.62	3.197	0.0251	1.286	522.1	113

Table 3: Table for parameters

Below the energy density 110 MeV/fm^3, the matter forms the inner and outer crust of the star made of nucleons arranged in a lattice, as well as neutron and electron gases. In this energy density region the QMC Equation of State (EoS) is matched with equations of state given by Baym-Pethick-Sutherland (BPS) EoS [201], reflecting the composition of the same matter in that energy density region. The BPS equation of state is used below 110 MeV/fm^3 in this thesis. And a strange matter EoS state is taken from Ref. [165], for comparison purposes. The EoS of a strange star matter (strange matter EoS or MIT EoS) is given by

$$P = \frac{1}{3}(\epsilon - 4B), \tag{47}$$

where B is the bag constant whose value is taken to be 10^{14}gm/cm^3. This EoS is based on the same MIT bag model, which suggests quark deconfinement at the higher energy densities. It only takes color singlet baryon into consideration [182]. This EoS poorly represents the crust region (See section 5.1 for details) where the energy density is low compared to the core. For the reason appropriate changes are made and nucleons EoS is used for equation (47), (i) for low density region below 300 MeV/fm^3, (ii) for energy density region below 500 MeV/fm^3. And comparative results are drawn.

4.2 Structural Equations

4.2.1 Non-rotating neutron star structure (Tolman-Oppenheimer-Volkoff (TOV) equation)

The structural equation for a static, spherical neutron star involves solving the TOV [7-8] equation, derived from the general theory of relativity equations [183][184], for a particular equation of state (EoS) . The TOV equation is the relation between pressure gradient (force), working outwards at the shell, and the Newtonian gravitational attraction due to the mass inside the shell and the correction term which is derived from general relativity. Force is different at different distances from the center of a star. In other words, the TOV equations are the balance between the gravitational attraction and the internal pressure that sustains the neutron star.

The TOV equation is the stellar structural equation for a static (non-pulsating), spherically symmetric, non-rotating neutron star which is considered to made of a perfect fluid (no heat and no viscosity), under the Einstein's general theory of relativity framework.

A direct manifestation of the definition of the perfect fluid gives the energy momentum tensor as

$$T^{\alpha\beta} = \begin{pmatrix} -\epsilon & 0 & 0 & 0 \\ 0 & P & 0 & 0 \\ 0 & 0 & P & 0 \\ 0 & 0 & 0 & P \end{pmatrix}$$

For the sake of convenience all calculations have been done in natural units (G = c = 1).

The line element for such a compact star is given by,

$$ds^2 = -e^{2\Phi(r)}dt^2 + e^{2\Lambda(r)}dr^2 + r^2 d\theta^2 + r^2 \sin^2\theta d\phi^2, \tag{48}$$

where $\Phi(r)$ and $\Lambda(r)$ are the metric functions depend on the radial distances. In covariant form the metric functions can be written as

$$g_{tt} = -e^{2\Phi(r)}, g_{rr} = e^{2\Lambda(r)}, g_{\theta\theta} = r^2, g_{\phi\phi} = r^2 \sin^2\theta, \tag{49}$$

The line element (48) can be written as a covariant expression,

$$ds^2 = g_{\mu\nu} dx^\mu dx^\nu. \tag{50}$$

Here, some of the steps are given to determine the relation between the energy density and the pressure. The Einstein mixed tensor is calculated by

$$G^\mu_\nu = R^\mu_\nu - \frac{1}{2}\delta^\mu_\nu R = 8\pi T^\mu_\nu. \tag{51}$$

This equation is the connection between the distribution of energy and matter, contained in the energy momentum tensor and the curvature (geometry) of spacetime in the physical sense. Here T^μ_ν is the fluid stress energy tensor given by

$$T^\mu_\nu = (\epsilon + P)\frac{dx^\mu}{d\tau}\frac{dx_\nu}{d\tau} + \delta^\mu_\nu P, \tag{52}$$

where x^μ is the fluid's four velocity. And

$$T^t_t = -\epsilon, T^i_i = P. \tag{53}$$

The tensor divergence of the left hand side of equation (51) identically vanishes. Therefore, using the rule of covariant differentiation, the four derivative of the stress-energy tensor (is equal to zero), determined by

$$T^\mu_{\nu;\mu} = \frac{\partial T^\mu_\nu}{\partial x^\mu} + \Gamma^\mu_{\kappa\mu} T^\kappa_\nu - \Gamma^\kappa_{\nu\mu} T^\mu_\kappa = 0. \tag{54}$$

The non vanishing Christoffel symbols for the line element, i.e equation (48), are

$$\begin{aligned} \Gamma^r_{tt} = e^{2\Phi-2\Lambda}\Phi', \Gamma^t_{tr} = \Phi', \Gamma^r_{rr} = \Lambda', \\ \Gamma^\theta_{r\theta} = 1/r, \Gamma^\phi_{r\phi} = 1/r, \Gamma^r_{\theta\theta} = -re^{-2\Lambda}, \\ \Gamma^\phi_{\theta\phi} = cot\theta, \Gamma^r_{\phi\phi} = \frac{-rsin^2\theta}{e^{2\Lambda}}, \\ \Gamma^\theta_{\phi\phi} = -sin\theta.cos\theta, \end{aligned} \tag{55}$$

where Φ' and Λ' are the derivative of Φ and Λ with respect to r, i.e $\frac{d\Phi}{dr}$ and $\frac{d\Lambda}{dr}$. In flat spacetime, i.e in a local inertial frame of reference equation (54) reduces to

$$T^{\mu}_{\nu;\mu} = \frac{\partial}{\partial x^{\mu}} T^{\mu}_{\nu} = 0. \tag{56}$$

For the line element given above (equation (48)), the covariant derivative of stress energy tensor, i.e equation (54) reduces to

$$T^{\mu}_{\nu;\mu} = (\epsilon + P)\Phi' + P', \tag{57}$$

which implies that the mixed energy momentum tensor, the middle term of equation (51), for the given spacetime matric, can be calculated using the expressions below (See appendix 7.2.1)

$$\begin{aligned} R^t_t &= [-\frac{1}{4}\Phi'^2 + \frac{1}{4}\Phi'\Lambda' - \frac{1}{2}\Phi'' - \frac{1}{r}\Phi']e^{-\Lambda}, \\ R^r_r &= [-\frac{1}{4}\Phi'^2 + \frac{1}{4}\Phi'\Lambda' - \frac{1}{2}\Phi'' - \frac{1}{r}\Lambda']e^{-\Lambda}, \\ R^{\phi}_{\phi} = R^{\theta}_{\theta} &= -\frac{1}{r^2}e^{-\Lambda}[1 - \frac{1}{2}r\Lambda' + \frac{1}{2}r\Phi'] + \frac{1}{r^2}, \end{aligned} \tag{58}$$

The Ricci scalar is given by

$$R = \frac{1}{r^2 e^{2\Lambda}}[2\Phi'\Lambda' r^2 - 2\Phi'' r^2 - 2(\Phi')^2 r^2 - 4r\Phi' + 4r\Lambda' + 2e^{2\Lambda} - 2]. \tag{59}$$

Therefore, Einsteins' curvature tensor is calculated as

$$G^t_t = R^t_t - \frac{1}{2}R = e^{-2\Lambda}(\frac{1}{r^2} - 2\frac{\Lambda'}{r}) - \frac{1}{r^2}, \tag{60}$$

$$G^r_r = R^r_r - \frac{1}{2}R = e^{-2\Lambda}(\frac{2\Phi'}{r} + \frac{1}{r^2}) - \frac{1}{r^2}, \tag{61}$$

$$G^{\theta}_{\theta} = R^{\theta}_{\theta} - \frac{1}{2}R = e^{-2\Lambda}(\Phi'' - \Phi'\Lambda' + \Phi'^2 + \frac{\Phi' - \Lambda'}{r}), \tag{62}$$

$$G^{\phi}_{\phi} = G^{\theta}_{\theta}. \tag{63}$$

Provided we are dealing with a static configuration, the following relations are used

$$\frac{dr}{d\tau} = \frac{d\theta}{d\tau} = \frac{d\phi}{d\tau} = 0, \tag{64}$$

and

$$\frac{dt}{d\tau} = e^{-\Phi}. \tag{65}$$

Using equations (60-63) and equation (53) in equation (51) gives the general relativistic equation,

at μ = ν = t

$$e^{-2\Lambda}(\frac{1}{r^2} - 2\frac{\Lambda'}{r}) - \frac{1}{r^2} = -8\pi\epsilon, \tag{66}$$

at μ = ν = r

$$e^{-2\Lambda}(\frac{2\Phi'}{r} + \frac{1}{r^2}) - \frac{1}{r^2} = 8\pi P, \tag{67}$$

at μ = ν = θ

$$e^{-2\Lambda}(\Phi'' - \Phi'\Lambda' + \Phi'^2 + \frac{\Phi' - \Lambda'}{r}) = 8\pi P. \tag{68}$$

To solve for $e^{2\Lambda}$, multiplying equation (66) with r^2 in both sides, implies

$$e^{-2\Lambda}2\Lambda' r - e^{-2\Lambda} + 1 = 8\pi\epsilon r^2. \tag{69}$$

Notice that left hand side can be written as the derivative of a function

$$-\frac{d}{dr}(e^{-2\Lambda}r - r) = 2(4\pi\epsilon r^2) \tag{70}$$

and the mass contained in radius 'r' is given by

$$m(r) = 4\pi \int_0^r dr.r^2\epsilon(r). \tag{71}$$

Integration of equation (70) yields

$$e^{-2\Lambda} = 1 - \frac{2m}{r}. \tag{72}$$

Eliminating Λ from equation (67) by using equation (69), one gets

$$8\pi P = \frac{-2m}{r^3} + 2(1 - \frac{2m}{r})\frac{\Phi'}{r}, \tag{73}$$

which gives expression for Φ'

$$\Phi' = \frac{4\pi r^3 P + m}{r^2(1 - \frac{2m}{r})}. \tag{74}$$

At the star's surface

$$\Phi = \frac{1}{2}\log(1 - \frac{2M}{R}), \tag{75}$$

where M and R are the total mass and the radius of the neutron star, respectively. From appendix (8.2.2) (equation (175)) the pressure gradient as a function of radius and density can be stated as

$$\frac{dP}{dr} = -\frac{[\epsilon(r) + P(r)][4\pi r^3 P(r) + m(r)]}{r^2(1 - \frac{2m(r)}{r})}. \tag{76}$$

This is the equation that was desired. This equation is called TOV equation which is paramount to getting the complete model of a neutron star (hydro-statically stable stellar configuration). This equation is to be integrated under the boundary conditions, which are pressure (P) $\rightarrow$ 0, energy density (ϵ) $\rightarrow$ 0 where r $\rightarrow$ radius (at the surface).

Both, in classical mechanics as well as in the general theory of relativity, the pressure inside the shell, which gives a force outwards on a mass shell, is equal to the gravitational force that acts inwards (towards the center). In classical mechanics neutron stars can be made as massive as one pleases with P$<<\epsilon$, P $<<$ m and m $<<$ r, which produces dP/dr = ϵm/r^2. However, in the general relativistic framework as compact stars become more massive at a certain point they collapse under their own gravity, into black holes.

To determine the full model of neutron stars, we need a pressure-energy ($P(\epsilon)$) relation, which is referred to the equation of state (EoS), as input to the structural equations (TOV). The numerical integration of the TOV equations, from the center towards the surface, takes place in the following way.

- First choose the central density (ϵ_c) and determine the pressure (P) at center from equation of state. These values serve as input to TOV equations (equation (76)).

-Determine the mass (m) of the shell by equation (71).
- Using these values determine the pressure gradient at an infinitesimal distance(r) by the TOV equations.
- Thus allowing us to determine the pressure (P) for next the step (Eular method).
- Determining the pressure (P) allows us to calculate the energy density by the EoS and the mass for the next shell of thickness (dr).
-Repeating these steps until meeting the boundary conditions, determines the total mass and the radius of the neutron star.

4.2.2 Rotating neutron star

Solving the structural equations for a rotating neutron star is more complex than a non-rotating star. Rotating neutron stars are slightly heavier than non rotating ones because rotating stars experience an additional centrifugal force that counterbalances the gravity, unlike the non-rotating stars. Due to rotation, the shape of a neutron star also deforms, at the equator their radii stretch and at the poles they tend to flatten. They are more massive (have a bulge) at the equator than the poles. This deformation of stars makes calculations a bit harder because being more massive and deformed means a change in the spacetime structure. This implies that the line element for a rotating neutron star depends on the rotational velocity of the star. Therefore, the general relativistic effect of the local inertial frame dragging demands an additional non-diagonal term ($g^{t\phi}$) in the metric tensor. This additional term imposes a self consistent condition on the stellar structure of the neutron stars and, to the extent to which the local inertial frame is dragged along the direction of rotation, is determined by the properties of a neutron star, like mass and rotational velocity. For slowly rotating neutron stars, Hartle's [185][186] approach is adopted. Structural equations are solved under the general relativistic frame work, in steps, by the perturbed metric methodology. That involves :
(1) Solve the TOV equation for a non-rotating neutron star case.

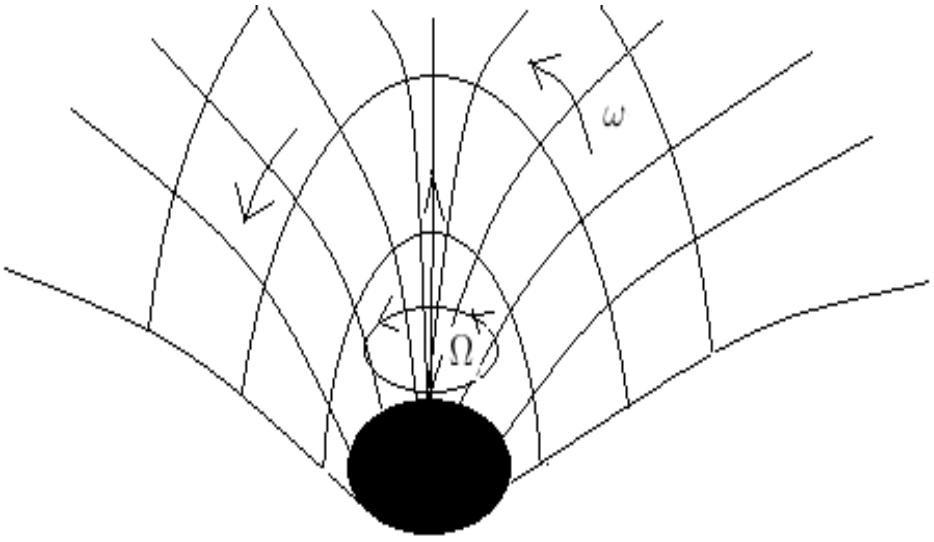

Figure 3: Curvature of spacetime around a rotating neutron star, rotating with rotational velocity Ω in general relativity framework and position dependent local frame dragging angular velocity $\omega(r, \theta, \phi)$.

(2) Solve the rotational perturbation expressions for determining the rotation of the neutron stars.
(3) Solve the monopole perturbation function to determine the extra mass and pressure, a neutron star may contain due to rotation.
(4) Solve the quadrupole perturbation function to determine the shape of the star.
(5) Solve the tidal deformability differential equations to get the Love number and tidal deformability of the neutron stars in a neutron star binary. We start at the second step, as step one is the non-rotating case which was considered in the last section

Rotational pertubation Hartle's approach to get the solution for a perturbed Schwarzschild metric is based on the idea that, as stars rotate their pressure, energy density and baryon number, all get perturbed.
The perturbed line element of rotating, axially symmetric equilibrium configura-

tion, is given by

$$ds^2 = -e^{2\nu(r,\theta,\Omega)}(dt)^2 + e^{2\psi(r,\theta,\Omega)}(d\phi - \omega(r,\theta,\Omega)dt)^2 + e^{2\mu(r,\theta,\Omega)}(d\theta)^2 + e^{2\lambda(r,\theta,\Omega)}(dr)^2 + \mathcal{O}(\Omega^3), \tag{77}$$

where

$$g^{tt} = -e^{-2\nu(r,\theta)}, \tag{78}$$

$$g^{t\phi} = -e^{-2\nu(r,\theta)}\omega(r,\theta), \tag{79}$$

$$g^{rr} = e^{-2\lambda(r,\theta)}, \tag{80}$$

$$g^{\theta\theta} = e^{-2\mu(r,\theta)}, \tag{81}$$

$$g^{\phi\phi} = e^{-2\psi(r,\theta)} - \omega^2(r,\theta)e^{-2\nu(r,\theta)}, \tag{82}$$

where ν, ψ, μ and λ are the perturbed metric functions , r, θ are polar coordinates and Ω is the uniform rotational velocity of the star. ω is the rotating velocity of the local inertial frame of reference dragged along the direction of rotation of the neutron star (Fig. 3). This dragged velocity also depends on the polar coordinates r, θ. Since the velocity of local dragging of the inertial reference frame depends on the neutron star's mass concentration inside and outside, which varies with Ω, makes ω is a function of Ω (Fig. 3). Relative angular velocity is denoted by, $\overline{\omega}$

$$\overline{\omega} = \Omega - \omega(r,\theta,\Omega). \tag{83}$$

It is this relative velocity ($\overline{\omega}$), which is of particular interest, when discussing the rotational flow of the fluid inside the neutron star.

The metric function is independent of both azimuthal angle (ϕ) and time, indicating stationary and axially symmetric rotation. Since, the neutron star is axially symmetric, this suggests that the star is required to not radiate any rotational energy in the form of gravitational radiation. Otherwise, there's a time dependent moment of the distribution of mass, which means the star could not remain in equilibrium over time.

Expansions of the metric functions through second order of Ω are denoted as

$$e^{2\nu(r,\theta,\Omega)} = e^{2\Phi(r)}[1 + 2(h_0(r,\Omega)) + h_2(r,\Omega)P_2(Cos\theta)], \tag{84}$$

$$e^{2\psi(r,\theta,\Omega)} = r^2 sin^2\theta[1 + 2(\nu_2(r,\Omega)) - h_2(r,\Omega)P_2(Cos\theta)], \tag{85}$$

$$e^{2\mu(r,\theta,\Omega)} = r^2[1 + 2(\nu_2(r,\Omega)) - h_2(r,\Omega)P_2(Cos\theta)], \tag{86}$$

$$e^{2\lambda(r,\theta,\Omega)} = e^{2\Lambda(r)}[1 + \frac{2}{r}\frac{m_0(r,\Omega) + m_2(r,\Omega)P_2(cos\theta)}{1 - 2m(r)/r}], \tag{87}$$

where the second order terms are introduced as

$$h(r,\theta,\Omega) = h_0(r,\Omega) + h_2(r,\Omega)P_2(cos\theta) + ..., \tag{88}$$

$$\nu(r,\theta,\Omega) = \nu_0(r,\Omega) + \nu_2(r,\Omega)P_2(cos\theta) + ..., \tag{89}$$

$$m(r,\theta,\Omega) = m_0(r,\Omega) + m_2(r,\Omega)P_2(cos\theta,\Omega). \tag{90}$$

Due to rotational perturbations, let's say pressure changes by an amount of ΔP, energy density by $\Delta\epsilon$ and baryon number density by $\Delta\rho$. Consequently, due to perturbation the stress-energy tensor changes, say, ΔT and the new stress-energy tensor for the perturbed metric is given by [187]

$$T_{\mu\nu} = T^0_{\mu\nu} + \Delta T_{\mu\nu} \tag{91}$$

where $T^0_{\mu\nu}$ denotes the perfect fluid energy-momentum tensor for a non-rotating neutron star given by

$$T^0_{\mu\nu} = (\epsilon + P)u_\mu u_\nu + P g_{\mu\nu}, \tag{92}$$

$$\Delta T_{\mu\nu} = (\Delta\epsilon + \Delta P)u_\mu u_\nu + \Delta P g_{\mu\nu}. \tag{93}$$

Here ϵ (energy density), P (pressure), and ρ (baryon number density) are measured in the local inertial frame co-moving with the fluid and u_ν is the fluid four velocity ($u_\nu u^\nu = -1$).

The individual changes can be given by

$$\Delta P = (\epsilon + P)(p_0 + p_2 P_2(cos\theta)), \tag{94}$$

$$\Delta\epsilon = \Delta P\frac{\partial\epsilon}{\partial P}, \tag{95}$$

$$\Delta\rho = \Delta P \frac{\partial\rho}{\partial P}, \tag{96}$$

where p_0 and p_2 are the monopole and the quadrupole pressure perturbation functions and $P_2(cos\theta)$ is the Legendre polynomial function given by

$$P_2(z) = \frac{3z^2 - 1}{2}. \tag{97}$$

After these initial remarks, lets move to get the structural equations in Hartle's framework. Frame dragging function ($\omega(r, \theta)$) is determined by the Einstein's field equations

$$G^t_\phi = R^t_\phi = 8\pi T^t_\phi, \tag{98}$$

$$T^t_\phi = (\epsilon + P)\overline{\omega} r^2 sin^2\theta e^{-2\nu}, \tag{99}$$

(See appendix 7.2.3)

$$\frac{1}{r^4}\frac{\partial}{\partial r}(r^4 e^{(\nu+\lambda)}\frac{\partial\overline{\omega}}{\partial r}) + \frac{e^{\lambda-\nu}}{r^2 sin^3\theta}\frac{\partial}{\partial\theta}(sin^3\theta\frac{\partial\overline{\omega}}{\partial\theta}) - 16\pi(\epsilon + P)\overline{\omega}e^{\lambda-\nu} = 0, \tag{100}$$

where following relations are used

$$\frac{\partial\lambda}{\partial\theta} = \frac{\partial\nu}{\partial\theta} = \frac{\partial\nu}{\partial\theta} = 0, \tag{101}$$

let

$$j(r) = e^{-(\Phi+\Lambda)} = e^{-\Phi(r)}\sqrt{1 - \gamma(r)}, \tag{102}$$

where $\gamma(r)$ is

$$\gamma(r) = 1 - \frac{2m(r)}{r}, \tag{103}$$

to express coefficient of $\overline{\omega}$ in terms of the unperturbed metric functions, differentiating equation (102), one gets

$$\frac{dj(r)}{dr} = -4\pi r\frac{[\epsilon(r) + P(r)]}{\sqrt{1 - \gamma(r)}}e^{\Phi(r)}, \tag{104}$$

where equation (74) is used and $d\Phi/dr$ is plugged as follows

$$\frac{d\Phi}{dr} = -\frac{1}{\epsilon(r) + P(r)}\frac{dP(r)}{dr}. \tag{105}$$

Now, simple algebraic manipulation in equation (100) leads to

$$\frac{1}{r^4}\frac{\partial}{\partial r}(r^4 j\frac{\partial\overline{\omega}}{\partial r}) + \frac{4}{r}\frac{dj}{dr}\overline{\omega} + \frac{e^{\lambda-\nu}}{r^2 sin^3\theta}\frac{\partial}{\partial\theta}(sin^3\theta\frac{\partial\overline{\omega}}{\partial\theta}) = 0. \tag{106}$$

Expanding ω in vector spherical harmonics

$$\overline{\omega}(r,\theta) = \Sigma_{l=1}^{\infty}\overline{\omega}_l(r)(-\frac{1}{sin\theta}\frac{dP_l}{\partial\theta}), \tag{107}$$

$\overline{\omega}_l(r)$ satisfies

$$\frac{1}{r^4}\frac{d}{dr}(r^4 j(r)\frac{d\overline{\omega}(r)}{dr}) + (\frac{4}{r}\frac{dj(r)}{dr} - e^{\lambda-\nu}\frac{l(l+1)-2}{r^2})\overline{\omega}_l(r) = 0. \tag{108}$$

For *l* = 1 and r $<$ R this yields

$$\frac{d}{dr}(r^4 j(r)\frac{d\overline{\omega}_l(r)}{dr}) + 4r^3\frac{dj(r)}{dr}\overline{\omega}(r) = 0. \tag{109}$$

Equation (109) is to be integrated from the center of the neutron star towards the surface under the boundary conditions that are

i) $\overline{\omega}$ must be regular at the center where r = 0.

ii)$\frac{\overline{d\omega}}{dr}$ vanishes at r = 0.

For numerical calculations an arbitrary value of ω is selected at the origin of the neutron star and integration takes place from there, towards the surface. Outside the neutron star $\overline{\omega}$ has the behavior

$$\overline{\omega}(r,\Omega) = \Omega - \frac{2}{r^3}J(\Omega), \tag{110}$$

where Ω is the rotation of the neutron star and J(Ω) is the angular momentum of the neutron star. The angular momentum can also be given by

$$J(\Omega) = \frac{R^4}{6}(\frac{d\overline{\omega}}{dr})_R, \tag{111}$$

$$J(\Omega) = I(\Omega)\Omega, \tag{112}$$

where R is the radius of the neutron star. Once $d\overline{\omega}/dr$ is calculated, the angular momentum can be calculated by equation (111) and the moment of inertia from equation (112).

Monopole equations The monopole equations (l = 0) can be calculated once $\overline{\omega}$ has been calculated from equation (109). These equations are helpful to determine the extra mass and the pressure on the neutron star due to rotation. By

$$G_t^t = 8\pi T_t^t, \tag{113}$$

$$G_r^r = 8\pi T_r^r, \tag{114}$$

the monopole mass, m_0 and the pressure perturbation, p_0, equations are coupled by,

$$\frac{dm_0}{dr} = 4\pi r^2 \frac{\partial \epsilon}{\partial P}(\epsilon + P)p_0 + \frac{1}{12}j^2 r^4 (\frac{d\overline{\omega}}{dr})^2 + \frac{8\pi r^4 j^2 (\epsilon + P)\overline{\omega}^2}{3(1-\gamma)}, \tag{115}$$

$$\frac{dp_0}{dr} = -\frac{(1+8\pi r^2 P)}{r^2(1-\gamma)^2}m_0 - 4\pi\frac{\epsilon + P}{1-\gamma}rp_0 + \frac{1}{12}\frac{r^3 j^2}{1-\gamma}(\frac{d\overline{\omega}}{dr})^2 + \frac{1}{3}\frac{d}{dr}(\frac{r^2 j^2 \overline{\omega}^2}{1-\gamma}). \tag{116}$$

Equations (115) and (116) are to be integrated from the center of the neutron star toward the surface under the boundary conditions $m_0 \to 0$ and $p_0 \to 0$ when $r \to 0$, to determine the pressure perturbation function and the mass perturbation function which will lead us to determine the extra mass the neutron star gets due to rotation.

Near r $\to$ 0 the pressure and mass perturbation functions have following behavior

$$p_0(r) \to \frac{(j_c \overline{\omega_c} r)^2}{3}, \tag{117}$$

$$m_0(r) \to \frac{4\pi(\epsilon + P)}{15}[2 + \frac{\partial \epsilon}{\partial P}]_c (j_c \overline{\omega})^2 r^5, \tag{118}$$

where 'c' subscript indicates the value at the center and $'j'$ is taken from equation (102). Let ΔM be the increment in mass due to rotation. One finds at r = R (surface)

$$\Delta M = m_0(\Omega) + \frac{1}{R^3}J(\Omega)^2, \tag{119}$$

where ΔM depends on the rotational velocity of the neutron star. Typically the value of ΔM is very small in comparison to the total mass of the neutron star, which is why it has been ignored by most authors.

Quadrupole equations - The quadrupole equations are essential to determine the shape and deformation of the neutron star caused by rotation. These equations can be solved once $\overline{\omega}$ has been calculated. The quadrupole differential equations are formed by the following field equations

$$R^{\theta}_{\theta} - R^{\phi}_{\phi} = 8\pi(T^{\theta}_{\theta} - T^{\phi}_{\phi}), \tag{120}$$

$$G^{r}_{r} = 8\pi P, R^{\theta}_{r} = 0. \tag{121}$$

One gets the following differential equations

$$\frac{dv_2}{dr} = -2\frac{d\phi}{dr}h_2 + (\frac{1}{r} + \frac{d\phi}{dr})(\frac{-r^3}{3}\frac{dj^2}{dr}\overline{\omega}^2 + \frac{j^2r^4}{6}(\frac{d\overline{\omega}}{dr})^2), \tag{122}$$

and

$$\begin{aligned}\frac{dh_2}{dr} = (-2\frac{d\phi}{dr} + \frac{2}{1-\gamma}(\frac{d\phi}{dr})^{-1}(2\pi\kappa(\epsilon+P) - m/r^3))h_2 \\ -\frac{2}{r^2(1-\gamma)}(\frac{d\phi}{dr})^{-1}v_2 + \frac{1}{6}(r\frac{d\phi}{dr} - \frac{1}{2r(1-\gamma)}(\frac{d\phi}{dr})^{-1})r^3j^2(\frac{d\overline{\omega}}{dr})^2 \\ -\frac{1}{3}(r\frac{d\phi}{dr} + \frac{1}{2r(1-\gamma)}(\frac{d\phi}{dr})^{-1})(r\overline{\omega})^2\frac{dj^2}{dr}.\end{aligned} \tag{123}$$

Equations (122) and (122) are to be integrated from the center of the star towards the surface under the boundary conditions $h_2(0) = 0, v_2(0) = 0$ and $h_2(\infty) = 0, v_2(\infty) = 0$.

Unlike the monopole equations, the quadrupole equations are more complex to solve. As $r \to 0$, functions h_2 and v_2 have following behavior

$$h_2(r) \to A_2r^2, v_2(r) \to B_2r^4, \tag{124}$$

where A_2 and B_2 are constants with dimensions, m^{-2} and m^{-4} and they must be selected such that they obey

$$B_2 + 2\pi A_2(P_c + \epsilon_c/3) = \frac{-4\pi}{3}(\epsilon_c + P_c)(j_c\overline{\omega_c})^2, \tag{125}$$

to get the particular solution. And for the homogeneous solution,
near $r \to 0$

$$h_2^{(h)}(r) \to \alpha r^2, v_2^{(h)}(r) \to \beta r^4, \tag{126}$$

where α and β are constant with dimensions m^{-2} and m^{-4}, respectively. They are to be chosen such that they follow

$$\beta + 2\pi\alpha(P_c + \epsilon_c/3) = 0. \tag{127}$$

The general solution of the functions h_2 and v_2 is the combination of the particular solution and the homogeneous solution.

$$\begin{aligned} v_2(r) &= C_2 v_2^{(h)} + v_2^p, \\ h_2(r) &= C_2 v_2^{(h)} + h_2^p. \end{aligned} \tag{128}$$

The exterior solutions of the quadrupole equations are given by

$$\begin{aligned} v_{2ext} &= -(\frac{J}{r^2})^2 + \alpha\frac{\gamma}{\sqrt{1-\gamma}}Q_2^1(\frac{2}{\gamma} - 1), \\ h_{2ext} &= (\frac{J}{r^2})^2(1 + \frac{2}{\gamma}) + \alpha Q_2^2(\frac{2}{\gamma} - 1), \end{aligned} \tag{129}$$

where Q_2^1 and Q_2^2 are Legendre polynomials of the second kind (y>1)

$$\begin{aligned} Q_2^1(y) &= \sqrt{y^2-1}(\frac{3y^2-2}{y^2-1} - \frac{3y}{2}\log\frac{y+1}{y-1}), \\ Q_2^2(y) &= \frac{3}{2}(y^2-1)\log\frac{y+1}{y-1} - \frac{3y^3-5y}{y^2-1}, \end{aligned} \tag{130}$$

exterior solution of the quadrupole function $h_{2ext}(R)$, i.e equation (129) and interior solution $h_2(R)$, i.e equation (128) and their first derivatives are to be matched at the surface of the neutron star in order to get the values of C_2 and K.

$$h_2(R) = h_{2ext}(R), \frac{d}{dr}h_2(R) = \frac{d}{dr}h_{2ext}(R). \tag{131}$$

These are the values that are required to determine the quadrupole moment and the eccentricity of the rotating neutron star.

Once α has been calculated, then the quadrupole moment is calculated by

$$Q = \frac{J^2}{m} + \frac{8\alpha m^3}{5}, \tag{132}$$

and the eccentricity is given by

$$e(r) = \frac{3(r-2m)}{2m}[h_2(r) + \frac{r^3}{3(r-2m)}(\Omega - \frac{2J}{r^3})^2]. \tag{133}$$

4.2.3 Tidal Love number and tidal deformability

To determine the tidal Love number and tidal deformability Hinderer and Flanagan's [158][159][160] method is taken into consideration. Suppose a spherically symmetric, static neutron star is placed in an external tidal quadrupole field (ϵ_{ij}) and in response the neutron star develops a tidal quadrupole moment (Q_{ij}). The the star's tidal deformability is λ

$$Q_{ij} = -\lambda\epsilon_{ij}. \tag{134}$$

The tidal deformability and the tidal Love number (k_2) are related by

$$\lambda = \frac{2}{3}k_2R^5. \tag{135}$$

The quadrupole moment developed in response to an external tidal field is the coefficient of the asymptotic expansion of total metric at a large distance from the star

$$-(\frac{1+g_{tt}}{2}) = -\frac{m}{r} - \frac{3Q_{ij}}{2r^3}n^in^j + ... + \frac{\epsilon_{ij}}{2}r^2n^in^j + ..., \tag{136}$$

where n^i = x^i/r and Q_{ij}& ϵ_{ij} both are traceless and symmetric. To compute the tidal Love number, following the work of Ref. [159], the perturbation metric of a spherically symmetric star in a tidal field in Regge Wheeler gauge [161] is simplified [158] as

$$\begin{aligned} ds^2 = -e^{2\Phi(r)}[1 + H(r)Y_{20}(\theta,\phi)]dt^2 + e^{2\Lambda(r)}[1 - H(r)Y_{20}(\theta,\phi)]dr^2 \\ +r^2[1 - k(r)Y_{20}(\theta,\phi)](d\theta^2 + sin^2\theta d\phi^2), \end{aligned} \tag{137}$$

where H and Y_{20} are the factors introduced by Regge-Wheeler gauge transformation (even parity perturbation) and K is connected to H by the relation

$$\frac{dK}{dr} = \frac{dH}{dr} + 2H\frac{d\Phi'}{dr}. \tag{138}$$

In equation (137), the azimuthal number 'm' is set to be zero without the loss of generality, because the tidal deformation will be symmetric around the axis connecting the two neutron stars, which is the axis of spherical harmonic decomposition.

The perturbation in stress-energy tensor components of a perfect fluid are

$$\begin{aligned} \delta T_0^0 &= -\delta\epsilon(r)Y_{20}(\theta,\phi), \\ \delta T_i^i &= \delta p(r)Y_{20}(\theta,\phi), \end{aligned} \tag{139}$$

where $\delta\epsilon$ and δp are changes in the energy density and pressure. The function H(r) is the solution of the differential equation

$$[-\frac{6e^{2\Lambda}}{r^2}-2(\Phi')^2+2\Phi''+\frac{3}{r}\Lambda'+\frac{7}{r}\Phi'-2\Phi'\Lambda'+\frac{f}{r}(\Phi'+\Lambda')]H+[\frac{2}{r}+\Phi'-\Lambda']H'+H''=0, \tag{140}$$

where f is $f = \delta\epsilon/\delta p$ and for slow changes in fluid configuration gives

$$f = \frac{d\epsilon}{dp}. \tag{141}$$

With the help of equations (57,71,72,76), equation (140) can be simplified into two first order differential equation as follows,

$$\frac{dH}{dr} = \beta \tag{142}$$

$$\begin{aligned} \frac{d\beta}{dr} = 2(1-2\frac{m}{r})^{-1}H[-2\pi(5\epsilon+9p+(\epsilon+p)f)+\frac{3}{r^2}+2(1-2\frac{m}{r})^{-1}(\frac{m}{r^2}+4\pi rp)^2] \\ +2\frac{\beta}{r}(1-2\frac{m}{r})^{-1}[-1+\frac{m}{r}+2\pi r^2(\epsilon-p)]. \end{aligned} \tag{143}$$

Equations (142 & 143) are to be integrated from just outside the center of the neutron star to the surface with the equations (57,71,72,76) . The expansion just

outside the center $H(r)$ = $a_0 r^2$ and $\beta(r)$ = $2a_0 r$, where 'r' is very small, $r \to 0$ and a_0 is the expansion factor which can be chosen to be arbitrary because it cancels in the end in the tidal Love number expression. Outside the neutron star $H(r)$ has a general solution in terms of the second order Legendre function, for large values of 'r'.

$$H = C_1 Q_2^2(r/M - 1) + C_2 P_2^2(r/M - 1) \tag{144}$$

and its coefficients ($C_1 \& C_2$) can be obtained by comparing its asymptotic expansion with equation (136) using equation (134) in terms of λ

$$C_1 = \frac{15}{8M^3}\lambda\epsilon, C_2 = \frac{M^2\epsilon}{3}. \tag{145}$$

Now, substituting the values of C_1 and C_2 in equation (144) one can solve for λ by matching the exterior solution (equation (144)) with the interior solutions (equation (140)) and their first derivatives, at the surface (r = R). Suppose, $C = M/R$ and $y = R\beta(R)/H(R)$. The tidal Love number can be calculated by using equation (135) as

$$k_2 = \frac{8C^5}{5}(1-2C)^2[2+2C(y-1)-y] \times [2C(6-3y+3C(5y-8))+ 4C^3(13-11y+C(3y-2)+2C^2(1+y))+3(1-2C)^2(2-y+2C(y-1)) \times \log(1-2C)]^{-1}. \tag{146}$$

Once k_2 has been calculated then the tidal deformability (λ) can be calculated by the equation (135).

5 Results

In this section the properties of neutron stars are calculated for the energy density from 0 to 1200 MeV/fm^3 for three EoSs and results are compared systematically. N-QMC700 and F-QMC700 EoSs are based on the parameterizations given in Table 2, while the third EoS is for strange matter (MIT), taken from reference [165].

5.1 Pressure and energy density relation

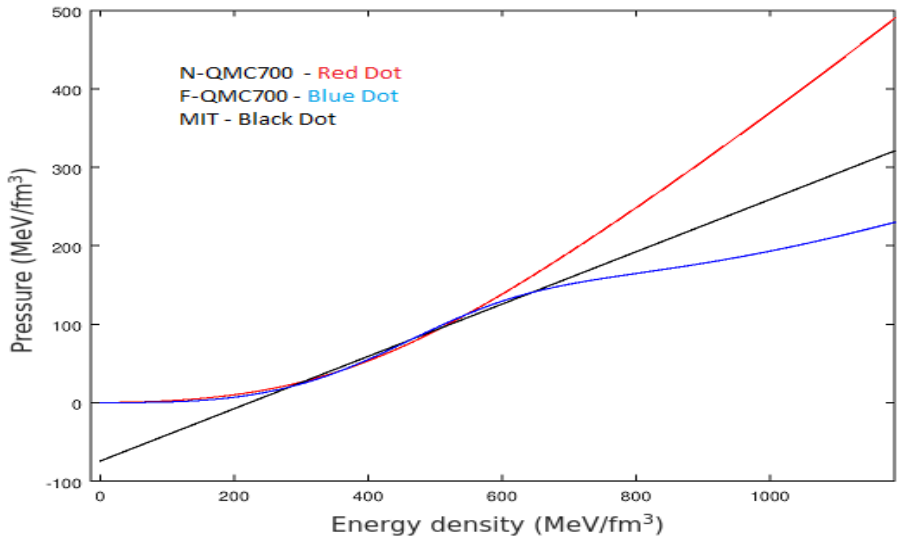

Figure 4: Pressure-energy density plot for different matter compositions. Strange star EoS is poorly behaving at the lower energy densities. Pressure is zero at the energy density 223.8 Mev/fm^3 for strange matter EoS.

Fig. 4 represents the pressure and energy relation, for all three chosen EoSs. The strange matter EoS (MIT - black dot) is unphysical in the low energy density region (at the crust). In particular, pressure is negative below the energy density 223.8 MeV/fm^3. Here, a key point must be stated, i.e. in the low energy density region, there is only nuclear matter, strange matter or hyperons only come into the

existence when the energy density increases a few times the nuclear matter density (at the core) and the chemical potential is favorable for their existence. All of them have only nuclear matter at low energy density, so they must show a similar characteristic in the region. As energy density increases, around 580 MeV/fm^3, F-QMC700 starts to deviate from the N-QMC700 and shows a softer EoS, because hyperons (Ξ^-, Λ, Ξ^0) start to develop at this point (see Ref. [154]). On the other hand the strange matter EoS, which is rather stiffer than former EoS and around the energy density 300 MeV/fm^3 and 500 MeV/fm^3 crosses the nucleons only matter EoS and at (one of) these energy densities it predicts to develop strange matter (deconfined quarks) which leads to a strange star. N-QMC700 is the most stiff EoS which is based on nucleon only matter. It does not show development of hyperons or strange matter at all.

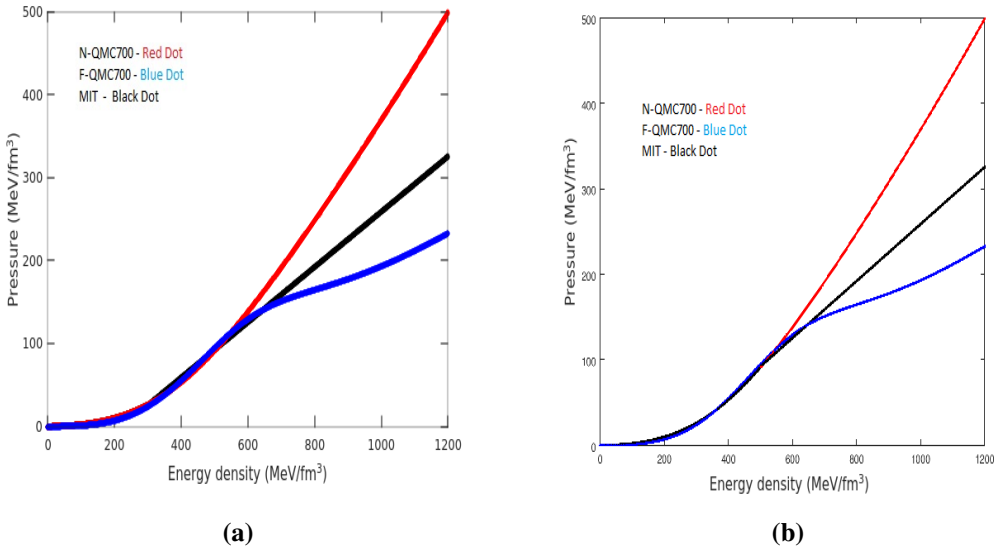

Figure 5: (a) Pressure-Energy density plot for different matter compositions with strange matter parameters changed to nucleons only EoS parameters for the lower energy densities below 300 MeV/fm^3, (b) Pressure-Energy density plot for different matter compositions with strange matter parameters changed to nucleons only EoS parameters for the lower energy densities below 500 MeV/fm^3

In Fig. 5, the strange matter EoS is corrected for the low energy density region with the parameters of nucleons only EoS (N-QMC700). In Fig. 5(a), the strange matter EoS parameters are matched to the nucleon only EoS parameters for the energy densities below 300 MeV/fm^3 and in Fig. 5(b), the nucleons only EoS is used up to 500 Mev/fm^3 in the same way and above that energy density strange matter EoS is used. Here, we are comparing two possibilities. First, when the strange matter starts to exist at 300 MeV/fm^3 and second, when the strange matter comes into existence at 500 MeV/fm^3. In Fig. 5, all three EoSs now show the same characteristic at the low energy densities.

5.2 Relation of mass with radius and compactness

Predicting the maximum mass of a neutron star is an important constraint on the EoS. Fig. 6 gives the relation between the mass and the radius. Although the strange matter EoS predicts a maximum mass of over 2 $M\odot$, it poorly predicts the mass and the radii of the neutron stars at the low energy densities. At the crust, where the energy density is low and stars are not so compact (compared to the core), it must show an expansion in the radius, like the N-QMC700 and F-QMC700 are showing. Fig. 7 and Fig. 8 are the figures with parameters for the strange stars at the low energy densities, below 300 MeV/fm^3 and 500 MeV/fm^3, are fixed to the nucleons only EoS parameters (N-QMC700) respectively. This means that up to the energy density 300 MeV/fm^3 and 500 MeV/fm^3 in Fig. 7 & 8, there are only nucleons while the strange matter come into existence at higher densities with this change the behavior of all the three EoS show similar radii at the low energy densities. And at the high energy densities, F-QMC700, which is rather softer than the other two EoSs, predicts a maximum mass of 1.999 $M_\odot$, whereas N-QMC700 EoS predicts a maximum mass of 2.226 $M_\odot$. Finallly, the strange matter EoS predicts a maximum mass of 2.121$M_\odot$ and 2.004 $M_\odot$ in both the possibilities, as shown in Fig. 7 and Fig. 8. But the strange star radii have

significantly changed between the energy density region 300-1200 MeV/fm^3 as shown in Fig. 8, if quark deconfinement takes place at the 500 MeV/fm^3 all the EoSs show similar relationship between the mass and the radius. They only differ near the maximum mass. Whereas in Fig. 7, if deconfinement takes place at the energy density 300 MeV/fm^3 the mass and the radius relationship is significantly different than N-QMC700 and F-QMC700. And as the energy density increases, neutron stars get heavy and their cores become more stiff. Eventually, at a critical point, they collapse into the black holes.

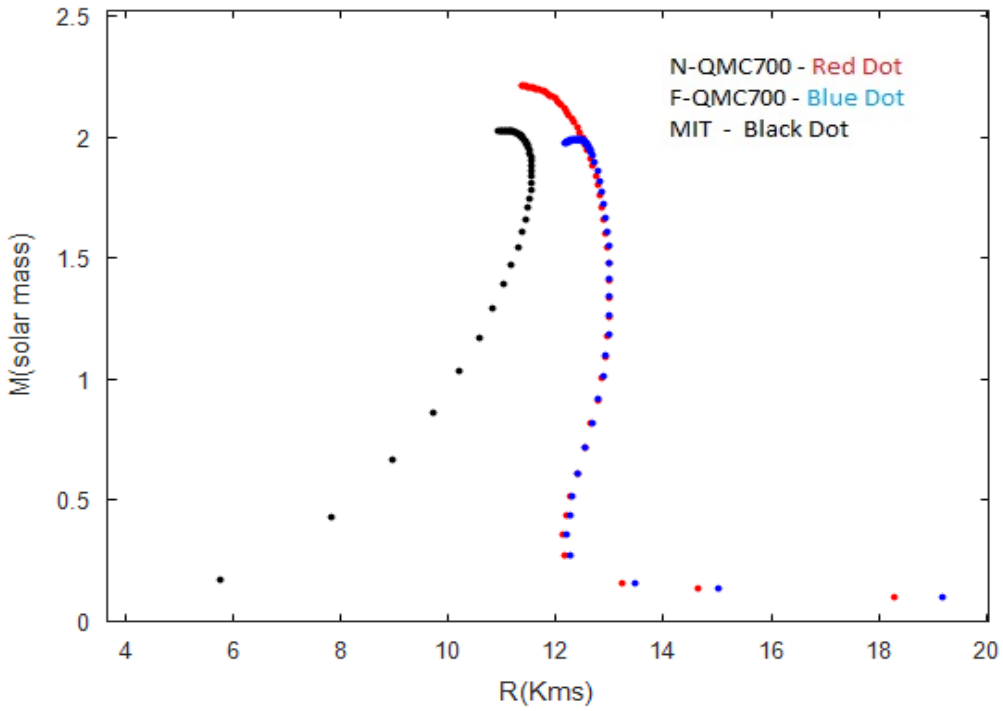

Figure 6: Mass vs Radius plot for different matter compositions without changing parameters for strange matter EoS (MIT) at the lower energy densities.

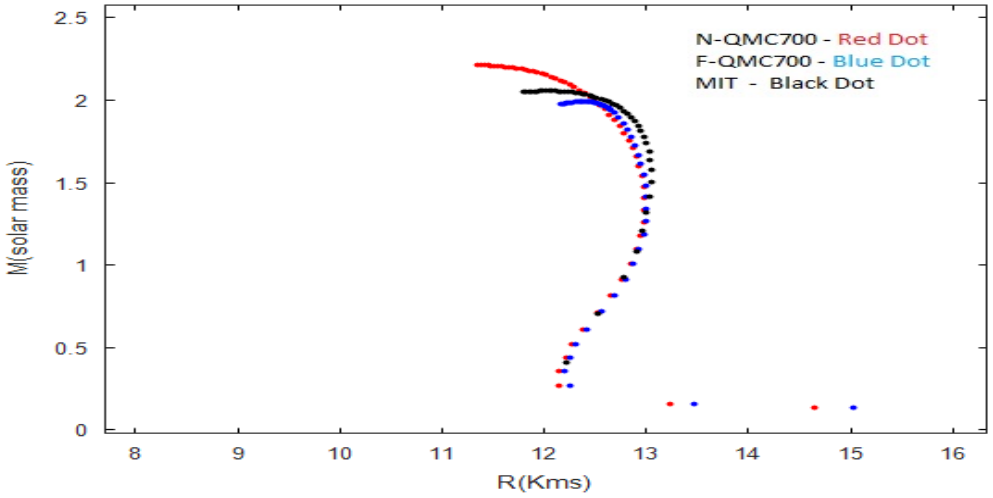

Figure 7: Mass vs Radius plot for different matter compositions with strange matter EoS parameters changed to nucleons only EoS parameters for the lower energy densities below 300 MeV/fm^3.

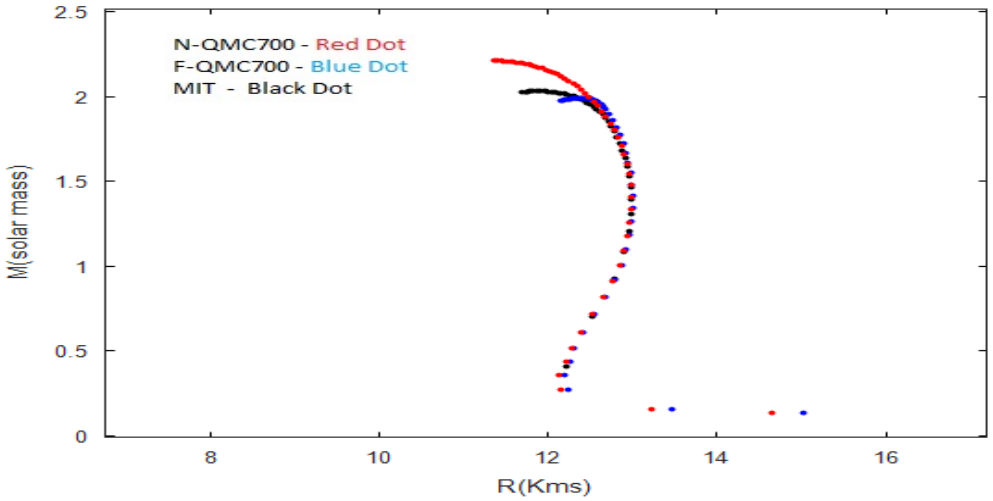

Figure 8: Mass vs Radius plot for different matter compositions with strange matter EoS parameters changed to nucleons only EoS parameters for the lower energy densities below 500 MeV/fm^3.

Fig. 9 depicts the mass and compactness relation without fixing parameters for

the strange matter EoS at the lower energy densities and behavior of the strange matter EoS is largely different than N-QMC700 and F-QMC700. Whereas in Fig. (10 & 11), with fixed parameters the mass and the compactness (R/2M) show a very similar behavior to N-QMC700 and F-QMC700. The compactness is more for the higher mass neutron stars. And when it reaches to a maximum mass, at that point neutron star is stiffest and if the mass (or the central energy density) is increased further the star will collapse. None of the EoSs allow R $\leq$ 3M which is the condition for extremely stiff black holes. At R = 3M, null geodesics are trapped inside (black holes) and nothing can come out of it (would not cool down by standard procedures [188]).

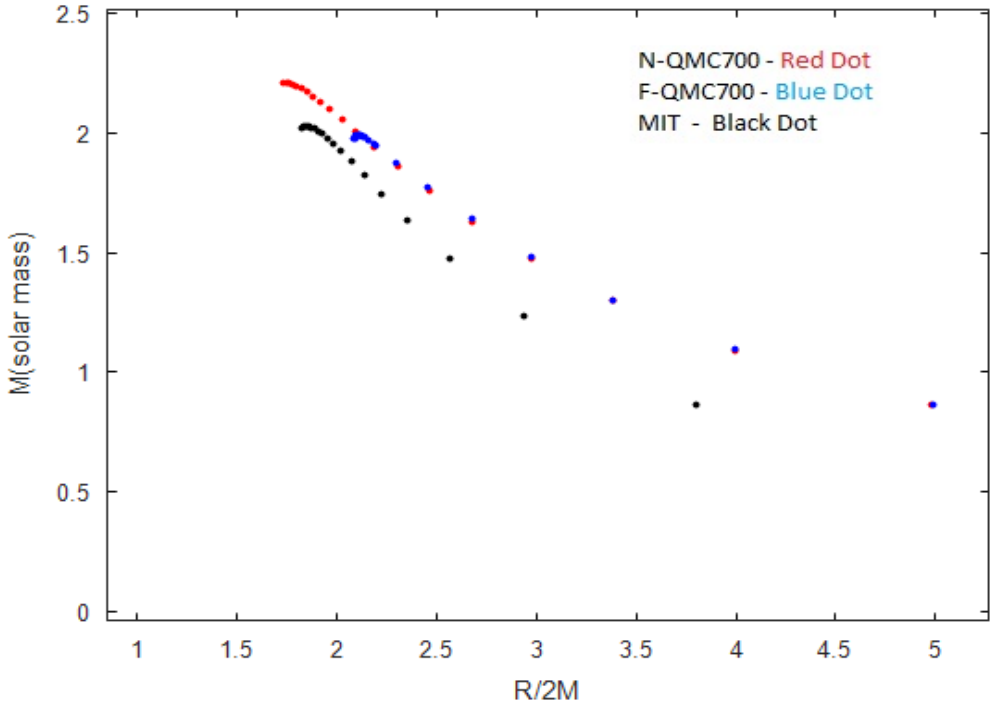

Figure 9: Mass vs Compactness plot for different matter composition without changing parameters of strange matter EoS at lower densities.

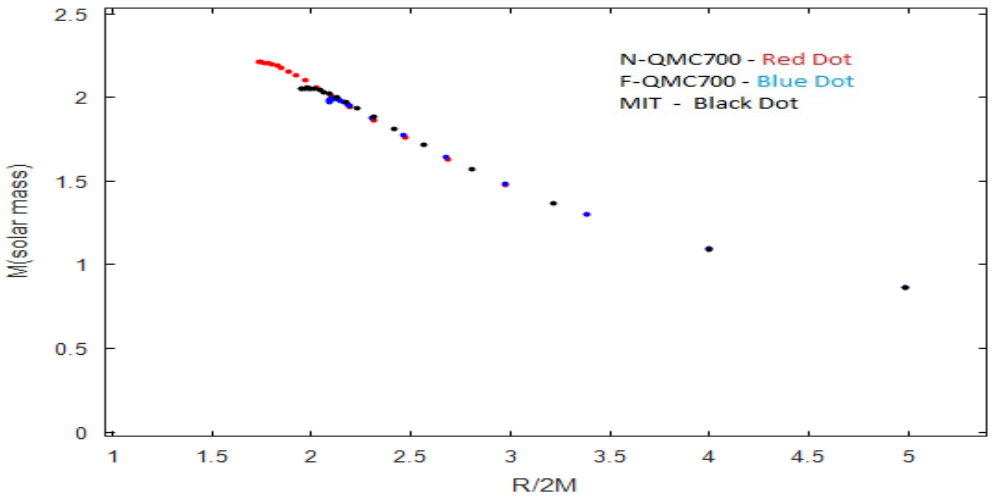

Figure 10: Mass vs Compactness plot for different matter compositions with strange matter EoS parameters changed to nucleons only EoS parameters for the lower energy densities below 300 MeV/fm^3.

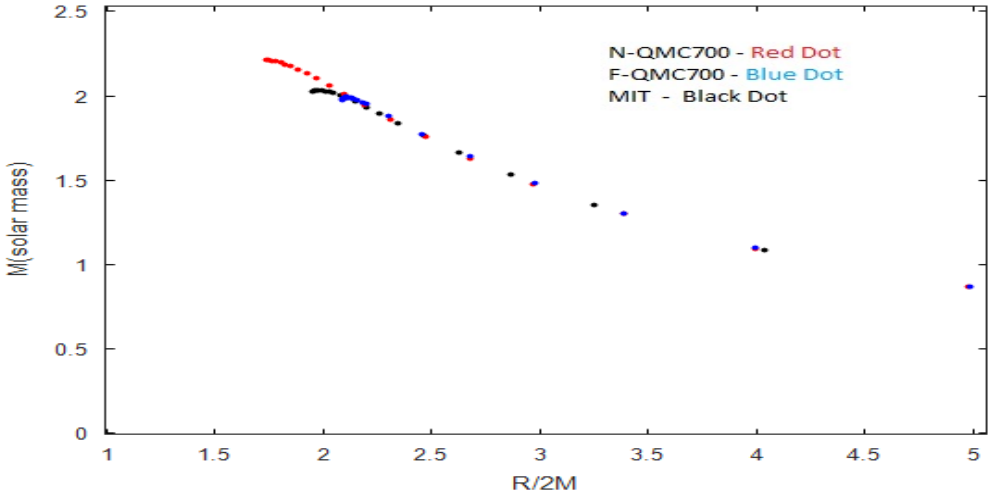

Figure 11: Mass vs Compactness plot for different matter compositions with strange matter EoS parameters changed to nucleons only EoS parameters for the lower energy densities below 500 MeV/fm^3.

5.3 Moment of inertia

In Fig. 12 the moment of inertia, which is calculated using the standard formula $I = \frac{J}{\Omega}$ (equation (112)), presented against mass for different EoSs. Since, the angular momentum is calculated only to the first order of Ω, dividing it by Ω gives a value which is independent of the rotational velocity (Ω) of the neutron star. In other words, the value of moment of inertia does not depend on the rotational velocity and only depends on the structure of a non-rotating neutron star. In this study, calculations have been done for the rotational velocity (Ω) 500 rotations/sec, which is high enough to see rotational effects on neutron star and low enough that it does not violate Hartle's method for the slow rotation.

In Fig. 12, we see that the moment of inertia for strange matter EoS is very different than N-QMC700 & F-QMC700. Whereas in Fig. 13 & 14 all three chosen EoSs yield similar values for the moment of inertia for the low mass (low energy density) neutron stars as the mass increases, around the value of maximum mass (at higher central energy densities), all the EoSs show different values for the moment of inertia. It was shown by Lattimer and Prakash [189], Bejger and Haesel [190], Lattimer and Schultz [158] that, the parameter of moment of inertia ($\frac{I}{M_0 R_0^2}$, where M_0 is the mass and R_0 is the radius of the neutron star) is related to compactness in such a way that the compactness vs moment of inertia parameter, is independent of EoSs and all of them fall almost on the same line. In Fig. 15, the moment of inertia and compactness is presented without changing parameters for the strange stars and compared to N-QMC700 $\&$ F-QMC700. We see that the moment of inertia parameter for the strange matter EoS is very different from N-QMC700 and F-QMC700 and it does not follow the moment of inertia constraint, while N-QMC700 and F-QMC700 EoS do. After fixing the parameters as shown in Fig. 16 and 17 at the lower energy densities (300 MeV/fm^3 & 500 MeV/fm^3) all three EoSs satisfy the relation independent of EoS. They fall almost on the same line [165].

As a further check, Fig. 18 shows the relation between the dimensionless mo-

ment of inertia ($\frac{I}{M^3}\frac{c^4}{G^2}$) and compactness ($M/R$). The strange matter EoS clearly deviates from the other two EoSs, while N-QMC700 and F-QMC700 both exhibit a Universal behavior. As the strange matter EoS parameters are fixed for the low energy densities 300 MeV/fm^3 & 500 MeV/fm^3, as shown in Fig. 19, the dimensionless moment of inertia and M/R factor plot for all EoSs fall almost on top of each other while in Fig. 20 all three EoSs show a relation independent of EoS as suggested in Ref. [191]. Accurate measurement of the mass with the help of Keplerian parameters and the precise measurement of the moment of inertia, can help us accurately measuring the radius [192].

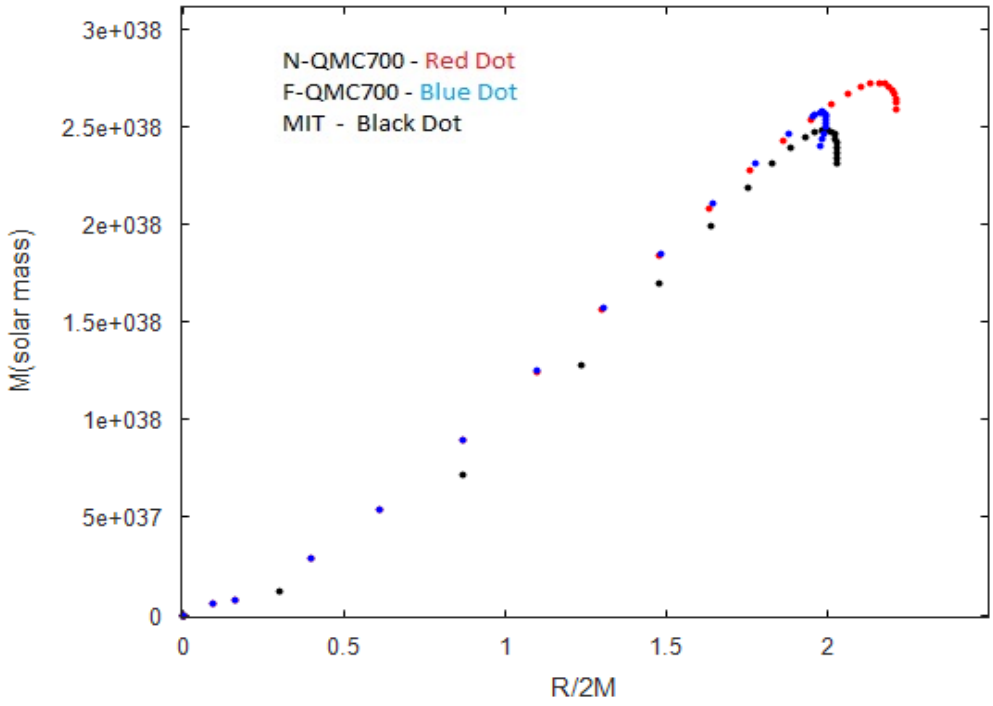

Figure 12: Moment of inertia vs Mass plot for different matter composition without changing parameters of strange matter EoS at lower densities.

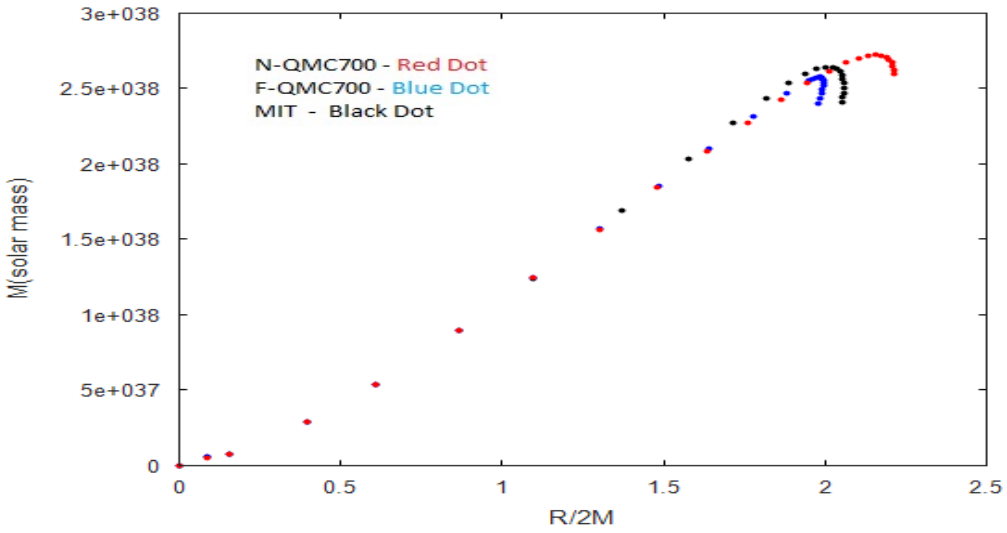

Figure 13: Moment of inertia vs Mass plot for different matter compositions with strange matter EoS parameters changed to nucleons only EoS parameters for the lower energy densities below 300 MeV/fm^3.

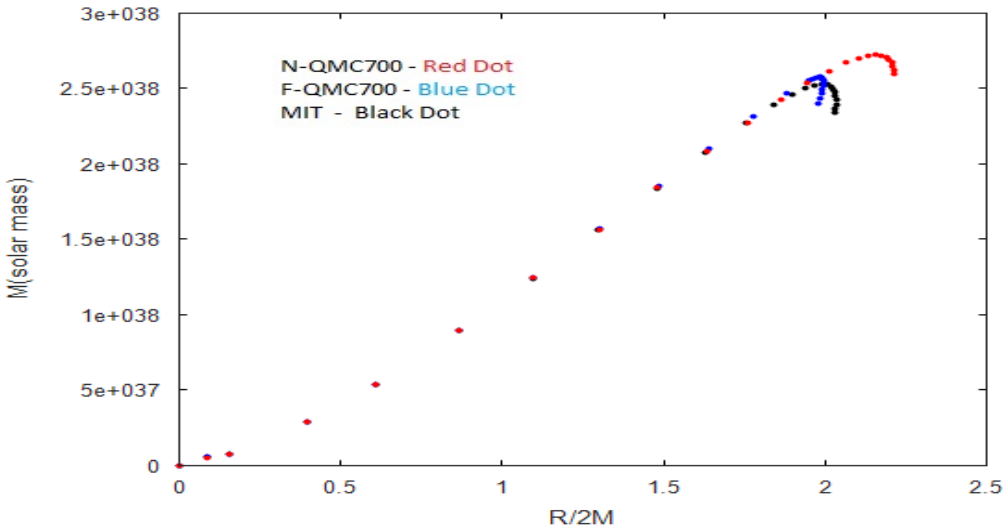

Figure 14: Moment of inertia vs Mass plot for different matter compositions with strange matter EoS parameters changed to nucleons only EoS parameters for the lower energy densities below 500 MeV/fm^3.

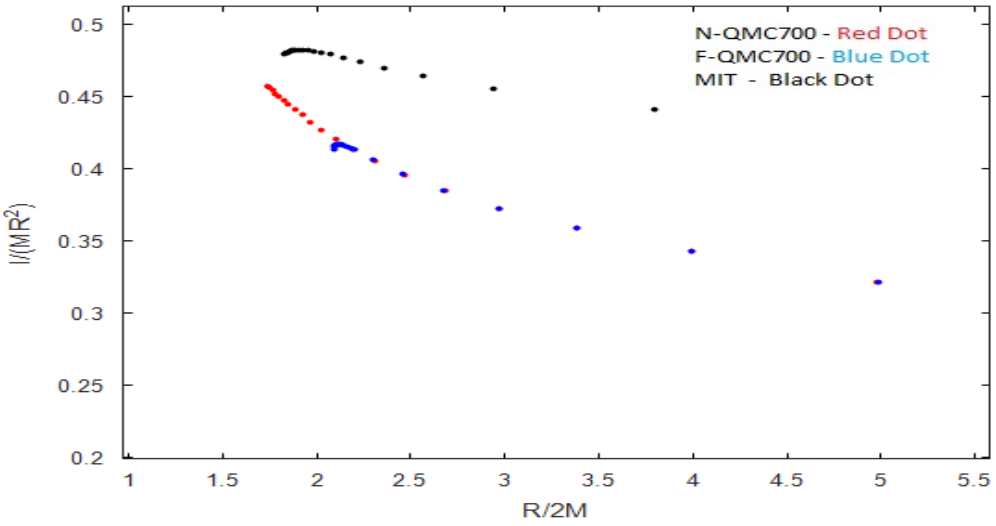

Figure 15: Moment of inertia parameter vs Mass plot for different matter composition without changing parameters of strange matter EoS at lower densities.

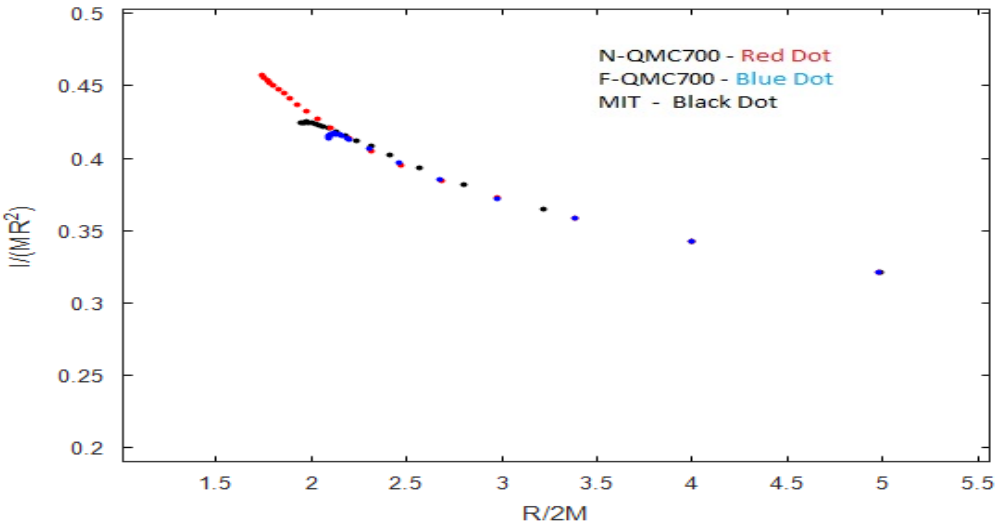

Figure 16: Moment of inertia parameter vs Mass plot for different matter compositions with strange matter EoS parameters changed to nucleons only EoS parameters for the lower energy densities below 300 MeV/fm^3.

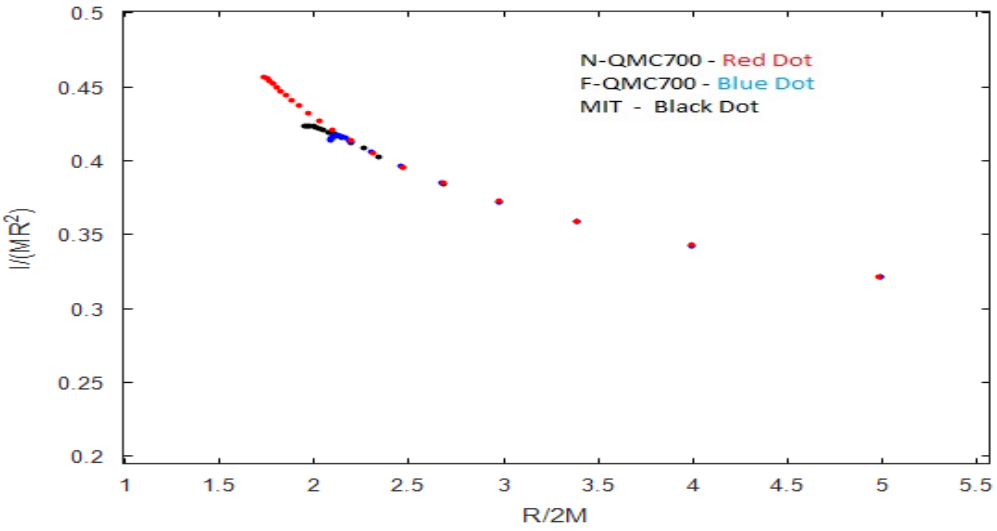

Figure 17: Moment of inertia parameter vs Mass plot for different matter compositions with strange matter EoS parameters changed to nucleons only EoS parameters for the lower energy densities below 500 MeV/fm^3.

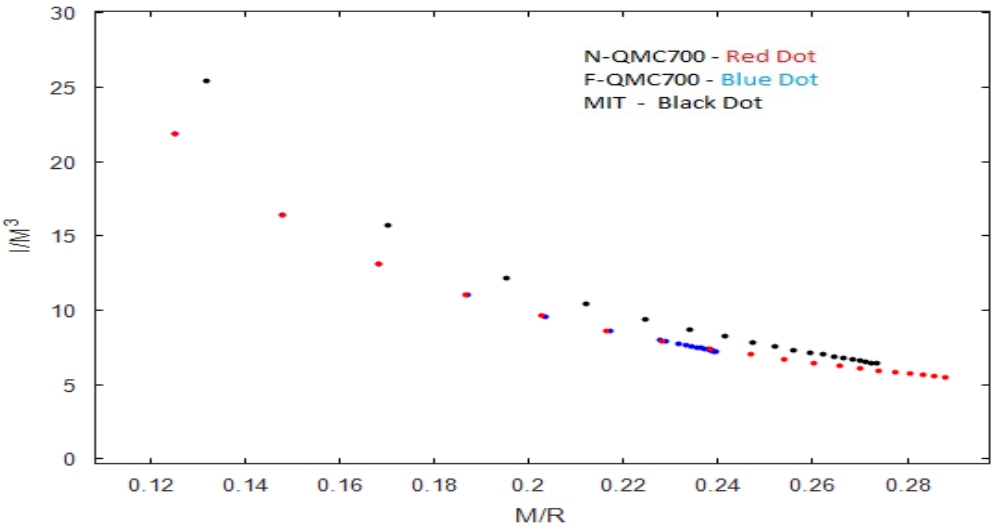

Figure 18: Dimensionless moment of inertia vs Mass/Radius plot for different matter composition without changing parameters of strange matter EoS at lower densities.

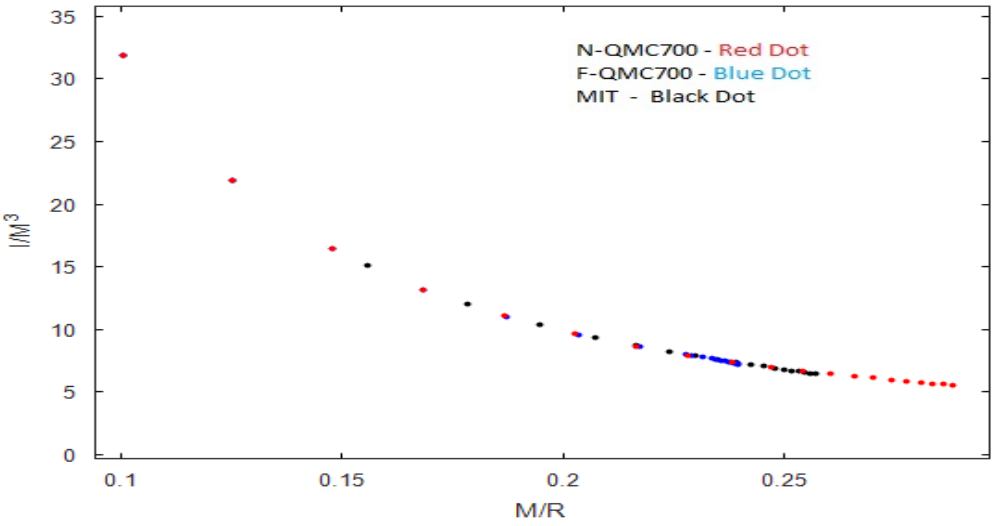

Figure 19: Dimensionless moment of inertia vs Mass/Radius plot for different matter compositions with strange matter EoS parameters changed to nucleons only EoS parameters for the lower energy densities below 300 MeV/fm^3.

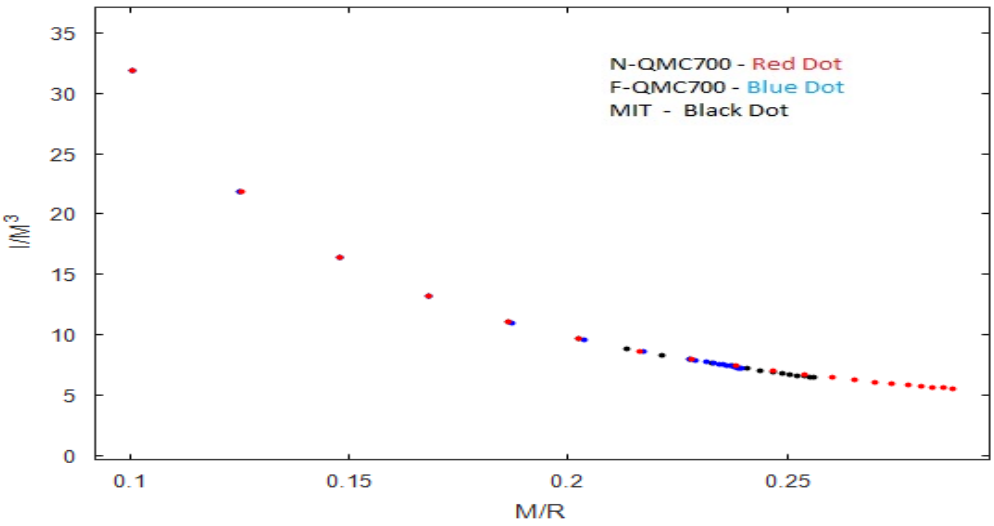

Figure 20: Dimensionless moment of inertia vs Mass/Radius plot for different matter compositions with strange matter EoS parameters changed to nucleons only EoS parameters for the lower energy densities below 500 MeV/fm^3.

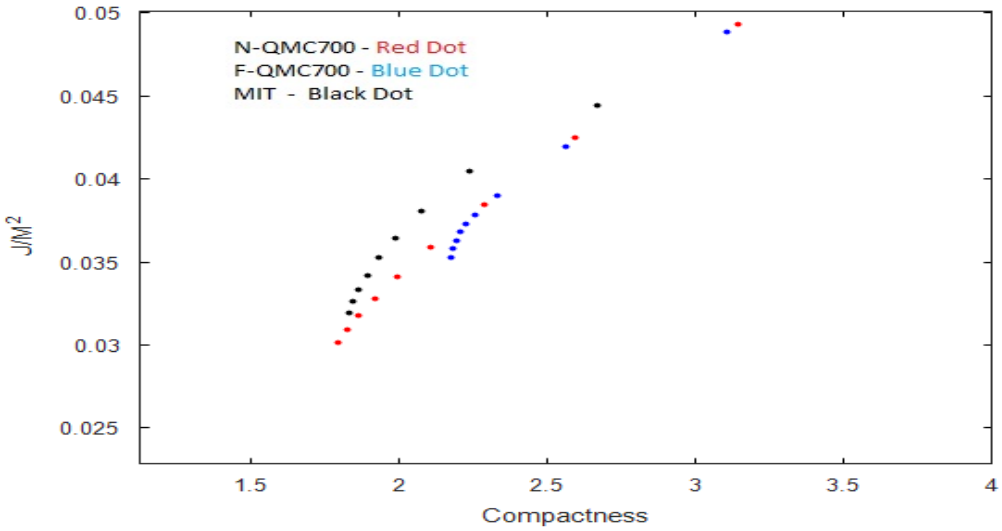

Figure 21: Dimensionless angular momentum vs Compactness plot for different matter composition without changing parameters for strange matter EoS at the lower energy densities.

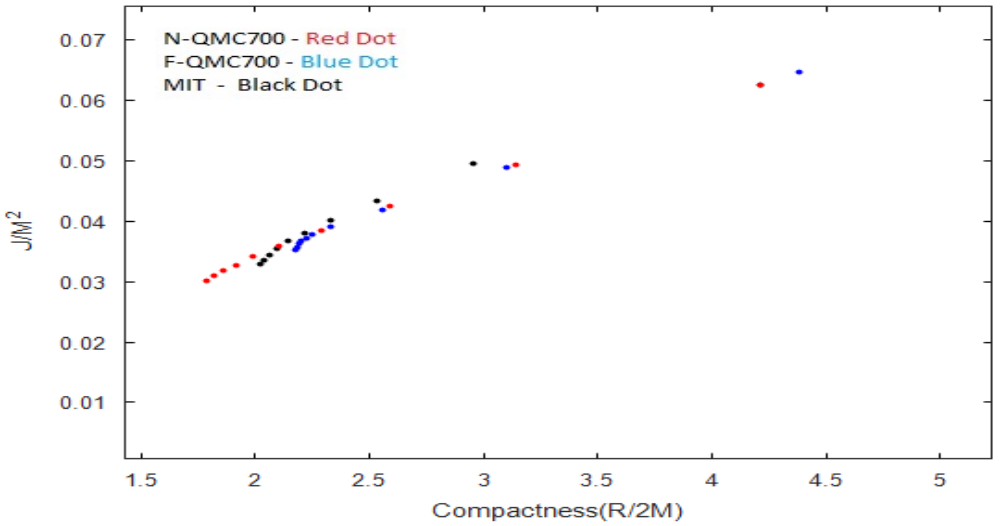

Figure 22: Dimensionless angular momentum vs Compactness plot for different matter compositions with strange matter EoS parameters changed to nucleons only EoS parameters for the lower energy densities below 300 MeV/fm^3.

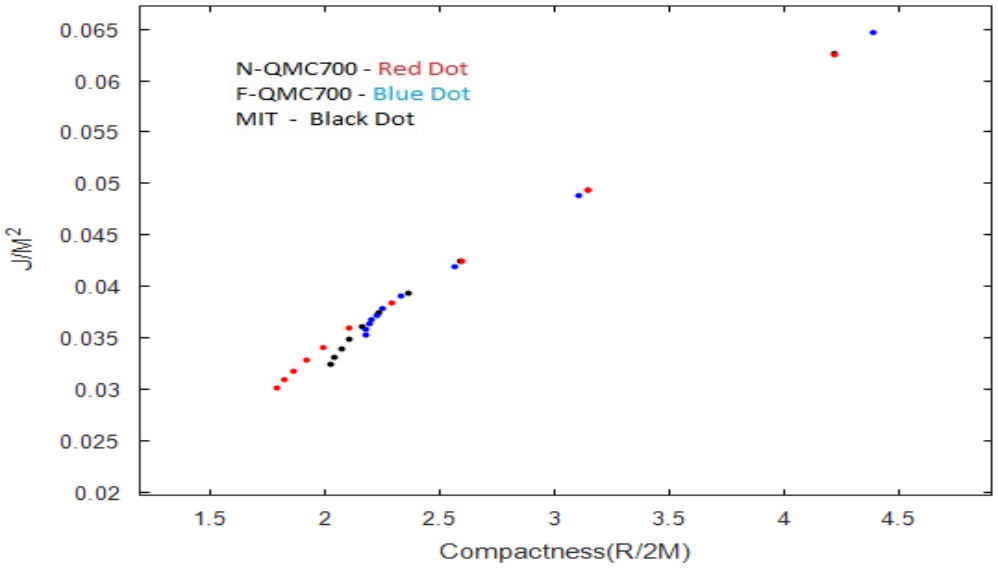

Figure 23: Dimensionless angular momentum vs Compactness plot for different matter compositions with strange matter EoS parameters changed to nucleons only EoS parameters for the lower energy densities below 500 MeV/fm^3

Fig. 21 shows the dimensionless angular momentum vs compactness for neutron stars which are rotating at frequency 500 Hz. At the higher energy densities at the core, the N-QMC700 and F-QMC700 EoSs show similar behavior, with the F-QMC700 deviating from the former only near the maximum compactness, while the strange matter EoSs shows higher values for dimensionless angular momentum than N-QMC700 and F-QMC700. In Fig. 22, after fixing the parameters for the strange matter EoS at the energy density below 300 MeV/fm^3, dimensionless angular momentum is still slightly higher than other two EoSs, while near the maximum allowed compactness (higher energy densities at the core) all three EoSs show very close values. In Fig. 23, we see that if strange matter comes into existence at the energy density 500 MeV/fm^3 then all three EoSs display same characteristic for angular momentum, only deviating near the maximum mass of the neutron star.

5.4 Relation of quadrupole moment with mass, compactness and dimensionless moment of inertia

The quadrupole moment of the rotating neutron star is another important quantity that determines the distribution of the mass and the deformation in shape of a neutron star. It plays an important role in determining the inner-most stable orbit of the low mass compact stars which can have significant effect on the quasi-periodic orbit, as suggested in Ref. [52]. It is important to include the quadrupole momentum particularly for the neutron stars that have mass close to 2 solar masses (maximum observed mass) [186][193]. As shown in Fig. 24, as the mass (or the central energy density) of the neutron stars increases, their quadrupole moment systematically decreases because the neutron stars become very compact. None of the EoSs allow dimensionless quadrupole moment (Kerr solution) = 1, which is the condition for black holes. For the low mass neutron stars the quadrupole moment is larger, which means that more deformation takes place. F-QMC700 and N-QMC700 EoSs both have larger quadrupole moment than strange matter (without changing parameters). This suggests that neutron stars with hyperons or nucleons present at the higher energy density are more deformed than the corresponding strange matter stars at that energy density. For the same reason the strange star dimensionless quadrupole moment is very different from the other EoSs. Near the maximum mass all EoSs are very close to having dimensionless quadrupole moment equal to 1 .

In Fig. 25 and 26 the dimensionless quadrupole momentum is presented with changed parameters for the strange matter EoS at the low energy densities. After fixing the parameter at 300 MeV/fm^3 and 500 MeVfm^3, all EoSs have almost similar values and show a Universal behavior (independent of EoSs) for both the cases. They only differ near the maximum mass of the neutron star.

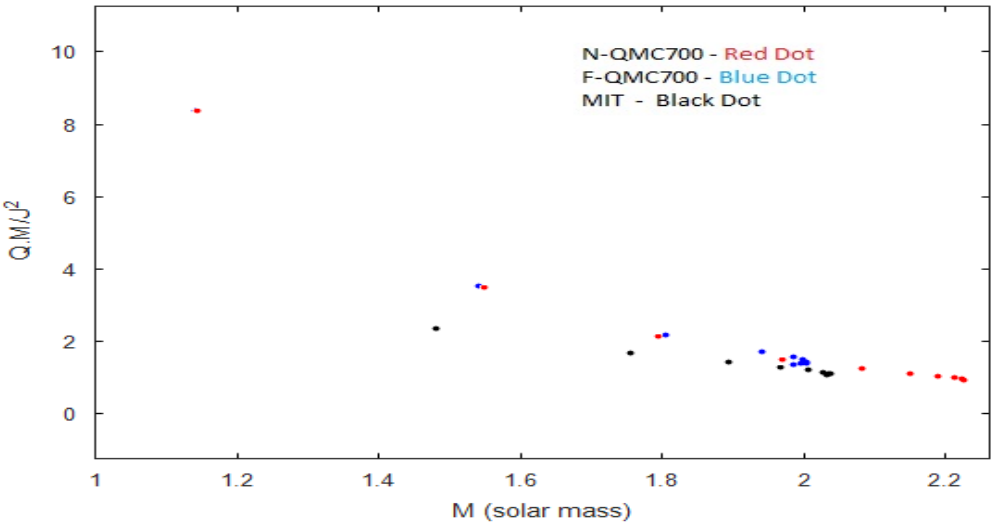

Figure 24: Dimensionless quadrupole momentum vs Mass for different matter composition without changing parameters of strange matter EoS.

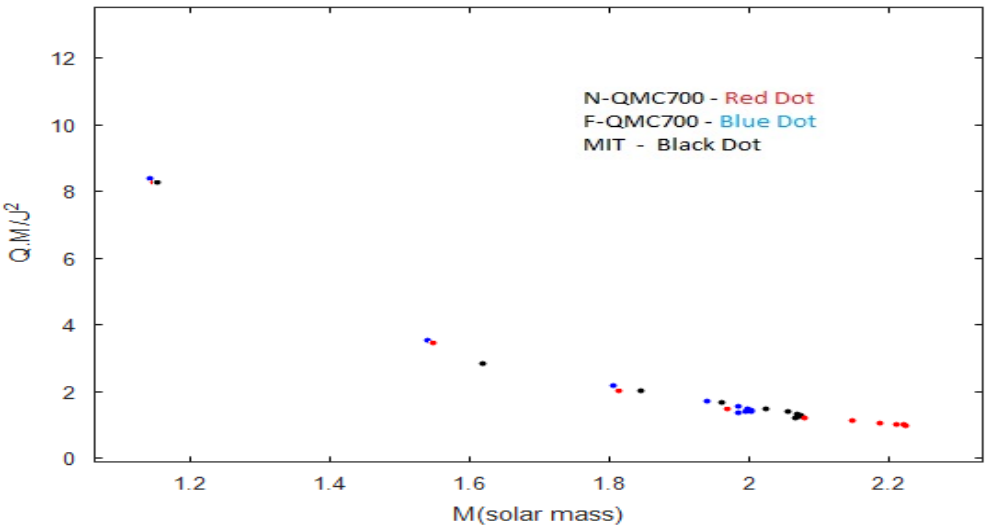

Figure 25: Dimensionless quadrupole momentum vs Mass for different matter compositions with strange matter EoS parameters changed to nucleons only EoS parameters for the lower energy densities below 300 MeV/fm^3.

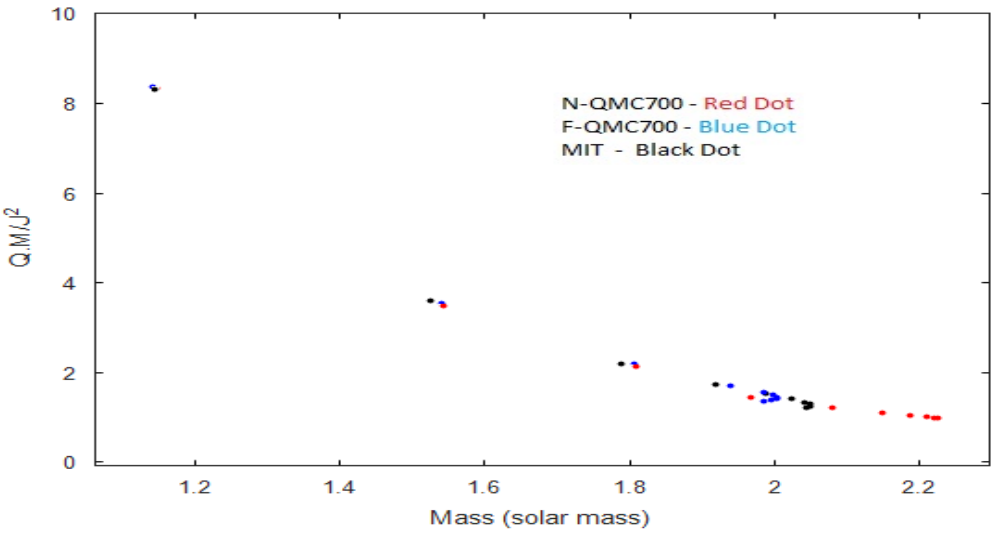

Figure 26: Dimensionless quadrupole momentum vs Mass for different matter compositions with strange matter EoS parameters changed to nucleons only EoS parameters for the lower energy densities below 500 MeV/fm^3.

As shown in Fig. 27, as the neutron stars reach near their maximum compactness their dimensionless quadrupole moments tend towards the value '1', which suggests that the neutron stars tend to become Schwarzschild black holes (at R/2M = 1.5, and the dimensionless quadrupole moment = 1). For low compactness neutron stars the strange star quadrupole moment is very different from N-QMC700 and F-QMC700. Some of the stiffest possible EoSs correspond to closest to Kerr solution are noted in References [194][195][165]. After fixing the parameters for strange matter EoS for the low energy densities in Fig. 28 and 29, the strange star display behavior similar to N-QMC700 and F-QMC700. The dimensionless quadrupole moment does not change much for the strange stars in both the condition about when strange degree of freedom comes in the picture at the energy density 300 MeV/fm^3 or 500 MeV/fm^3.

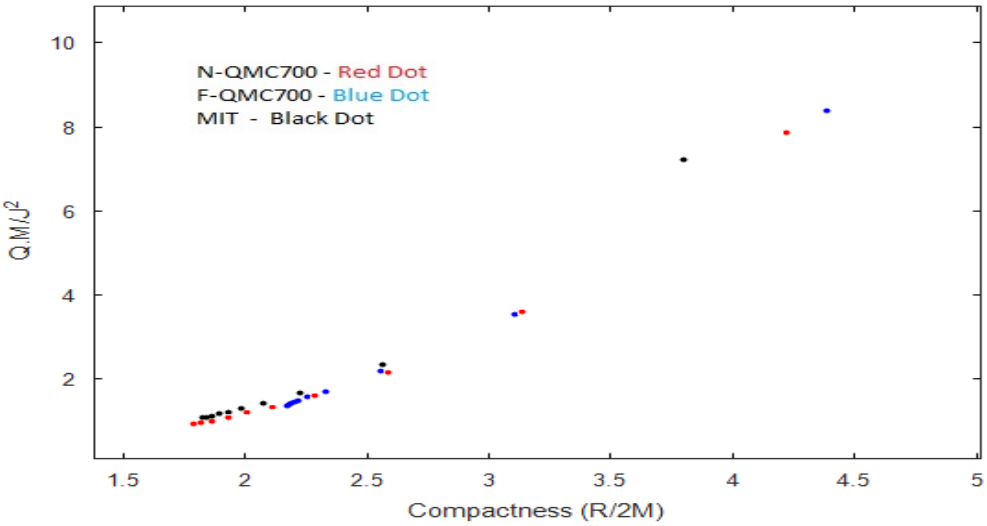

Figure 27: Dimensionless quadrupole momentum vs Compactness plot for different matter composition without changing parameters of strange matter EoS at the lower energy densities.

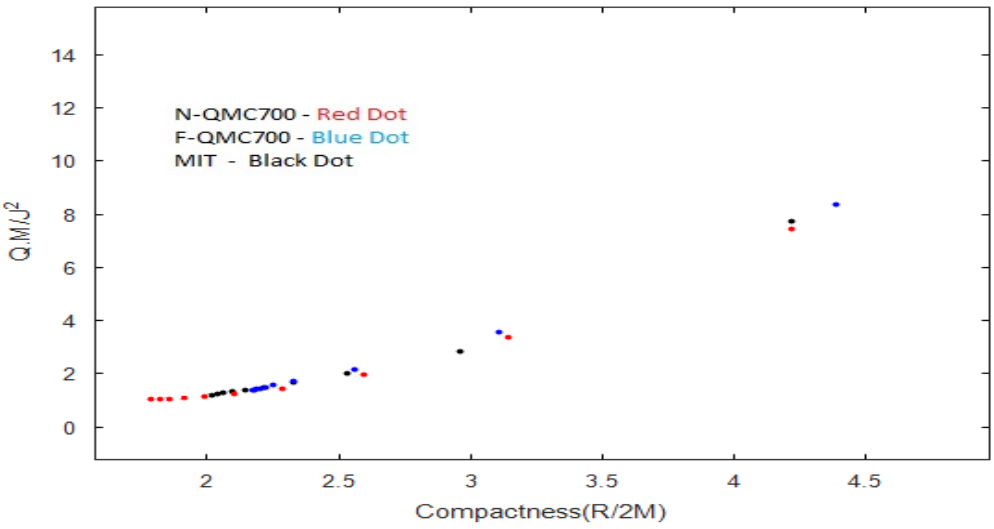

Figure 28: Dimensionless quadrupole momentum vs Compactness plot for different matter compositions with strange matter EoS parameters changed to nucleons only EoS parameters for the lower energy densities below 300 MeV/fm^3.

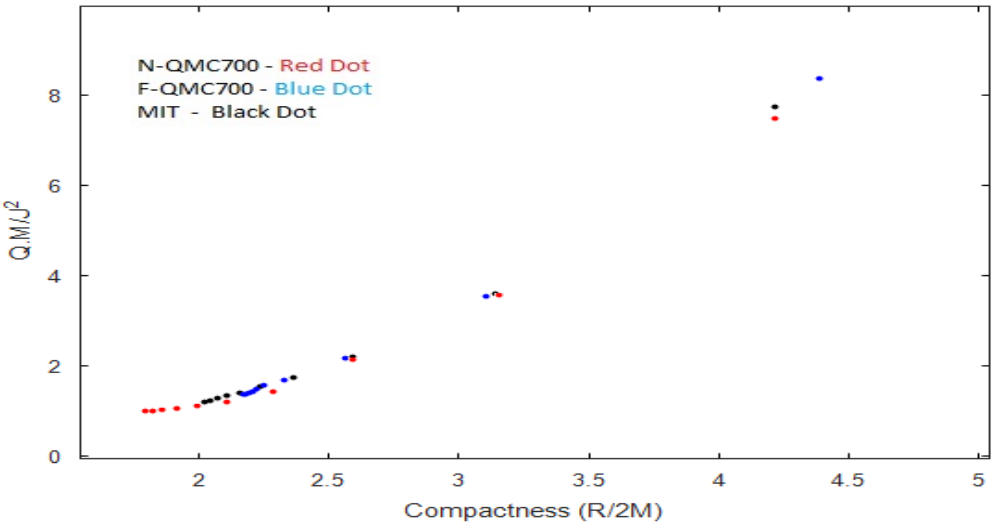

Figure 29: Dimensionless quadrupole momentum vs Compactness plot for different matter compositions with strange matter EoS parameters changed to nucleons only EoS parameters for the lower energy densities below 500 MeV/fm^3.

Although the quadrupole moment and the moment of inertia are both very sensitive to the EoSs, both of them have a Universal relationship that is, most of the EoSs dimensionless moment of inertia vs dimensionless quadrupole moment (I-Q relation) plots fall on the top of each other and show a characteristic which is (almost) independent of EoSs, predicted by Yagi and Yunes [196]. In Fig. 30, N-QMC700 and F-QMC700 both show the same characteristic and follow the universality while strange matter EoS behavior is very different and it does not follow the universality. As shown Fig. 31 and Fig. 32 after fixing the parameters for strange star at 300 MeV/fm^3 and 500 MeV/fm^3 energy densities, the I-Q relation for all the EoS is almost independent of EoSs.

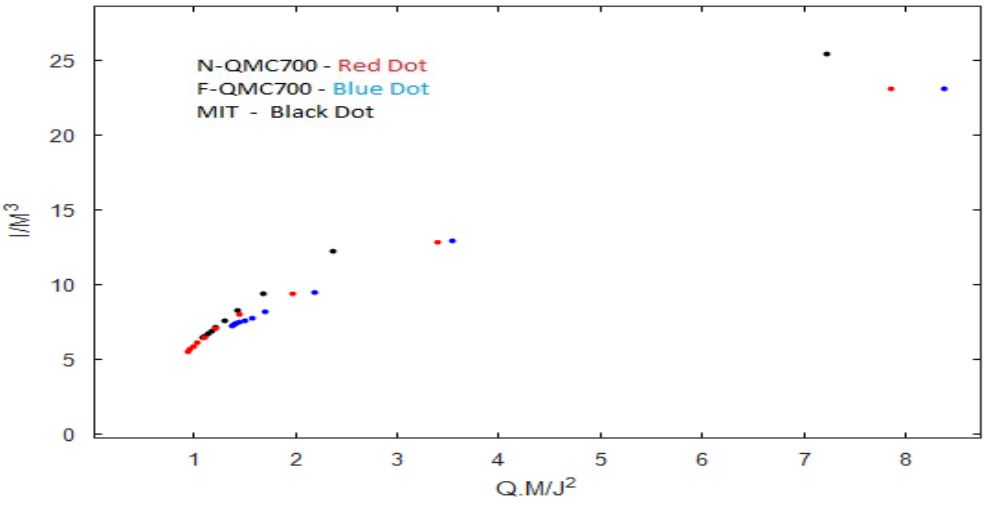

Figure 30: Dimensionless quadrupole momentum vs Dimensionless moment of inertia plot for different matter composition without changing parameters for strange matter EoS at the lower energy densities.

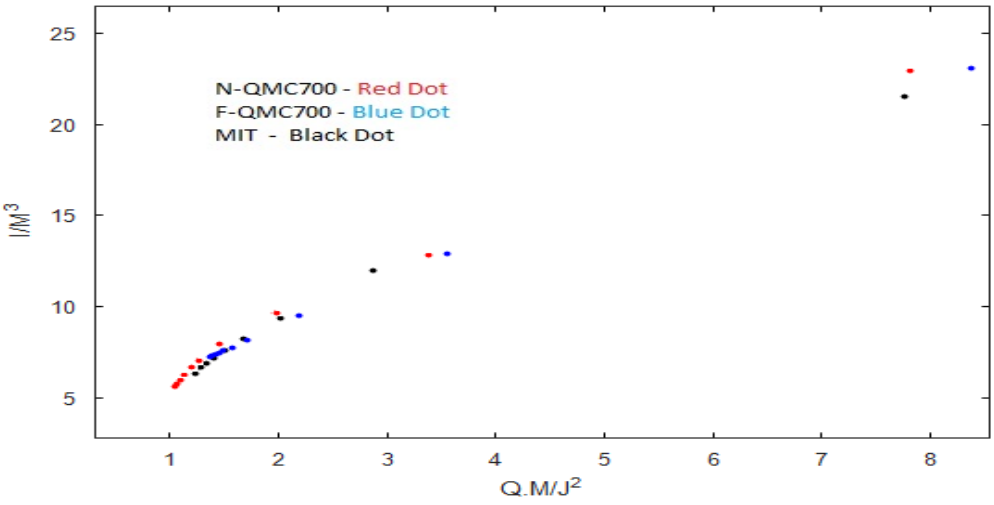

Figure 31: Dimensionless quadrupole momentum vs Dimensionless moment of inertia plot for different matter compositions with strange matter EoS parameters changed to nucleons only EoS parameters for the lower energy densities below 300 MeV/fm^3.

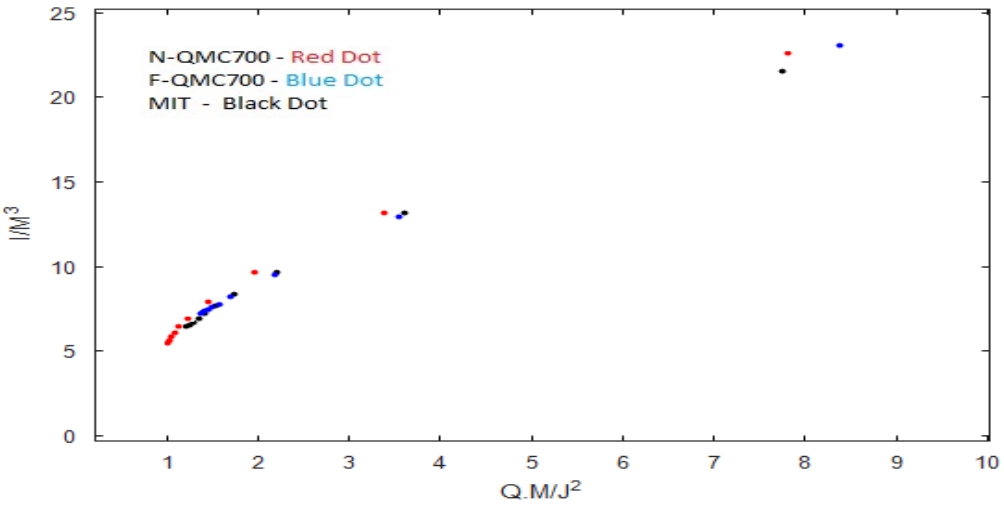

Figure 32: Dimensionless quadrupole momentum vs Dimensionless moment of inertia plot for different matter compositions with strange matter EoS parameters changed to nucleons only EoS parameters for the lower energy densities below 500 MeV/fm^3.

5.5 Tidal Love number and tidal deformability

Fig. 33 depicts the relation between tidal Love number (k_2) and M/R ratio for non-spinning neutron stars. All three EoSs Love numbers tend to zero (which is the Love number for black holes) as the value of M/R increases. This is expected because as the neutron stars become more massive, their mass is more centrally concentrated and they are extremely unlikely to get deformed. For low mass compact stars, the strange matter EoS is very different from those of N-QMC700 and F-QMC700. The low mass stars are not so compact at the center and they are more likely to get deformed, as shown at small values of M/R for the QMC EoSs. In comparison, the strange matter EoS predicts a non deformability for the low mass stars. For the reason strange matter EoS parameters are fixed with N-QMC700 EoS at the lower energy densities $\leq$ 300 MeV/fm^3 and $\leq$ 500 MeV/fm^3 in Fig. 34 and Fig. 35, respectively.

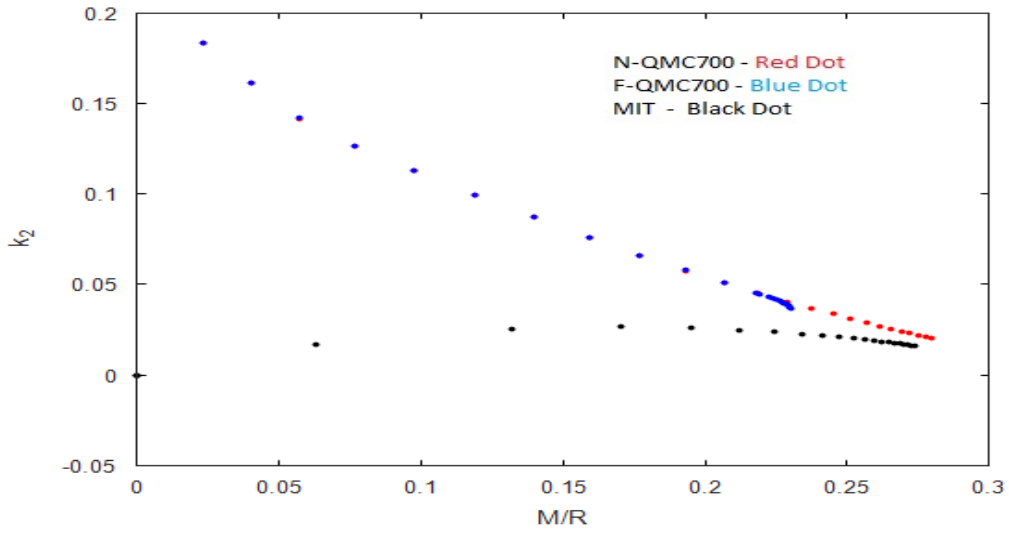

Figure 33: Tidal Love number vs M/R plot for different matter composition without changing parameters of strange matter EoS at the lower energy densities.

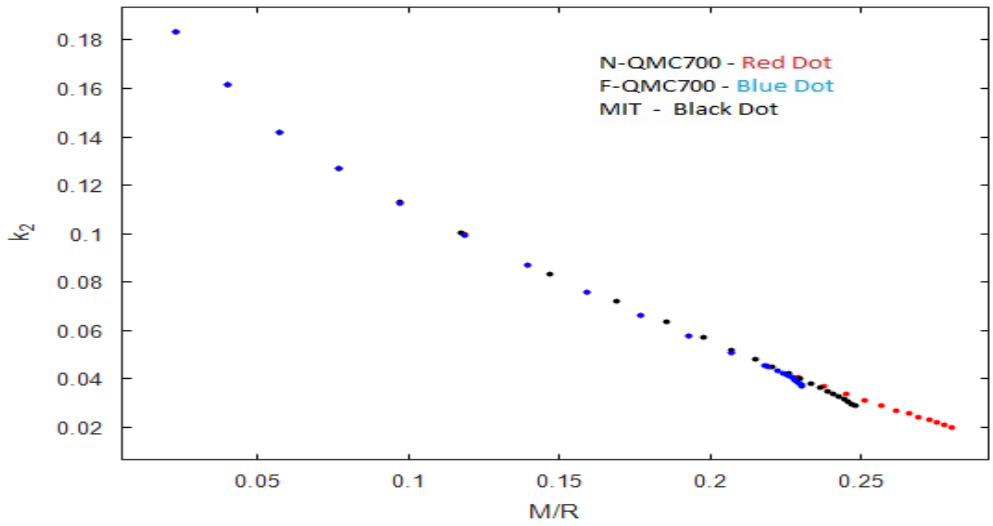

Figure 34: Tidal Love number vs M/R plot for different matter compositions with strange matter EoS parameters changed to nucleons only EoS parameters for the lower energy densities below 300 MeV/fm^3.

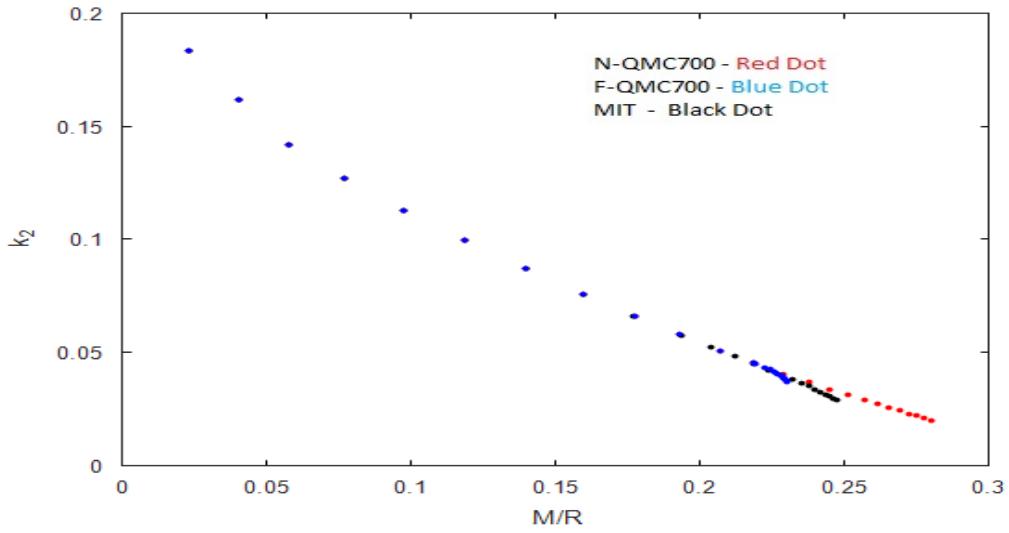

Figure 35: Tidal Love number vs M/R plot for different matter compositions with strange matter EoS parameters changed to nucleons only EoS parameters for the lower energy densities below 500 MeV/fm^3.

After fixing the parameters of strange matter EoS, its Love number has changed significantly and it shows high deformability, like N-QMC700 and F-QMC700, for the low mass compact stars and in both Figs. 34 and 35, the value of k_2 for strange matter EoS has not changed much. It is almost same in both cases (see Table 10).

As predicted by Yagi and Yunes [196], dimensionless tidal deformability (λ/M^5) vs dimensionless moment of inertia (I/M^3) plot shows a behavior which is independent of EoS. As shown in Fig. 36, both N-QMC700 and F-QMC700 EoSs fall exactly on top of each other and follow universality, whereas the strange matter EoS is very different and falls far away from them and does not follow the universality.

Next the parameters of the strange matter EoS are fixed for the energy density below 300 MeV/fm^3 and 500 MeV/fm^3 with N-QMC700. As shown in Fig. 37 and Fig. 38, the strange matter EoS dimensionless moment of inertia vs dimensionless tidal deformability then follows the universality like QMC EoS, in both

cases.

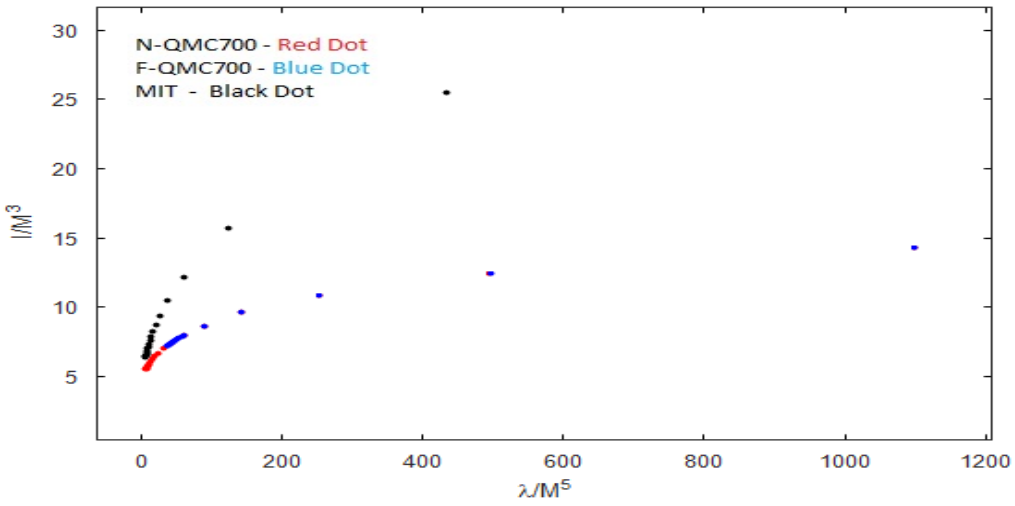

Figure 36: Dimensionless moment of inertia vs Dimensionless tidal deformability plot for different matter composition without changing parameters of strange matter EoS at the lower energy densities.

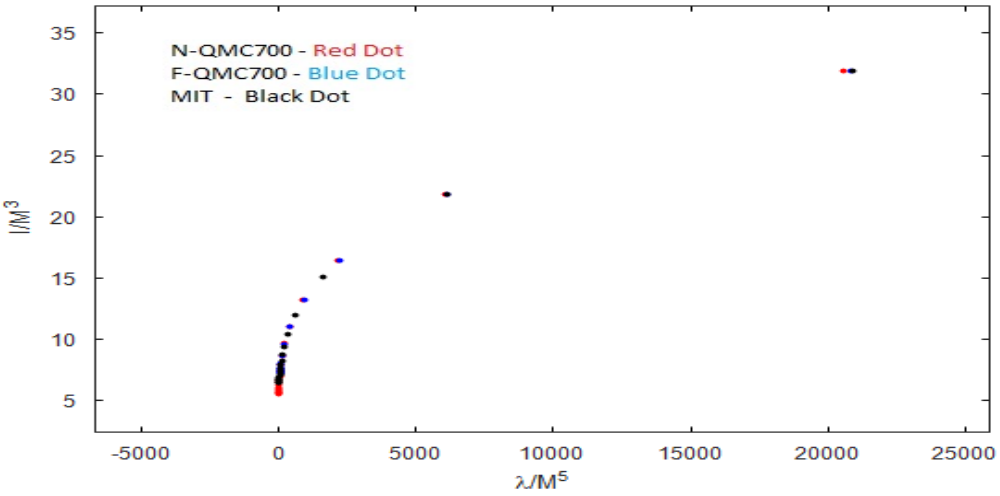

Figure 37: Dimensionless moment of inertia vs Dimensionless tidal defromability plot for different matter compositions with strange matter EoS parameters changed to nucleons only EoS parameters for the lower energy densities below 300 MeV/fm^3.

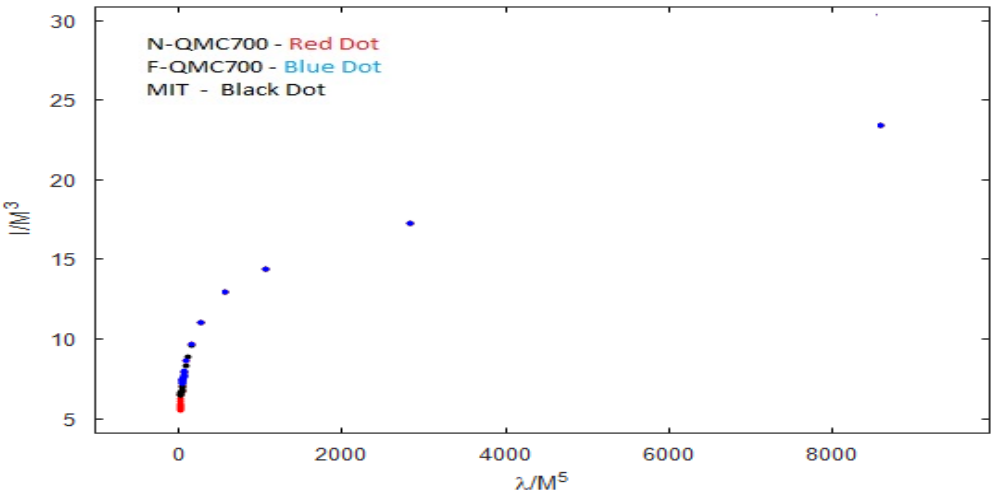

Figure 38: Dimensionless moment of inertia vs Dimensionless tidal defromability plot for different matter compositions with strange matter EoS parameters changed to nucleons only EoS parameters for the lower energy densities below 500 MeV/fm^3.

There are EoSs given in the tabular form with the strange matter EoS parameters are changed to nucleons only EoS (N-QMC700) for the low energy density $\leq$ 500 MeV/fm^3. Observables are calculated at the different energy densities. Each EoS's observables are divided in two tables. One table with observables that do not strictly depend on the rotation of the neutron star and other table with the observables that are directly related to the rotations of the neutron star.

In Tables 4,5 and 6, ϵ_c represents the central energy density in MeV/fm^3, R denotes the radius in 'Kilometers', M stands for the mass (in solar mass), τ represents the Kepler period (in milliseconds) of the neutron star which is calculated by

$$\tau = 0.82\sqrt{M/M_{sun}}.(R/10)^{3/2}. \tag{147}$$

The shortest period observed so far is 0.887 ms and values for F-QMC700 for minimum rotations are closest to it [23] but this observation may rely on the techniques used for the measurement.

z_{surf} stands for the gravitational red-shift at the surface of the neutron star, calculate by

$$z_{surf} = \sqrt{(1 - \frac{2GM}{c^2R})} - 1 \tag{148}$$

The gravitational red-shift is significant for determining the mass and the radius separately [197]. It covers a wide range of values from 0.11 to 0.52 as suggested in Ref. [198][199].

C denotes the compactness of the neutron stars, calculated by

$$C = \frac{Rc^2}{2GM}. \tag{149}$$

I stands for the moment of inertia [157], given in units of 10^{45}gm.cm^2. And Ω is the rotational velocity of the neutron star, which is calculated for the central rotating velocity 100.82342 rotations/sec, showing the Lense-Thirring effect or frame dragging effect. This value is related to the curvature of the spacetime and displays that the dragging is greater as the neutron stars become more compact.

Although the effect is small but it may change the properties of the neutron stars significantly.

Whereas, the observables which are directly related to the rotations (monopole and quadrupole equations) of the neutrons stars are given for each EoS at the different energy densities in Tables 7, 8 and 9. In these tables, the rotational velocity is taken as 500 rotations/sec which is considered as uniform. 'Mass increment' is the value of additional mass (in terms of solar mass) a neutron star can have due to rotations, the quadrupole momentum is given in units $kg.m^2$ and the eccentricity is given in the last column that represents the distortion in the shape of the neutron stars due to rotations.

In Table (10), tidal Love numbers (k_2) and tidal deformabilty (λ in units $kg.m^2.sec^2$) is given for non-spinning neutron stars with changed parameters of strange matter EoS at the energy density below 300 MeV/fm^3 (MIT-300) and 500 MeV/fm^3 (MIT-500), at the different energy densities.

ϵ_c	$R(Km)$	$M/M_\odot$	τ	z_{surf}	C	I	Ω
100	13.230	0.15743	3.1449	0.018053	28.449	0.074691	113.672
200	12.385	0.60830	1.4491	0.081533	6.8923	0.53693	127.947
300	12.905	1.0941	1.1492	0.15505	3.9927	1.2433	148.0
400	12.975	1.52488	0.99707	0.22754	2.9730	1.8431	173.843
500	12.825	1.7578	0.89829	0.29628	2.4699	2.2741e	203.77
600	12.590	1.9446	0.83069	0.35615	2.1917	2.5358	235.34
700	12.345	2.0618	0.78330	0.40492	2.0269	2.6693	266.582
800	12.110	2.1326	0.74830	0.44370	1.9223	2.7192	296.435
900	11.890	2.1742	0.72100	0.47470	1.8513	2.7194	324.644
1000	11.695	2.1974	0.69961	0.49915	1.8016	2.6911	351.343
1100	11.515	2.2089	0.68174	0.51913	1.7647	2.6467	376.8 2
1200	11.355	2.2127	0.66701	0.53510	1.7372	2.5934	401.279

Table 4: Table for N-QMC700.

ϵ_c	$R(Km)$	$M/M\odot$	τ	z_{surf}	C	I	Ω
100	13.475	0.15774	3.2295	0.017715	28.976	00.074949	113.67
200	12.410	0.60997	1.4515	0.081416	6.9011	0.53923	127.95
300	12.925	1.0973	1.1502	0.15493	3.9952	1.2493	148.01
400	12.990	1.4818	0.99731	0.22748	2.9735	1.8522	173.842
500	12.855	1.7743	0.89724	0.29850	2.4575	2.3138	203.75
600	12.630	1.9506	0.83337	0.35495	2.1963	2.5574	229.988
700	12.565	1.9735	0.82213	0.36467	2.1597	2.5745	242.019
800	12.495	1.9879	0.81231	0.37235	2.1321	2.5727	248.417
900	12.430	1.9929	0.80496	0.37710	2.1156	2.5543	253.55
1000	12.355	1.9924	0.79780	0.38068	2.1034	2.4682	258.873
1100	12.260	1.9862	0.78983	0.38359	2.0937	2.52254	264.499
1200	12.160	1.9756	0.78228	0.38540	2.0878	2.4042	270.241

Table 5: Table for F-QMC700.

ϵ_c	$R(Km)$	$M/M\odot$	τ	z_{surf}	C	I	Ω
100	13.455	0.15707	3.2292	0.017712	28.982	0.074407	113.68
200	12.400	0.4525	1.4525	0.081376	6.5088	1.9041	127.96
300	12.910	1.0931	1.1505	0.15490	3.9958	1.2411	148.03
400	12.975	1.4761	0.99751	0.22745	3.1423	2.9738	173.89
500	12.820	1.7562	0.89817	0.29632	2.4696	2.2707	203.84
600	12.645	1.8941	0.84721	0.33960	2.2586	2.4597	226.70
700	12.465	1.9653	0.81403	0.36848	2.1458	2.5235	245.36
800	12.295	2.0036	0.78978	0.38898	2.0761	2.5256	261.51
900	12.125	2.0230	0.76974	0.40463	2.0278	2.4956	275.76
1000	11.970	2.0311	0.75350	0.41643	1.9938	2.4495	288.52
1100	11.830	2.0322	0.74013	0.42532	1.9694	2.3954	300.09
1200	11.700	2.0288	0.72858	0.43229	1.9511	2.3382	310.68

Table 6: Table for strange star EoS (MIT EoS) with parameters changed to nucleons only EoS for the low energy densities ($\leq$ 500 MeV/fm^3).

ϵ_c	Mass increment (Solar mass)	Quadrupole moment	Eccentricity
100	0.96340e-006	1.91375e+036	0.022202
200	3.0890e-006	4.9979e+035	0.0060785
300	7.7259e-006	1.9942e+035	0.0028223
400	1.4936e-005	1.1244e+035	0.0016898
500	2.3132e-005	8.0178e+034	0.0011724
600	3.0423e-005	6.5848e+034	8.9791e-004
700	3.5942e-005	5.8033e+034	7.3620e-004
800	3.9674e-005	5.2842e+034	6.3350e-004
900	4.2028e-005	4.8846e+034	5.6309e-004
1000	4.3407e-005	4.5512e+034	5.1173e-004
1100	4.4040e-005	4.2622e+034	4.7353e-004
1200	4.4250e-005	4.0041e+034	4.4264e-004

Table 7: Table for N-QMC700 for neutron stars rotating at 500 rotation/sec.

ϵ_c	Mass increment (in Solar mass)	Quadrupole moment	Eccentricity
100	1.050e-006	1.6729e+036	0.02029
200	3.3454e-006	4.7919e+035	0.006309
300	8.0049e-006	2.262e+035	0.0029845
400	1.4708e-005	1.3898e+035	0.0017421
500	2.24375e-005	1.0049e+035	0.0011988
600	2.6019e-005	8.5086e+034	9.8311e-004
700	3.1425e-005	7.7999e+034	9.0368e-004
800	3.0260e-005	7.3582e+034	8.6689e-004
900	3.1936e-005	6.9927e+034	8.4089e-004
1000	3.2013e-005	6.6422e+034	8.1937e-004
1100	3.1717e-005	6.2780e+034	7.9915e-004
1200	3.1112e-005	5.9069e+034	7.8035e-004

Table 8: Table for F-QMC700 for neutron stars rotating at 500 rotation/sec.

ϵ_c	Mass increment (in Solar mass)	Quadrupole moment	Eccentricity
100	1.0511e-006	1.6098e+036	0.019926
200	3.3459e-006	4.6043e+035	0.0062294
300	8.0054e-006	2.1738e+035	0.0029548
400	1.4708e-005	1.3386e+035	0.0017269
500	2.2475e-005	9.7176e+034	0.0011894
600	2.7533e-005	8.1813e+034	9.7526e-004
700	3.2040e-005	7.4406e+034	8.9912e-004
800	3.6183e-005	6.614e+034	7.968e-004
900	3.9339e-005	6.0618e+034	7.3705e-004
1000	4.1354e-005	5.5293e+034	6.9366e-004
1100	4.2549e-005	5.1067e+034	6.5803e-004
1200	4.3051e-005	4.7192e+034	6.3084e-004

Table 9: Table for strange star EoS (MIT EoS) with changed parameters to nucleons only EoS for low densities ($\leq$ 500 MeV/fm^3) for stars rotating at 500 rotation/sec

ϵ_c	N-QMC700		F-QMC700		MIT-500		MIT-300	
	K_2	λ	K_2	λ	K_2	λ	K_2	λ
100	0.161	2.257	0.161	2.267	0.161	2.252	0.161	2.252
200	0.126	1.115	0.126	1.121	0.126	1.113	0.126	1.113
300	0.099	0.6750	0.099	0.6784	0.099	0.6735	0.099	0.6789
400	0.075	0.4242	0.075	0.4265	0.075	0.4232	0.071	0.3981
500	0.057	0.2737	0.057	0.2749	0.057	0.2704	0.057	0.2805
600	0.045	0.1846	0.045	0.1865	0.048	0.2128	0.048	0.2128
700	0.036	0.1316	0.043	0.1726	0.042	0.1623	0.042	0.1695
800	0.031	0.0989	0.041	0.1601	0.038	0.1343	0.038	0.1401
900	0.027	0.0774	0.040	0.1509	0.035	0.1139	0.034	0.1188
1000	0.024	0.0628	0.039	0.1417	0.032	0.0988	0.032	0.1028
1100	0.021	0.0523	0.038	0.1321	0.030	0.0871	0.030	0.0907
1200	0.020	0.0445	0.036	0.1225	0.029	0.0779	0.029	0.0810

Table 10: Tidal Love number (k_2) and tidal deformability ($\lambda \times 10^{30} kg.m^2.sec^2$) for the different matter compositions with strange matter EoS parameters changed to nucleons only EoS at the energy density (ϵ_c (MeV/fm^3)) below 300 MeV/fm^3(MIT-300) and 500 MeV/fm^3(MIT-500).

6 Conclusion

In this thesis, comparative models for the rotating neutron stars have been successfully calculated within the Hartle's framework at frequency 500 Hz for the different EoSs under the constraints imposed in section 3.

It is shown that the presence of strange matter or hyperons at the core at the higher energy densities makes the EoS softer in comparison to the nucleons only EoS, as demonstrated in Fig 4. The strange matter EoS is linearly varying with the energy density and at low energy densities yields inappropriate properties for the neutron stars. Hyperons only come into existence when the energy density is 580 MeV/fm^3. The possibilities and consequences of having strange matter at the energy density 300 Mev/fm^3 and 500 MeV/fm^3 are shown in Fig. 5. Because in the lower energy density region there are only nucleons. Therefore, the strange matter EoS is fixed with nucleons only EoS at the lower energy densities.

The significance of the crust region in exploited for determining the radius for the neutron star in Figs. 6, 7 and 8. The QMC EoSs show expansion in the radius at the low energy densities, at the crust which is expected, whereas the strange matter EoS does not show this nature, at the crust region as shown in Fig. 6. Due to the poor parameterization of strange matter EoS at the crust (or the low energy density region) it yields inappropriate value for radii (and the moment of inertia see Fig. 12). After fixing the parameters of strange matter EoS in lower energy densities region the results are shown Fig. 7 and Fig 8. The mass and the radius relation for strange matter EoS in Fig. 7 is stiffer than Fig. 8.

Selected QMC EoSs have successfully predicted maximum mass close to what has been observed ($2M\odot$) at the energy density less than 6 times the nuclear matter density. The presence of hyperons at the core reduces the maximum mass of the neutron star significantly. The significance of nuclear physics at the lower energy density is shown in Figs. 6, 7, 8 and 9 which suggests that if the nuclear physics at the energy density in the nuclear density region in (1-3) times normal

nuclear density is not precisely known, then values calculated by an EoS can be drastically different. In Figs. 10 and 11, we see that the compactness of the nucleons only EoS is very close to the compactness of the black holes (1.5).

The moment of inertia grows in a similar way for all EoSs, as plotted Figs. 13 and 14. After fixing the parameters for the strange matter EoS. The presence of strange matter above the energy density 300 MeV/fm^3 or 500 MeV/fm^3 does not make a significant change in the moment of inertia for the low mass neutron stars but as it approaches to the maximum mass the moment of inertia is different for each EoS.

Although every EoS predicts different properties for the neutron stars, certain combinations of these properties show a universality. Without fixing the strange matter EoS parameters at the lower energy density, the plots of moment of inertia parameter against compactness, Fig. 15 and dimensionless moment of inertia against (M/R), Fig. 18, do not follow the universality between them as suggested in Refs. [192][194][165] and Ref. [191] respectively, while the hyperons and the nucleons EoSs show universality. After fixing the parameters at the energy density below 300 MeV/fm^3 and 500 MeV/fm^3 in Figs. 16 and 17 and Figs. 19 and 20, respectively, the predictions of strange matter at 500 MeV/fm^3 show the universality like N-QMC700 and F-QMC700. In Fig. 21 also, the dimensionless angular momentum is very different for the strange matter EoS from QMC EoSs [165] while fixing the strange matter EoS at the energy density 500 MeV/fm^3 in Fig. 23 predicts a Universal relation between the dimensionless angular momentum and the compactness .

Fig. 24 shows that the dimensionless quadrupole moment for the low mass strange star is very different and small comparative to QMC EoSs that suggests strange stars are not much deformed while it is supposed to be similar to QMC EoS because there is no strange matter in the low mass neutron star. After fixing the parameters in Figs. 25 and 26 the quadrupole moment for the strange star is almost the same as thte QMC EoS whether the strange matter comes into existence

at the energy density 300 MeV/fm^3 or 500MeV/fm^3. Fig. 27 shows a Universal relation between the dimensionless quadrupole moment and compactness as suggested in Ref. [165]. The dimensionless quadrupole moment for the strange star is different than QMC EoS, whereas all EoS show similar values near the maximum mass. After fixing the parameters for strange matter EoS in Figs. 28 & 29 all three EoSs show the compactness vs dimensionless characteristic independent of EoSs. Due to high compactness the nucleons only EoS shows a slightly deviated behavior than hyperons and strange matter EoS which fall almost on top of each other.

There is a unique relation between the dimensionless quadrupole moment and the dimensionless moment of inertia. That is, when they are plotted, the result is independent of the EoS (I-Q relation), which means to say that all EoSs fall approximately on top of each other as demonstrated after fixing the parameters for the strange matter EoS in Fig. 31 and 32. F-QMC700 and strange matter EoS follow the universality while N-QMC700 is slightly away from them.

In Fig. 33, calculated tidal Love number for QMC EoSs follow the behavior suggested by most authors, for instance see Ref. [160][161][162][163], while the strange matter EoS doesn't unless its parameters are fixed at the lower energy density region as shown in Fig. 34 and 35. In Fig. 36, the QMC EoSs follow the I/M^3-λ/M^5 universality whereas the strange matter EoS doesn't. After fixing the parameters for the strange matter EoS for the lower energy density regions below 300 MeV/fm^3 & 500 MeV/fm^3. The strange matter EoS follows the universality as shown in Figs. 37 and 38. Although the tidal Love number and the tidal deformability both are highly sensitive to the EoSs yet the tidal Love number does not change for the strange matter EoS, whether it comes into existence at the energy density 300 MeV/fm^3 or 500 MeV/fm^3 while tidal deformability changes.

It is explicitly shown in Tables 7, 8 and 9 that rotations can increase the mass of the neutron stars around the mass of the Earth by an amount which is very small in comparison to the total mass of the neutron star, so it does not have much impact

on most of the neutron star properties and it can be ignored for future studies. The quadrupole moment decreases as the compactness of the neutron star increases. As the neutron stars tend to become more compact they are very unlikely to get deformed due to rotations as shown by eccentricity which is decreasing with the mass (energy density). It is predicted that as the central energy density of the neutron star increases, its quadrupole moment decreases and so does the deformation in the shape.

In nutshell, it is shown that EoSs based on the nuclear structure, does follow the imposed EoS constraint which is a clear indication that the nuclear structure may play a significant role in defining the properties of matter at the energy density several times the nuclear matter density. Precisely knowing the nuclear physics at the energy density 1-3 times the nuclear matter density is extremely important to calculate the properties of neutron stars particularly radius and the moment of inertia. The quadrupole moment of a strange star does not depend much on the energy density of phase transition. If the phase transition, into hyperons or strange matter, happens approximately at the same energy density then the properties of corresponding neutron star and strange star are very likely the same to each other. Several unique universalities are predicted among the neutron star properties such as moment of inertia parameter (I/MR^2) vs compactness ($R/2M$), dimensionless moment of inertia vs M/R, dimensionless quadrupole momentum (QM/J^2) vs compactness, dimensionless quadrupole momentum vs dimensionless moment of inertia, dimensionless moment of inertia vs dimensionless tidal deformability.

6.1 Future work

In the future, with better technology and more observational data, we may have more precise measurements of luminosity, mass, radius and we can further improve constraints on EoS. With the discovery of gravitational waves we may impose a new constraint on EoS in a neutron star binary system, which may provide

further information for understanding the interior of the neutron star.

Furthermore, recently improvements have been made in the QMC model, and with these advancements we can improve our EoS and can get better results. In future it will be interesting to see how QMC EoS can explain the neutron star cooling process, magnetic fields and the tidal deformability of the spinning neutron stars merger.

7 Appendix

7.1 Nuclear Theory

Free mass of baryons in the bag model

The free mass of the baryon (flavor f), containing quarks (N_{ud}, N_s) is given by

$$M_f = \frac{N_{ud}\Omega(m_{ud}) + N_s\Omega(m_s)}{R} - \frac{Z_0}{R} + \Delta E_M(f) + (4/3)\pi B R^3, \tag{150}$$

where $\Omega(m)$ (quark mode) is calculated by following boundary condition, in terms of bag constant(B)

$$\frac{Sinx}{x} + \frac{Cosx - \frac{sinx}{x}}{\Omega + mR} = 0, x = \sqrt{\Omega^2 - (mR)^2}. \tag{151}$$

In the presence of scalar field, $\Omega^2 - (mR)^2 < 0$ but the equation remains valid by analytical continuation. The bag radius is kept fixed for baryon of each flavor by the stability condition $\frac{\delta M_f}{\delta R} = 0$. Up and down quark masses are set to zero and the zero point parameter Z_0 is taken(assumed) to be same for all particles.
Hyperfine color interaction is evaluated by ref [200], for color singlet baryon

$$\Delta E_M = \Sigma_i^j E_{ij} \vec{\sigma_i}.\vec{\sigma_j}, i < j, \tag{152}$$

where σ_i is Pauli matrix for i^{th} quark and

$$E_{ij} = 8 g_c \frac{\mu_i(R)\mu_j(R) I_{ij}}{R^3}, \tag{153}$$

$$\mu_i(R) = \frac{4R\Omega(m_i) + 2R^2 m_j - 3R}{12\Omega(m_i)(\Omega(m_i) - 1) + 6Rm_i}, \tag{154}$$

where g_c is the color coupling constant and μ_i is magnetic moment. It is noted that quark mass dependence produces a non-trivial flavor dependence of the coupling to the nuclear scalar field. The expression for the overlapping integral I_{ij} is :

$$I_{ij} = 1 + \frac{-3y_i y_j - 4x_i x_j sin^2 x_i sin^2 x_j + x_i x_j K_{ij}}{2(x_i sin^2 x_j - (3/2)y_i)(x_j sin^2 x_j - (3/2)y_j)}, \tag{155}$$

$$K_{ij} = 2x_i S_i(2x_i) + 2x_j S_j(2x_j) - (x_i + x_j) S_i(2x_i + 2x_j) - (x_i - x_j) S_i(2x_i - 2x_j), \tag{156}$$

$$y_i = x_i - sinx_i cosx_i, x_i = \sqrt{\Omega(m_i)^2 - (Rm_i)^2}. \tag{157}$$

Effective Mass

In the effect of constant scalar field over the volume of baryon, variations of the field just yields the spin-orbit interaction, which can be ignored in uniform matter consideration. Let strange quark does not interact with the scalar field.

$$m_{ud} \to m_{ud} - g^q_\sigma \sigma, m_s \to m_s, \tag{158}$$

where σ is scalar field and g^q_σ is its coupling strength to u and d quarks. These couplings must be substituted in equation (150) and stability condition is followed to determine the actual radius. Then mass becomes a function of σ and parameters (B,Z_0,m_s,g_c) which all depend on R_N^{free}. So, in a medium

$$M_f \to M_f(m_{u,d} - g^q_\sigma, R_N^{free}). \tag{159}$$

Simply a fit of $M_f(\sigma, R_N^{free}) - M_f(0, R_N^{free})$ is made in powers of $m_{u,d} - g^q_\sigma \sigma$, with also coefficients also fitted as polynomials in R_N^{free}. σ - N coupling is defined as

$$g_\sigma = \frac{\partial M_N(\sigma, R_N^{free})}{\partial \sigma}|_{\sigma=0} = -g^q_\sigma \frac{\partial M_N(\sigma, R_N^{free})}{\partial m}|_{m=0}, \tag{160}$$

which permit to eliminate g^q_σ in favor of g_σ. And following expression is formed

$$M_f(\sigma, R_N^{free}) - M_f(0, R_N^{free}) = P_f^{(1)}(R_N^{free}) g_\sigma \sigma + P_f^{(2)}(R_N^{free})(g_\sigma \sigma)^2 + ..., \tag{161}$$

where by construction

$$P_N^{(1)}(R_N^{free}) = -1, \tag{162}$$

if the mass is given by(approximated)

$$M_f = \frac{N_u \Omega(m_{ud}) + N_s \Omega(m_s)}{R_N^{free}}, \tag{163}$$

then

$$P^1_{\Lambda\Sigma} = -2/3, P^1_{\Xi} = -1/3, \tag{164}$$

Following the work given by reference [69], $M_f(\sigma)$ is given by

$$M_f(\sigma) = M_f - \omega^\sigma_f g_\sigma \sigma + (d/2)\tilde{\omega}^\sigma_f (g_\sigma \sigma)^2, \tag{165}$$

where d is scalar polarisability and values of ω^σ_f & $\tilde{\omega}^\sigma_f$ are given in table 10. And preferred value of $R_N free$ = 0.8 fm.

	N	Λ	Σ	Ξ
d(fm)	0.15	0.15	0.15	0.15
ω^σ_f	1	0.703	0.614	0.353
$\tilde{\omega^\sigma_f}$	1	0.68	0.673	0.371

Table 11: Table for d, ω^σ_f, and $\tilde{\omega^\sigma_f}$.

7.2 Structural equations

7.2.1 Christoffel symbols and Ricci scalar

$$\begin{aligned}
\Gamma^{\lambda}_{t\kappa}\Gamma^{\kappa}_{\lambda t} &= (\Gamma^{t}_{tt})^2 + 2\Gamma^{t}_{ti}\Gamma^{i}_{tt} + \Gamma^{i}_{tj}\Gamma^{j}_{it} = 2(\Phi')^2 e^{2\nu-2\Lambda}, \\
\Gamma^{\lambda}_{r\kappa}\Gamma^{\kappa}_{\lambda r} &= (\Gamma^{t}_{rt})^2 + 2\Gamma^{t}_{ri}\Gamma^{i}_{tr} + \Gamma^{i}_{rj}\Gamma^{j}_{ir} = (\Phi')^2 + (\Lambda')^2 + \frac{2}{r^2}, \\
\Gamma^{\lambda}_{\theta\kappa}\Gamma^{\kappa}_{\lambda\theta} &= (\Gamma^{t}_{\theta t})^2 + 2\Gamma^{t}_{\theta i}\Gamma^{i}_{t\theta} + \Gamma^{i}_{\theta j}\Gamma^{j}_{i\theta} = -2e^{-2\lambda} + cot^2\theta, \\
\Gamma^{\lambda}_{\phi\kappa}\Gamma^{\kappa}_{\lambda\phi} &= (\Gamma^{t}_{\phi t})^2 + 2\Gamma^{t}_{\phi i}\Gamma^{i}_{t\phi} + \Gamma^{i}_{\phi j}\Gamma^{j}_{i\phi} = -2(sin^2\theta e^{-2\Lambda} + cos^2\theta),
\end{aligned} \tag{166}$$

Non-vanishing components of Riemann-Christoffel symbols

$$\begin{aligned}
R^{t}_{rtr} &= -\Phi'' - (\Phi')^2 + \Phi'\Lambda', \\
R^{t}_{\theta t\theta} &= r\Phi' e^{-2\Lambda}, \\
R^{t}_{\phi t\phi} &= r\Phi' sin^2\theta e^{-2\Lambda}, \\
R^{r}_{ttr} &= [-\Phi'' - (\Phi')^2 + \Phi'\Lambda']e^{2\Phi-2\Lambda}, \\
R^{r}_{\theta r\theta} &= r\Lambda' e^{-2\Lambda}, \\
R^{r}_{\phi r\phi} &= r\Lambda' sin^2\theta e^{-2\Lambda}, \\
R^{\theta}_{tt\theta} &= -\Phi' r e^{2(\Phi-\Lambda)}, \\
R^{\theta}_{rr\theta} &= -\frac{\Lambda'}{r}, \\
R^{\theta}_{\phi\theta\phi} &= sin^2\theta(1 - e^{-2\Lambda}), \\
R^{\phi}_{tt\phi} &= -\Phi' r e^{2(\Phi-\Lambda)}, \\
R^{\phi}_{rr\phi} &= \frac{\Lambda'}{r}, \\
R^{\phi}_{\theta\theta\phi} &= -1 + e^{-2\Lambda},
\end{aligned} \tag{167}$$

Ricci tensors are given by,

$$\begin{aligned} R_{tt} &= [-\Phi'\Lambda' + \Phi'' + (\Phi')^2 + 2\frac{\Phi'}{r}]e^{2(\Phi-\Lambda)}, \\ R_{rr} &= -\Phi'' - \Phi'^2 + \Phi'\Lambda' + \frac{2\Lambda'}{r}, \\ R_{\theta\theta} &= [-r\Phi' + r\Lambda' + e^{2\Lambda} - 1]e^{-2\Lambda}, \\ R_{\phi\phi} &= -sin^2\theta[r\Phi' - r\Lambda' - e^{2\Lambda} + 1]e^{-2\Lambda}, \end{aligned} \tag{168}$$

Individual components of mixed Ricci tensors are calculated by the relation,

$$R^{\mu}_{\nu} = g^{\mu\lambda}R_{\lambda\nu}, \tag{169}$$

And Ricci scalar is obtained form the relation,

$$R = g^{\mu\nu}R_{\mu\nu}, \tag{170}$$

7.2.2 Relation between Φ and P

From equation (54),

$$T^{\mu}_{\nu;\mu} = 0 = (\epsilon + P)u_{\sigma;\mu}u^{\mu} + P_{,\sigma} + P_{,\mu}\,u^{\mu}u_{\sigma}, \tag{171}$$

here σ is dummy index and following relations are used to get the right hand side

$$u^{\nu}_{;\mu}u_{\nu} = u^{\nu}u_{\nu;\mu} = 0. \tag{172}$$

One notices that $P_{,r}$ is non-zero and non-trivial component of equation (158) is

$$(\epsilon + P)u_{r;\mu}u^{\mu} + P_{,r} = 0 \tag{173}$$

and

$$u_{r;\mu} = \frac{\partial u_r}{\partial x^{\mu}} - \Gamma^{\lambda}_{r\mu}u_{\lambda} = -\Gamma^{\lambda}_{r\mu}u_{\lambda} \tag{174}$$

which enable us to get the final relation

$$\frac{dP}{dr} = (\epsilon + P)\Gamma^{\lambda}_{r\mu}u_{\lambda}u^{\mu} = -(\epsilon + P)\frac{d\Phi}{dr} \tag{175}$$

7.2.3 Rotational equations

Mixed tensor R^t_ϕ is calculated ($R^t_\phi = R_{\phi\nu}g^{\nu t}$) as,

$$\begin{aligned}R^t_\phi = (-1/2)[&e^{2\mu(r,\theta)}\frac{\partial^2}{\partial r^2}\omega(r,\theta) + e^{2\lambda(r,\theta)}\frac{\partial^2}{\partial\theta^2}\omega(r,\theta) + (\frac{\partial}{\partial\theta}\lambda(r,\theta)) \times e^{2\lambda(r,\theta)}\frac{\partial}{\partial\theta}\omega(r,\theta)\\
&+ (\frac{\partial}{\partial r}\mu(r,\theta))e^{2\mu(r,\theta)}\frac{\partial}{\partial r}\omega(r,\theta) + 3(\frac{\partial}{\partial\theta}\psi(r,\theta))e^{2\lambda(r,\theta)}\frac{\partial}{\partial\theta}\omega(r,\theta)\\
&- (\frac{\partial}{\partial r}\lambda(r,\theta))e^{2\mu(r,\theta)} \times \frac{\partial}{\partial r}\omega(r,\theta) - (\frac{\partial}{\partial r}\omega(r,\theta))e^{2\mu(r,\theta)}\frac{\partial}{\partial r}\nu(r,\theta)\\
&- (\frac{\partial}{\partial\theta}\omega(r,\theta)) \times e^{2\lambda(r,\theta)}\frac{\partial}{\partial\theta}\nu(r,\theta) + 3(\frac{\partial}{\partial r}\psi(r,\theta))e^{2\mu(r,\theta)}\frac{\partial}{\partial r}\omega(r,\theta)\\
&- (\frac{\partial}{\partial\theta}\mu(r,\theta))e^{2,\lambda(r,\theta)}\frac{\partial}{\partial\theta}\omega(r,\theta)] \times e^{2\psi(r,\theta)-2\nu(r,\theta)-2\lambda(r,\theta)-2\mu(r,\theta)}\end{aligned} \tag{176}$$

$$T^t_\phi = -\frac{e^{2\psi(r,\theta)}[\epsilon+P][\Omega-\omega(r,\theta)]}{-e^{2\nu(r,\theta)}+[\Omega-\omega(r,\theta)]^2e^{2\psi(r,\theta)}}, \tag{177}$$

$$e^{2\psi} \to r^2sin^2\theta, \tag{178}$$

$$T^t_\phi = \frac{r^2sin^2\theta[\epsilon+P]\overline{\omega}e^{-2\nu}}{1-\overline{\omega}^2e^{2\psi-2\nu}}, \tag{179}$$

$$T^t_\phi = r^2sin^2\theta[\epsilon+P]\overline{\omega}e^{-2\nu} + O(\Omega^2), \tag{180}$$

In equation (176), using

$$\frac{\partial\lambda}{\partial\theta} = \frac{\partial\nu}{\partial\theta} = \frac{\partial\mu}{\partial\theta} = 0, \tag{181}$$

one gets,

$$\begin{aligned}R^t_\phi = -\frac{1}{2}[&e^{2\mu}\frac{\partial^2\omega}{\partial r^2} + e^{2\lambda}\frac{\partial^2\omega}{\partial\theta^2} + \frac{\partial\mu}{\partial r}e^{2\mu}\frac{\partial\omega}{\partial r} - \frac{\partial\lambda}{\partial r}e^{2\mu}\frac{\partial\omega}{\partial r} - \frac{\partial\nu}{\partial r}e^{2\mu}\frac{\partial\omega}{\partial r}\\
&+3\frac{\partial\psi}{\partial r}e^{2\mu}\frac{\partial\omega}{\partial r}]e^{2\psi-2\nu-2\lambda-2\mu}\end{aligned} \tag{182}$$

$$\begin{aligned}R^t_\phi = -\frac{1}{2}[&\frac{\partial^2\omega}{\partial r^2} + e^{2\lambda-2\mu}\frac{\partial^2\omega}{\partial\theta^2} + \frac{\partial\mu}{\partial r}\frac{\partial\omega}{\partial r} - \frac{\partial\lambda}{\partial r}\frac{\partial\omega}{\partial r} - \frac{\partial\nu}{\partial r}\frac{\partial\omega}{\partial r}\\
&+3\frac{\partial\psi}{\partial r}\frac{\partial\omega}{\partial r}]e^{2\psi-2\nu-2\lambda}\end{aligned} \tag{183}$$

$$R^t_\phi = 8\pi T^t_\phi, \tag{184}$$

$$-\frac{1}{2}[\frac{\partial^2\omega}{\partial r^2}+e^{2\lambda-2\mu}\frac{\partial^2\omega}{\partial\theta^2}+\frac{\partial\mu}{\partial r}\frac{\partial\omega}{\partial r}-\frac{\partial\lambda}{\partial r}\frac{\partial\omega}{\partial r}-\frac{\partial\nu}{\partial r}\frac{\partial\omega}{\partial r}+3\frac{\partial\psi}{\partial r}\frac{\partial\omega}{\partial r}]e^{2\psi-2\nu-2\lambda}$$
$$=8\pi r^2 sin^2\theta[\epsilon+P]\overline{\omega}e^{-2\nu} \tag{185}$$

Simple algebraic manipulation leads to equation (100),

8 References

[1] I. Vidana, Eur. Phys. J. Plus, 133 (2018) 445.

[2] W. Greiner and H Stocker 1990 *proc. NATO Advanced Study Institute on the Nuclear Equation of State(Peniscola)* NATO ASI Series is vol 261A & B(New York: Plenum Press).

[3] W. Greiner , H. Stocker and Gallmann A 1994 *proc NATO Advanced Study on Hot and Dense Nuclear Matter(Bodrum)* NATO ASI Series B Vol 335(New York: Plennum Press).

[4] H. Stocker, A. Gallmann and J.H. Hamilton 1997 Iporc INt Conf. on Nuclear Physics at the Turn of the Millennium: Structue of Vacuum and Elementary Matter (Wilderness)(Singapore: World Scientific).

[5] J. Chadwick, Nature 129, (1932) 312.

[6] W. Baade and F. Zwicky. Phys. Rev. 45, (1934) 138.

[7] R. C. Tolman, Phys. Rev. C 55, (1939) 364.

[8] J. R. Oppenheimer and G. M. Volkoff, Phys. Rev. C 55, (193) 374.

[9] B. K. Harrison, M. Wakano, J. A. Wheeler, "Matter-energy at high density: end point of thermonuclear evolution" in la structure at evolution de l'univers (Brussels: R. Stoops), 124-140 (1958).

[10] T. H. R. Skyrme, Nucl. Phys. 9, (1959) 615.

[11] A. G. W. Cameron, Astrophys. J 130, (1959) 916.

[12] M. Gell-Mann, Phys. Lett. 8, (1964) 214.

[13] D. Ivanenko and D. F. Kurdgelaidze, Astrozika 1, (1965) 479.

[14] D. Ivanenko and D. F. Kurdgelaidze, Lett. Nuovo Cimento 2, (1969) 13.

[15] A. Hewish, S. J. Bell, J. D. H. Pilkington, P. F. Scott, and R. A. Collins, Nature 217, (1968) 709.

[16] T. Gold, Nature 218, (1968) 731.

[17] A. M. Lenchek 1972 *The Physics of Pulsars*(New York: Gordon and Breach).

[18] F. G. Smith 1977 *Pulsars* (Cambridge: Cambridge University Press).

[19] R. N. Manchester and J. H. Taylor 1977 *Pulsars* (San Francisco: Freeman).

[20] A. G. Lyne and F. Graham-Smith 1990 *Pulsar Astronomy* (Cambridge:Cambridge University Press).

[21] S. J. Bell, (1969), *The measurement of radio source diameters using a diffraction method*, Ph.D. thesis, The University of Cambridge, 6567.

[22] S. J. Bell, (1977) Petit Four. Annals of the New York Academy of Science 302, 685-689.

[23] J. W. T. Hessels, S. M. Ransom, I. H. Stairs, P. C. Freire, V. M. Kaspi, F. Camilo, (2006). "A Radio Pulsar Spinning at 716 Hz". Science. 311 (5769): 1901–1904.

[24] R. N. Manchester, G. B. Hobbs, A. Tech & M. Hobbs, Astron. J. 129, 1993 (2005).

[25] G. S.Bisnovatyi-Kogan Phys. Usp. 49, 53 (2006).

[26] V. M. Lipunov Astrophysics of Neutron Stars (Berlin: Springer, 1992).

[27] V. E. Zavlin Astrophys. Space Sci. 308, 297 (2007).

[28] S. Mereghetti Astron. Astrophys. Rev. 15, 225 (2008).

[29] I. F. Malov and G Z Machabeli Anomal'nye Pulsary (Anomalous Pulsars) (Moscow: Nauka, 2009).

[30] K. Mori, Ho W C G Mon. Not. R. astron. Soc. 377, 905 (2007).

[31] M. van der Klis et al. Nature 316, 225 (1985).

[32] M. van der Klis Annu. Rev. Astron. Astrophys. 38, 717 (2000).

[33] M. Kluzniak et al. Rev. Mex. Astron. Astrophys. 27, 18 (2007)

[34] M. Tagger Rev. Mex. Astron. Astrophys. 27, 26 (2007).

[35] N. Shaposhnikov and L. Titarchuk Astrophys. J. 606, L57 (2004) 111

[36] E.F Brown, L. Bildsten , R. E. Rutledge Astrophys. J. 504, L95 (1998)

[37] E. F. Brown, A Cumming Astrophys. J. 698, 1020 (2009).

[38] P. S. Shternin et al. Mon. Not. R. astron. Soc. 382, L43 (2007)

[39] N. K. Glendenning 1985 Astrophys. J 293 470.

[40] C. Kettner, F. Weber, M. K. Weigel and N. K. Glendenning 1995 Phys. Rev.

D 51 1440.

[41] I. Vidana, A. Polls and A. Ramos, Phys. Rev. C 65, (2001) 035804.

[42] R. P. Feynmann , N. Metropolis and E. Teller 1949 Phys. Rev 75 1561.

[43] B. K. Harrison and J. A. Wheeler 1965 Gravitational Theory and Gravitational Collapse ed B. K. Harrison, K. S. Thorne, M. Wakano and J. A. Wheeler (Chicago: University of Chicago Press) pp 1-177.

[44] G. Baym , H. A. Bethe and C. J. Pethick 1971 Astrophys. J. 175 225.

[45] J. W. Negele and D. Vautherin 1973 Nucl. Phys. A 178 123.

[46] G. Baym, C. Pethick and P. Sutherland P 1971 Astrophys. J 170 299.

[47] E. Witten 1984 phys Rev. D 30 272.

[48] C. Alcock , E. Farhi and A. V. Olinto A V 1986 Astrophys. J 310 261.

[49] P. Haensel , J. L. Zdunik and R. Schaeffer 1986 Astron. Astrophys. 160 121.

[50] G. Baym Neutron stars and the physics of matter at high density, in: Nuclear Physics with Heavy Ions and Mesons (Les Houches) session XXX vol 2 ed R Balian, M Rho and G Ripka (Amsterdam: North-Holland) p 745, 1978.

[51] M. Urbanec, E. Betak, Z. Stuchlık , 2010, Acta Astronomica, 60, 149.

[52] F. Weber and N. K. Glendenning, 1993, ed D. H. Feng, G. Z. He and X. Q. Li (Singapore: World Scientific) p 64-183.

[53] S. A. Moszkowski 1974 Phys. Rev D 9 1613.

[54] Y. C. Leung 1989 Physics of Dense Matter (Singapore: World Scientific).

[55] F. Weber and M. K. Weigel 1989 Nucl. Physc A 493 549.

[56] F. Weber and M. K. Weigel 1989 Nucl. Physc A 495 363c.

[57] N. K. Glendenning, F. Weber and S. A. Moszkowski 1992 Phys. Rev C 45 844.

[58] N. K. Glendenning 1991 Nucl. Phys. B Proc. Suppl. 24B 110.

[59] N. K. Glendenning 1992 Phys Rev. D 46 1274.

[60] N. K. Glendenning Pei S 1995 Acta Phys. Hungarica (New Ser.) Heavy Ion Phys. 1 323.

[61] N. K. Glendenning 1995 Phys. Rep. 264 143.

[62] J. N. Bahcall, R. A. Wolf Phys. Rev. 140, B1452 (1965).

[63] A. B. Migdal Sov. Phys.–JETP 34, 1184 (1972).

[64] R. F. Sawyer Phys. Rev. Lett. 29, 382 (1972); erratum: ibid., 29, 823 (1972).

[65] D. J. Scalapino Phys. Rev. Lett. 29, 386 (1972).

[66] A. B. Migdal Sov. Phys. Uspekhi 20, 879 (1977).

[67] D. B. Kaplan, A. E. Nelson Phys. Lett. B 175, 57 (1986).

[68] A. Ramos, J. Schaffner-Bielich, J. Wambach Lecture Notes in Phys. 578, 175 (2001).

[69] E. E. Kolomeitsev, D. N. Voskresensky Phys. Rev. C 68, 015803 (2003).

[70] I. M. Dremin, A. B. Kaidalov Phys. Usp. 49, 263 (2006).

[71] D. D. Ivanenko, D. F. Kurdgelaidze, Astrophysics 1, 251 (1965).

[72] J. C. Collins, M. J. Perry Phys. Rev. Lett. 34, 1353 (1975).

[73] A. Kurkela , P. Romatschke, A. Vuorinen Phys. Rev. D 81, 105021 (2010).

[74] D. Blaschke et al. Phys. Rev. C 80, 065807 (2009).

[75] I. Iosilevskiy Acta Physica Polonica B (Proc. Suppl.) 3, 589 (2010).

[76] N. K. Glendenning N K Phys. Rev. D 46, 1274 (1992).

[77] P. Cazzola, L. Lucaroni, C. Scaringi Nuovo Cimento B 43, 250 (1966).

[78] V. L. Ginzburg Sov. Phys. Usp. 14, 83 (1971); High- lights of Astronomy 2, 20 (1971).

[79] M. T. Takemori, R. A. Guyer Phys. Rev. D 11, 2696 (1975).

[80] V. R. Pandharipande, R. A. Smith Phys. Lett. B 59, 15 (1975).

[81] T. Takatsuka, R. Tamagaki Prog. Theor. Phys. 58, 694 (1977).

[82] M. Scott Ransom et al. Twenty-One Millisecond Pulsars in Terzan 5 Using the Green Bank Telescope. Science, 307:892896, 2005.

[83] P. C. C. Freire, A. Wolszczan, M. van den Berg, and J. W. T. Hessels, ApJ, 679:14331442, June 2008.

[84] D. J. Champion, et. al., Science, 320:1309, June 2008.

[85] J. P. W. Verbiest, et. al., ApJ, 679:675-680, May 2008.

[86] F. Nagase, 1992, ed D Pines, R Tamagaki and S Tsuruta (New York: Addison

- Wesley) p 77.

[87] S. L. Shapiro and S. A. Teukolsky, 1983, Black Holes, White Dwarfs, and Neutron stars (new York: Wiley).

[88] J. N. Bahcall 1978 Ann. rev. Astro. Astrophys. 16 241.

[89] J. W. T. Hessels et al., Science, 311:19011904, 2006.

[90] P. Kaaret et al., Astrophys. J., 657:L97100, 2007.

[91] I. Vidana, A. Polls and A. Ramos, Phys. Rev. C 65, (2001) 035804.

[92] I. Vidana and I. Bombaci, Phys. Rev. C 66, (2002) 045801. 16. F. Pacini, Nature 216, (1967) 567.

[93] F. Pacini, Nature 216, (1967) 567.

[94] M. F. Ryba, & J. H. Taylor, 1991a, ApJ, 371, 739.

[95] M. F. Ryba, & J. H. Taylor, 1991b, ApJ, 380, 557.

[96] B. Haskell, & A. Melatos 2015, Int. J. Mod. Phys. D, 24, 1530008.

[97] P. W. Anderson, & Itoh, N. 1975, Nature, 256, 25.

[98] M. A. Alpar, D. Pines, P. W. Anderson, & J . Shaham, 1984, ApJ, 276.

[99] R. Dib, & V. M. Kaspi, 2014, ApJ, 784, 37.

[100] A. G. Lyne, V. M. Kaspi, M. Bailes, R. N. Manchester, H. Taylor and Z. Arzoumanian 1996 Mon. Not. R. Astron. Soc. 281 L14.

[101] B. Link, R. I. Epstein, & J. M. Lattimer, 1999, Phys. Rev. Lett., 83, 3362.

[102] N. Chamel, 2012, Phys. Rev. C, 85, 035801.

[103] N. Chamel, 2013, Phys. Rev. Lett., 110, 011101.

[104] W. C. G. Ho, C. M. Espinoza, D. Antonopoulou, & N. Andersson, 2015, Sci. Adv., 1, e1500578.

[105] P. M. Pizzochero,M. Antonelli, B. Haskell, & S. Seveso, 2017, Nat. Astron., 1, 0134.

[106] A. G. Lyne, R. S. Pritchard, F. Graham-Smith, & F. Camilo, 1996, Nature, 381, 497.

[107] A. G. Lyne, C. A. Jordan, F. Graham-Smith, et al. 2015, MNRAS, 446, 857.

[108] C. M. Espinoza, A. G. Lyne, & B. W. Stappers, 2017, MNRAS, 466, 147.

[109] J. McKenna, & A. G. Lyne, 1990, Nature, 343, 349.

[110] A. G. Lyne, S. L. Shemar, & F. G. Smith, 2000, MNRAS, 315, 534.

[111] C. M. Espinoza, A. G. Lyne, B. W. Stappers, & M. Kramer, 2011, MNRAS, 414, 1679.

[112] A. W. Steiner, J. M. Lattimer and E. F. Brown, Astrophys. J. 765, (2013)L5.

[113] J. M. Lattimer and A. W. Steiner, Astrophys. J. 784, (2014) 123.

[114] S. D. Yancopoulos, T. T. Hamilton and D. J. Helfand 1994 Astrophys. J.429 832.

[115] M. Ruderman 1972 Ann. Rev. Astron. Astrophys. 10 427.

[116] G. Baym and C. Pethick C 1975 Ann. Rev.Nucl.Sci 25 27.

[117] V. Trimble and M. Rees 1970 Astrophys. Lett 5 93.

[118] G. Borner and J. M. Cohen J M 1973 Astrophys. J.185 959.

[119] J. M. Lattimer and B. F. Schutz, ApJ, 629:97(984), 2005.

[120] M. Bejger, T. Bulik, and P. Haensel, MNRAS, 364:635(639), 2005.

[121] I. A. Morrison, T. W. Baumgarte, S. L. Shapiro, and V. R. Pandharipande, ApJ, 617:L135(L138), 2004.

[122] F. Ozel, T. Guver, and D. Psaltis, ApJ, 693:1775(1779), March 2009.

[123] T. Guver, F. Ozel, A. Cabrera-Lavers, and P. Wroblewski, ApJ, 712:964(973), 2010.

[124] E. P. Liang, Astrophys. J. 304, (1986) 682.

[125] J. Cottam, F. Paerels, and M. Mendez, Nature, 420:51(54), 2002.

[126] F. Ozel, Nature, 441:1115(1117), 2006.

[127] J. M. Lattimer, C. J. Pethick, M. Prakash and P. Haensel, Phys. Rev. Lett. 66, (1991) 2701.

[128] S. Balberg and N. Barnea, Phys. Rev. C 57, (1998) 409.

[129] T. Takatsuka and R. Tamagaki, Prog. Theor. Phys. 102, (1999) 1043.

[130] T. Takatsuka, S. Nishizaki, Y. Yamamoto and R. Tamagaki, Prog. Theor. Phys. 105, (2000) 179.

[131] T. Takatsuka, S. Nishizaki, Y. Yamamoto and R. Tamagaki, Prog. Theor.

Phys. Suppl. 146, (2002) 279.

[132] I. Vidana and L. Tolos, Phys. Rev. C 70, (2004) 028802.

[133] X.-R. Zhou, H.-J. Schulze, F. Pan and J. P. Drayer, Phys. Rev. Lett. 95, (2005) 051101.

[134] Y. N. Wag and H. Shen, Phys. Rev. C 81, (2010) 025801.

[135] B. P. Abbot et al., Phys. Rev. Lett. 119, (2017) 161101.

[136] A. Y. Potekhin et al. Astrophys. J. 612, 1034 (2004)

[137] W. C. G. Ho, A. Y. Potekhin, G. Chabrier Astrophys, J. Suppl. Ser. 178, 102 (2008).

[138] K. Mori, W. C. G. Ho Mon. Not. R. astron. Soc. 377, 905 (2007).

[139] L.V. JONES, Stars and Galaxies. Westport, CT: Greenwood Press, 2009.

[140] J. C. Wheeler, *Cosmic Catastrophes*, Cambridge University Press, 2000.

[141] V. S. Beskin, Radio pulsars. P. N. Lebedev Physical Institute, Russian Academy of Sciences, Moscow. Physics-Uspekhi 42(11):1071-1098, 1999.

[142] F. Weber, *Pulsars as Astrophysical Laboratories for Nuclear and Particle Physics*, (Institute of Physics Publishing, Bristol 1999).

[143] D. G. Ravenhall, C. J. Pethick and J. R. Wilson, Phys. Rev. Lett. 50, (1983) 2066.

[144] C. J. Pethick, D. G. Ravenhall Annu. Rev. Nucl. Sci. 45, 429 (1995).

[145] P. Haensel, A. Y. Potekhin, D. G. Yakovlev, *Neutron Stars 1: Equation of State and Structure*, (New York: Springer, 2007).

[146] A. I. Chugunov, P. Haensel Mon. Not. R. astron. Soc. 381, 1143 (2007).

[147] D. N. Aguilera et al. Phys. Rev. Lett. 102, 091101 (2009).

[148] A. R. Bodmer, Phys. Rev. D 4, (1971) 1601.

[149] E. Witten, Phys. Rev. D 30, (1984) 272.

[150] H. Terezawa, INS Rep. 336 (Tokyo. Univ. Tokyo, INS), (1979).

[151] H. Terezawa, J. Phys. Soc. Japan 58, (1989) 3555.

[152] H. Terezawa, J. Phys. Soc. Japan 58, (1989) 4388.

[153] P. A.M Guichon, *Phys.Lett, B200:235,1988*.

[154] J. R. Stone, P.A.M. Guichon, H.H. Matevosyan, A.W. Thomas, Nucl. Phys. A, 792(3), 341 - 369, 2007.

[155] P. Demorest et al., Nature 467, (2010) 1081.

[156] J. Antoniadis et al., Science 340, (2013) 6131.

[157] J. M. Lattimer, B. F. Schultz, Astrophys.J. 629 (2005) 979-984.

[158] T. Hinderer, ApJ 677, (2008) 1216.

[159] T. Hinderer, B. D. Lackey, R. N. Lang and J.S. Read, Phys. Rev. D 81, (2010) 1230161.

[160] E. E. Flanagan and T. Hinderer, Phys. Rev. D 77, 021502 (2008), 0709.1915.

[161] T. Regge and J. A. Wheeler, Physical Review 108, 1063 (1957).

[162] B. P. Abbott et al., Phys. Rev. Lett., 119:161101, Oct 2017.

[163] B. P. Abbott et al., Phys. Rev. Lett., 121:161101, Oct 2018.

[164] J. B. Hartle and K. S. Thorne, Astrophys. J 153, (1968) 807.

[165]. M. Urbanec, J. C. Miller and Z. Stuchlik, MNRAS 443, (2013) 1903.

[166] P. A. M. Guichon, Phys. Lett., B200:235, 1988.

[167] P. A. M. Guichon, K. Saito, E. Rodionov, A.W. Thomas, Nucl. Phys. A601, 349 (1996); K. Saito, K. Tsushima, A.W. Thomas, Nucl. Phys. A609, 339.

[168] P. A. M. Guichon, H. H. Matevosyan, N. Sandulescu, and A. W. Thomas. Nucl.Phys., A772:1, 2006.

[169] P. A. M. Guichon, K. Saito, E. N. Rodionov, and A. W. Thomas. Nucl. Phys., A601:349, 1996.

[170] B. D Serot, J. D. Walecka, Adv. Nucl. Phys, 16:1,327, 1986.

[171] G. Krein, A. W. Thomas, and K. Tsushima. Nucl. Phys., A650:313–325, 1999, nucl-th/9810023.

[172] A. W. Thomas, Adv. Nucl. Phys., 13:1–137, 1984.

[173] N. K. Glendenning. In Compact Stars. Springer, Berlin, Heidelberg, New York, 2000.

[174] J. R. Stone, P.A.M. Guichon, H.H. Matevosyan, A.W. Thomas, Nucl. Phys A792 (2007) 341.

[175] W. D. Arnett and R. L. Bowers. Astrophys. J. Supplement, 33:415, 1977.

[176] V. R. Pandharipande. Nucl. Phys., A178:123, 1971.

[177] S. Balberg, I. Lichtenstadt, and G. B. Cook. Astrophys. J. Supplement, 121:515, 1999.

[178] R. B. Wiringa. Rev. Mod. Phys., 65:231, 1993.

[179] F. Hofmann, C. M. Keil, and H. Lenske. Phys. Rev., C64:025804, 2001.

[180] A. Akmal, V. R. Pandharipande, and D. G. Ravenhall. Phys. Rev., C58:1804, 1998.

[181] E. Chabanat, P. Bonche, P. Hansel, J. Meyer, and R. Schaeffer. Nucl. Phys.,A627:710, 1997.

[182] A. Chodos, R. L. Jaffe, K. Johnson, C. B. Thorn, 1974, Phys. Rev. D, 10, 2599.

[183] S. Weinberg, Gravitation and Cosmology (John Wiley and Sons, New York 1972).

[184] C. W. Misnes, K. S. Thorne, and J. A. Wheeler, Gravitation (W. H. Freeman, San Francisco 1973).

[185] J.B. Hartle, Astrophys. J 150, (1967) 1005.

[186] G. Torok, P. Bakala, E. Sramkova, Z. Stuchlık, M. Urbanec, 2010, ApJ, 714, 748.

[187] J. M. Irvine 1978, Neutron Stars (Oxford: Clarendon Press).

[188] Z. Stuchlik, G. Torok, S. Hledik, M. Urbanec, 2009, Classical and Quantum Gravity, 26, 035003.

[189] J. M. Lattimer, Prakash M., 2001, ApJ, 550, 426.

[190] M. Bejger, P. Haensel, 2002, A & A, 396, 917.

[191] D. Bandyopadhyay, S. A. Bhat, P. Char, D. Chatterjee, Eur. Phys. J. A54, 2018.

[192] J. M. Lattimer and B. F. Schutz, ApJ 629, (2005) 979.

[193] G. Torok, P. Bakala, E. Sramkova, Z. Stuchlık, M. Urbanec, K. Goluchova, 2012, ApJ, 760, 138.

[194] K. Yagi and N. Yunes, Phys. Rev. D 88, (2013) 023009.

[195] F. Cipolletta, C. Cherubini, S. Filippi, J.A. Rueda and R. Ruffini, Phys. Rev. D 92, (2015) 023007.

[196] K. Yagi and N. Yunes, Science 341, (2013) 365.

[197] J. M. Lattimer and M. Prakash. Phys. Rev. Lett., 94:111101, 2005.

[198] X. F. Zhao and H.Y. Jia, Revista Mexicana de Astronomıa y Astrofisica, 50, 103–108 (2014).

[199] L. Lindblom, Astrophysical Journal, Part 1 (ISSN 0004-637X), vol. 278, March 1, 1984, p. 364-368.

[200] T. A. DeGrand, R. L. Jaffe, K. Johnson, and J. E. Kiskis. Phys. Rev., D12:2060, 1975.

[201] G. Baym, C. Pethick, and P. Sunderland. ApJ, 170:299, 1971.